Unraveling the Function of Sll0944 in the Regulation of Carbon and Nitrogen Metabolism in *Synechocystis* sp. PCC6803

Dissertation

der Mathematisch-Naturwissenschaftlichen Fakultät
der Eberhard Karls Universität Tübingen
zur Erlangung des Grades eines
Doktors der Naturwissenschaften
(Dr. rer. nat.)

vorgelegt von
Tim Orthwein
aus Meschede

Tübingen
2024

Gedruckt mit Genehmigung der Mathematisch-Naturwissenschaftlichen Fakultät der Eberhard Karls Universität Tübingen.

Tag der mündlichen Qualifikation:	03.04.25
Dekan:	Prof. Dr. Thilo Stehle
1. Berichterstatter/-in:	Prof. Dr. Karl Forchhammer
2. Berichterstatter/-in:	Prof. Dr. Hannes Link

Erklärung

Ich erkläre hiermit, dass ich die zur Promotion eingereichte Arbeit selbständig verfasst, nur die angegebenen Quellen und Hilfsmittel benutzt und Stellen, die wörtlich oder inhaltlich nach den Werken anderer Autoren entnommen sind, als solche gekennzeichnet habe. Eine detaillierte Abgrenzung meiner eigenen Leistungen von den Beiträgen meiner Kooperationspartner habe ich in „Declaration of author contribution" vorgenommen.

Tübingen _____

“I am among those who think that science has great beauty.”

Marie Curie (Marie Salomea Skłodowska**)**

Contents

Abbreviations

2-OG	2-oxoglutarate
2-PGA	2-phosphoglycerate
3-PGA	3-phosphoglycerate
A. variabilis	*Anabaena variabilis*
AA	Amino acids
ACC	Acetyl-CoA carboxylase carboxyl transferase
ADP	Adenosine diphosphate
ADP-Glc	ADP-glucose
APC	Allophycocyanin
AMP	Adenosine monophosphate
ArgA	Amino-acid acetyltransferase
ArgE	Acetylornithine deacetylase
ArgJ	Arginine biosynthesis bifunctional protein
ATP	Adenosine triphosphate
B. subtilis	*Bacillus subtilis*
C	Carbon
CA	Carbonic anhydrase
CBB	Calvin Benson Bassham cycle
CCM	Carbon concentrating mechanism
CoA	Coenzyme A
CoIP	Co-Immunopecipitation
COX	cytochrome c oxidase
CP	Cyanophycin
Cyt b_6f	Cytochrome *b6f*
DHAP	Dihydroxyacetone phosphate
DNA	Desoxyribonucleic acid
dPGAM	2,3-bisphosphoglycerate dependent PGAM
e^-	Electrons
E. coli	*Escherichia coli*
ED	Entner Doudoroff cycle
Eda	KDPG aldolase
Edd	phosphogluconate dehydratase
EMP	Embden-Meyerhof-Parnas pathway
Eno	Enolase
ETC	Electron transport chain
F6P	Fructose 6-phosphate
FA	Fatty acid
FBP	Fructose 1,6-bisphosphate
FD	Ferredoxin
FNR	Ferredoxin-NADP+ reductase
G1P	Glucose 1-Phosphate
G6P	Glucose 6-phosphate
GAP	Glyceraldehyde 3-phosphate
GAPDH	GAP dehydrogenase
gifA/B	Genes of IF7/IF17
GLDH	Glutmate dehydrognase
GlgA	Glycogen synthase
GlgB	Branching enzyme
GlgC	G1P adenylyltransferase
GlgP	Glycogen phosphorylase
GlgX	Debranching enzyme
glnB/K	The gene encoding for the P_{II} nitrogen regulator protein
GlnB/K	P_{II} protein
GOE	Great oxygenation event
GOGAT	Glutamate-2-Oxogulatrate aminotransferase

Abbreviations

GS	Glutamine synthetase
H^+	Protons
IF7/17	inhibitory factors
iPGAM	2,3-bisphosphoglycerate independent PGAM
ipTM	Interface predicted template modelling
Kdg	2-oxoglutarate dehydrogenase
KDPG	2-keto-3-deoxy-6-phosphogluconate
N	Nitrogen
NAD(P)$^+$/H	Nicotinamidadenindinukleotid(phosphate)
NDH-1	NADH dehydrogenase
ntcA	The gene encoding for the global nitrogen regulator protein
NtcA	Global nitrogen regulator Portein
Pc	Plastocyanin
PCC	Pastuer culture collection
PDB	Protein Data Bank
PE	Phycoerythrin
PepC	Phosphoenolpyruvate carboxylase
Pfk	Phosphofructo kinase
PGAM	Phosphoglycerate mutase
PGI	Phosphoglycerate isomerase
Pgl	6-Phosphogluconolactonase
Pgm	Phosphogluco mutase
PHB	Polyhydroxy butyrate
PipX	P_{II} interacting protein X
PirC	P_{II} interacting regulator of carbon metabolism
PPP	Pentose phosphate pathway
PQ	Plastoquinone
PQH2	Plastoquinol
PRK	Pyruvate kinase
PRPP	Ribose-5-Phosphate pyrophosphate
PRPPS	PRPP-Synthetase
PS	Photosystem
PTM	Posttranslational modification
pTM	Predicted template modelling
R1,5BP	Ribulose-1,5-bisphosphat
RNA	Ribonucleic acid
Ro5P	Ribose 5-phosphate
RuBP	Ribulose-1,5-bisphosphate
Ru5P	Ribulose 5-phosphate
RuBisCO	Ribulose-1,5-bisphosphate carboxylase/Oxygenase
SDH	Succinate dehydrogenase
Ta	Transaldolase
TCA	Krebs- or Tricarbonic acid cycle
Tk	Transketolase
Zwf	G6P dehydrogenase

Summary

Cyanobacteria are considered to be the inventors of oxygenic photosynthesis. Two billion years ago, they shaped the atmosphere by releasing oxygen. Through this time, they evolved various species with plenty of mechanisms to adapt to the constantly changing environment. Among all those mechanisms, some structures became established and further functions evolved around this basis. One of the most prominent examples of this is the regulatory network of the nitrogen-regulatory protein P_{II}. In the non-diazotroph cyanobacterium *Synechocystis* sp. PCC 6803, P_{II} regulates a plethora of reactions that maintain the Carbon/Nitrogen homeostasis. The regulations depend on the binding of either ATP or ADP during high energy and nitrogen availability and 2-oxoglutarate (2-OG) during low nitrogen availability. In a balanced proportion of energy and nutrition, P_{II} ensures sufficient amounts of amino acid precursors by activating the phosphoenol pyruvate carboxylase and mitigating the fatty acid synthesis. It also binds the P_{II} interacting protein X to prevent the activation of the global nitrogen transcriptional regulator NtcA. With the increase of 2-oxoglutarate, P_{II} releases its binding partners, which cancels its regulations. It was suggested that P_{II} also regulate carbon storage during low nitrogen availability.

This work clarified P_{II}'s involvement in carbon storage regulation during chlorosis. The novel discovered that the P_{II} interacting regulator of carbon metabolism (PirC) changes the direction of fixed CO_2 from lower glycolysis to glycogen synthesis by inhibiting the 2,3-bisphosphoglycerate-independent phosphoglycerate mutase. P_{II} regulates this inhibition by binding the PirC during high ADP and ATP and releasing it during high 2-OG levels. PirC mediates the inhibition by interacting with two cyanobacteria-exclusive structural elements within their phosphoglycerate mutase. Furthermore, the elements also have a strong influence on the activity of the enzyme. This work also created the basis on which *Synechocystis* sp. PCC 6803 can be edited to create a chassis for the sustainable production of polyhydroxybutyrate (PHB) or other metabolism-derived valuable compounds. A strain derived from this work produced 80 % PHB of their cell dry mass.

Zusammenfassung

Cyanobakterien sind als die Pioniere der oxygenen Photosynthese anerkannt und haben vor zwei Milliarden Jahren maßgeblich zur Umgestaltung der Erdatmosphäre beigetragen. Im Laufe ihrer Evolution haben sie eine Vielzahl von Anpassungsmechanismen entwickelt, um sich an ständig wechselnde Umweltbedingungen zu gewöhnen. Ein zentraler Bestandteil dieser Anpassungen ist das regulatorische Netzwerk des Stickstoff-Regulations-Proteins P_{II}. In dem nicht-diazotrophen Cyanobakterium *Synechocystis sp. PCC 6803* steuert P_{II} eine Vielzahl von Stoffwechselprozessen, die für die Aufrechterhaltung der Kohlenstoff- und Stickstoff-Homöostase essentiell sind. Die Regulation erfolgt über die Bindung von ATP, ADP und 2-Oxoglutarat, die je nach Energie- und Nährstoffverfügbarkeit als Signalmoleküle dienen. Unter Bedingungen eines ausgeglichenen Energiehaushalts und ausreichender Nährstoffversorgung gewährleistet P_{II} eine effiziente Bereitstellung von Aminosäurevorläufern und reguliert die Fettsäuresynthese. Zudem hemmt es die Aktivierung des globalen Stickstoff-Transkriptionsregulators NtcA durch Bindung an das P_{II}-interagierende Protein X.

Unsere Ergebnisse belegen eine entscheidende Rolle von P_{II} bei der Regulation der Kohlenstoffspeicherung unter Stickstoffmangelbedingungen. Wir konnten zeigen, dass der P_{II}-interagierende Regulator des Kohlenstoffstoffwechsels (PirC) die Umwandlung fixierten Kohlenstoffs von der Glykolyse zur Glykogensynthese durch Hemmung der 2,3-Bisphosphoglycerat-unabhängigen Phosphoglycerat-Mutase beeinflusst. Diese Hemmung wird durch P_{II} reguliert, wobei die Bindung von PirC an P_{II} von den intrazellulären Konzentrationen von ATP, ADP und 2-Oxoglutarat abhängt. Strukturanalysen deuten darauf hin, dass PirC spezifisch mit cyanobakterien-spezifischen Elementen der Phosphoglycerat-Mutase interagiert und somit deren Aktivität beeinflusst. Unsere Studie legt den Grundstein für die Entwicklung von *Synechocystis sp. PCC 6803* als Chassisorganismus für die nachhaltige Produktion von Polyhydroxybutyrat (PHB) und anderen wertvollen Verbindungen. Durch gezielte genetische Modifikationen konnten wir Stämme generieren, die bis zu 80% ihres Trockengewichts in Form von PHB speichern.

Publications

Related to the topic of this thesis.

Publication 1

Research Article

Tim Orthwein, Jörg Scholl, Phillip Spät, Stefan Lucius, Moritz Koch, Boris Macek, Martin Hagemann and Karl Forchhammer

"The novel PII-interactor PirC identifies phosphoglycerate mutase as the key control point of carbon storage metabolism in cyanobacteria."
PNAS February 9, 2021, 118 (6)

Status: Published

Contribution: I have conducted Co-Immunoprecipitation experiments (cultivation and sample preparation) and biolayer interferometry analysis (BLI) to detect the binding kinetics of Protein-Protein interactions and the enzymatic assays. I also did all bioinformatic analyses of the proteins. I prepared the main figures and most of the figures in the supplement.

Publication 2

Research Article

Tim Orthwein, Luciano F. Huergo, Karl Forchhammer and Khaled A. Selim *"Kinetic Analysis of a Protein-protein Complex to Determine its Dissociation Constant (KD) and the Effective Concentration (EC50) of an Interplaying Effector Molecule Using Bio-layer Interferometry"*

Bio-protocol 11(17): e4152

Status: Published

Contribution: I planned, performed, and interpreted all experiments. I have written the first draft, edited the manuscript, and prepared all the figures.

Publication 3

Research Article

Tim Orthwein, Janette T. Alford, Nathalie Sofie Becker, Phillipp Fink, & Karl Forchhammer

„Structural elements of cyanobacterial co-factor-independent phosphoglycerate mutase that mediate regulation by PirC."

mBio: e03378-24

Status Published

Contribution: I planned and participated in all experiments. I wrote the first draft, edited the manuscript, and prepared all the figures.

Publications

Publication not related to the topic of this thesis

Publication 4

Research Article

M. Mager, H. Pineda Hernandez, F. Brandenburg, L. López-Maury, A.J. McCormick, D. J. Nürnberg, **Tim Orthwein**, D. A. Russo, A. J. Victoria, X. Wang, J. A. Z. Zedler, F. Branco dos Santos, and N. M. Schmelling

"*Interlaboratory Reproducibility in Growth and Reporter Expression in the Cyanobacterium Synechocystis* sp. PCC 6803"

ACS Synth. Biol. 2023, 12, 1823−1835

Status	Published
Contribution	I performed the experiments conducted in Tübingen.

Publication 5

Research Article

Sarah Wilcken, P.-H. Koutsandrea, T. Bakker, A. Kulik, **Tim Orthwein**, M. Franz-Wachtel, T. A. Harbig, Kay Nieselt, K.Forchhammer, H. Brötz-Oesterhelt, B. Macek, L. Kaysser, B. Gust

"*The TetR-like regulator Sco4385 and Crp-like regulator Sco3571 modulate heterologous production of antibiotics in Streptomyces coelicolor M512*"
Applied and Environmental Microbiology

Status	Submitted/Under Review
Contribution	I revised the BLI measurements and analysed the BLI data.

I Introduction

1 Cyanobacteria

In the kingdom of Eubacteria, cyanobacteriota represents a unique and versatile phylum. They are the only prokaryotes capable of performing oxygenic photosynthesis, a process that relies on light and oxygen (O_2) to fix carbon dioxide (CO_2). This process requires compartmentalisation within the cells. Almost all cyanobacteria contain an inner thylakoid membrane, essential for the light-dependent phase of photosynthesis. Embedded in the thylakoid is chlorophyll, the photosensitive molecule that gives cyanobacteria its characteristic green colour. The thylakoid membrane also contains light-harvesting antenna proteins called phycobilisomes, which contribute to the bluish appearance of cyanobacteria. Additionally, they have carboxysomes, which enhance CO_2 fixation during the light-independent part of photosynthesis. A diagram illustrating the general structure of cyanobacteria is shown in Figure 1A.

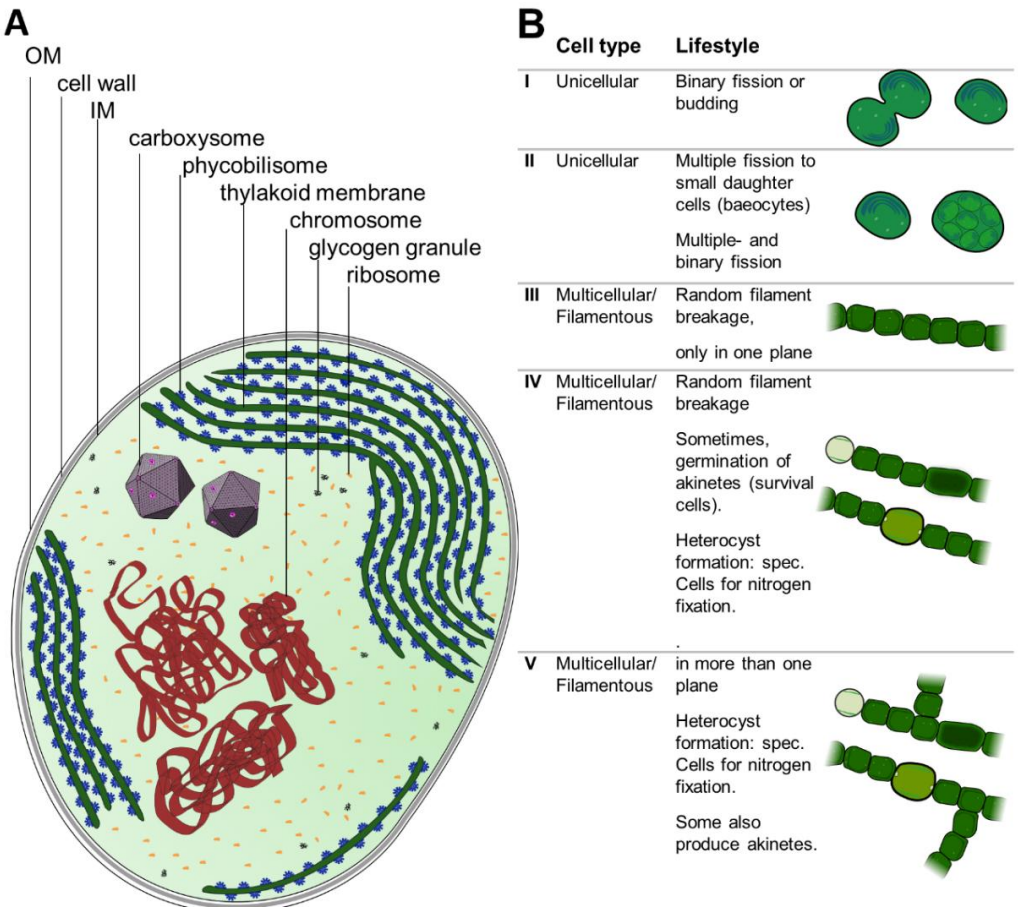

Figure 1 – (**A**) The general structure of a cyanobacterial cell, based on the model organism *Synechocysis* sp. PCC 6803. (**B**) Classification of cyanobacteria according to Rippka (1). Created with Inkscape 1.3 and Gimp 2.1.

Besides this uniqueness, cyanobacteria evolved into many different species, which can be classified into five sections regarding lifestyle, adaptation and morphology (Figure 1. B) (1). Along with their tremendous existence of around 2.4 billion years (2), cyanobacteria evolved various mechanisms to overcome hundreds of stress periods, such as nutrition deprivations or dry periods.

1.1 *Synechocystis* sp. PCC 6803

Due to their diverse abilities, cyanobacteria became an important phylum in natural research. One of the most studied cyanobacteria is the unicellular *Synechocystis* sp. PCC 6803. This section one cyanobacteria, now only termed *Synechocystis*, was used to discover many cyanobacterial phenomena. *Synechocystis* has a very accessible genome due to its natural competence, and easy-to-use protocols for genetic modifications are available (3, 4). Furthermore, its versatile metabolism and the various adaptation mechanisms to environmental changes make it an attractive target for investigating the physiology and metabolism of cyanobacteria (5, 6).

2 Cyanobacterial Metabolism

Cyanobacteria are mainly responsible for the great oxygenation event (GOE) approximately two billion years ago (7). This was only possible because of the evolution of oxygenic photosynthesis, in which CO_2 is captured from the ambient air and transformed mainly into cellular building blocks. In the light-dependent reaction, cyanobacteria obtain energy for the energy-intense CO_2 fixation and other pathways. In the *Calvin-Benson-Bessham* cycle (CBB), the light-independent reaction of photosynthesis, the CO_2, is fixed and channelled into the metabolism. Some cyanobacterial species require nitrate, nitrite, ammonia or urea to gain sufficient nitrogen, whereas others can fix atmospheric nitrogen (N_2) in periods of low availability. The intermediates must be distributed accurately. Therefore, the physiology of cyanobacteria is strictly regulated to maintain their homeostasis (8).

2.1 Energy Metabolism

2.1.1 Light Reaction of Photosynthesis

For the energy-consuming metabolism of the cell, cyanobacteria mainly gain their energy from the light reaction of photosynthesis (9), which takes place in the photosynthetic apparatus of the thylakoid (Figure 1). The light's energy is transformed into the energy-dense molecules of $NADPH^+$ and ATP. In the first step, at the

manganese cluster of Photosystem II (PSII), two molecules of H_2O are cleaved into four protons (H^+), one O_2 and four electrons (e^-) fueled by the absorption of light (Photolysis) (10). The four protons are released into the thylakoid lumen, and the electrons are transferred onto plastoquinone with two protons from the cytoplasm, forming plastoquinol (PQH_2). PQH_2 diffuse through the thylakoid membrane to cytochrome *b_6f* (Cyt *b_6f*). Cyt *b_6f* oxidises PQH_2 by means of a sequence of redox reactions known as the Q-cycle, resulting in a release of four protons into the lumen of th thylakoid again. The electrons are transferred to plastocyanin (Pc), in the next step. Then, Pc transfers the electrons in a secound light-driven reaction onto photosystem I (PSI). Subsequently, the terminal electron acceptor $NADP^+$ is reduced to NADPH by ferredoxin (FD) and ferredoxin-NADP+ reductase (FNR). Some of the electrons cycle back to Cyt *b_6f* for further H^+ pumping. The proton$^+$ membrane transport, driven by this electron transport chain (ETC), creates a proton motive force, which an F_1F_0-ATPase then uses to generate ATP (11).

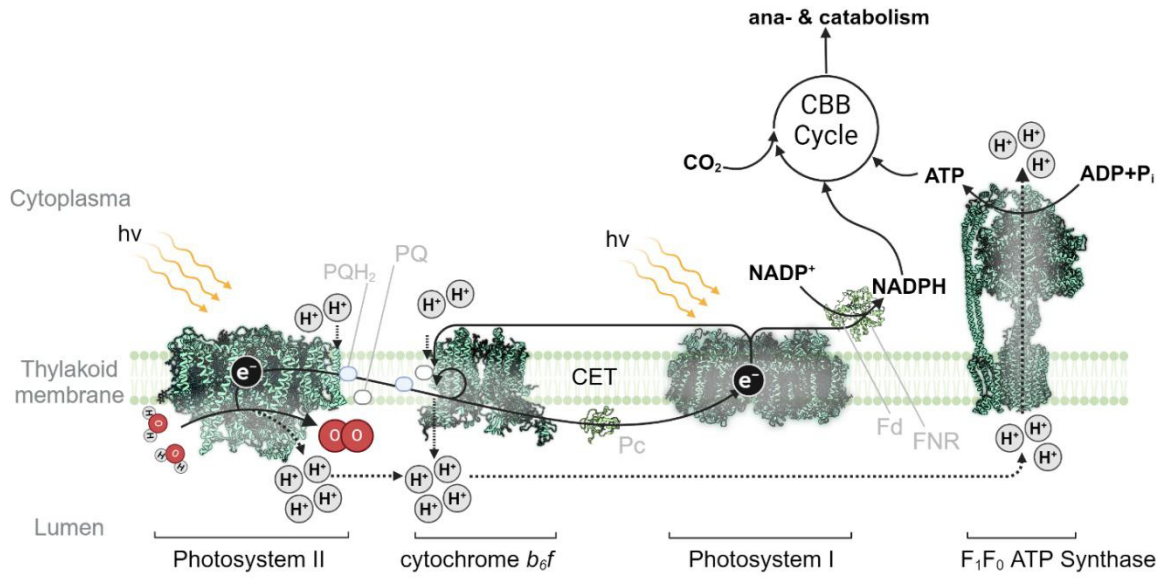

Figure 2 - Schematic representation of the photosynthetic machinery with e^- and H^+ flow inspired by Shevela *et al.* (12). PQ = Plastoquinone, PQH_2 = Plastoquinol, CET= cyclic electron transport, Pc = Plastocyanin, FD = Ferredoxin, FNR = Ferredoxin-NADP+ reductase. Structures used: PSII = PDB: 3KZI (13), Cytocrome *b6f* = PDB: 2ZT9 (14), Pc = PDB: 1BXV (15), PSI = PDB: 1JB0 (16), Fd-FNR-Complex = PDB: 1EWY (17). Created with biorender.com

In contrast to most algae and higher plants, cyanobacteria have specialised light-harvesting complexes called phycobilisomes (Figure 3). This multi-protein complex is located on the cytoplasmatic site of the thylakoid membrane. It is mainly built up by three individual light-capturing proteins: allophycocyanin (APC),

phycocyanin (PC) and phycoerythrin (PE), which are connected to the membrane by an anchoring protein (18, 19).

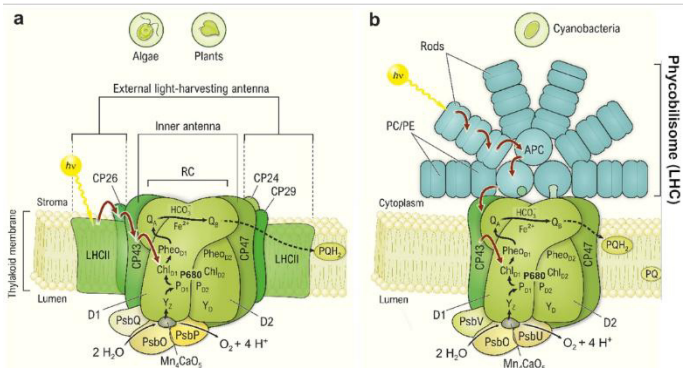

Figure 3 – Comparison of light-harvesting complexes of algae/plant PSII and cyanobacteria PSII Shevela *et al.* 2023 (12). (**a**) PSII of algae and plants, the LHC mainly integrated in the lipid-biolayer. (**b**) PSII of cyanobacteria with the PBS on the top of the membrane.

The PBS absorbs light in ranges between λ 530 – 650 nm, whereas chlorophyll a, the main chlorophyll in cyanobacteria, primarily absorbs light at λ 680 nm (20, 21). Consequently, cyanobacteria are more flexible in using light and can live in greater depths.

2.2.2 Respiration

In nature, cyanobacteria live under light-changing conditions. During dark periods when they cannot perform photosynthesis, cyanobacteria gain energy through oxidative phosphorylation, also known as respiration (22). Here, the proton motive force is also generated by an ETC, fueled by electrons of NADH and succinate oxidation. The components of the respiratory machinery are also located in the thylakoid and share redox-active components with the photosynthetic apparatus (23, 24). Additionally to the plastoquinone, Cyt b_6f complex, and plastocyanin, the respiratory apparatus possesses NADH dehydrogenase (NDH), succinate dehydrogenase (SDH) and a terminal cytochrome c oxidase (COX). NDH and SDH provide the electrons either through NADPH or succinate oxidation. Those electrons are then transferred to plastoquinone and transported to the Cyt b_6f. Again, during the electrons transferred onto plastocyanin, the protons are transported into the thylakoid lumen. Unlike photosynthesis, Pc transfers the electrons to COX, where the e^- is transferred to the terminal acceptor O_2 (25–27). The same ATP synthase during photosynthesis uses the protons to phosphorylate ADP to ATP.

2.2 Carbon Metabolism

Most eubacteria use glucose for energy and carbon incorporation. For this purpose, glucose is broken down depending on the metabolic status by the pentose phosphate- (PPP), the Embden–Meyerhof–Parnas- (EMP) and the *Entner-Doudoroff* (*ED*) pathway. All pathways are directed to the *Krebs Cycle* (*TCA*) or its variants, depending on the organism, in which NAD(P)H and ATP are formed. Furthermore, the intermediate molecules are used for the biosynthesis of building blocks such as nucleotides, fatty acids (FA) and amino acids (AA). Some cyanobacteria, such as Synechocystis, can use glucose as a carbon source, while obligate photosynthetic cyanobacteria, such as Synechococcus, cannot. However, all cyanobacteria primarily use CO_2 as a carbon source instead of glucose, incorporated mainly in the *Calvin-Benson-Bassham Cycle* (CBB). They also utilise the above-mentioned PPP, EMP, ED and TCA in their metabolism. The occurrence of all the paths enables a flexible adaptation to various conditions.

2.2.1 Calvin-Benson-Bassham-Cycle & Carbon Concentrating Mechanism

The main CO_2-fixing activity in cyanobacteria takes place in the CBB. In the first step, the Ribulose-1,5-bisphosphate-carboxylase/oxygenase (RuBisCO) adds CO_2 to Ribulose-1,5-Bisphosphate (RuBP) and splits RuBP into two 3-PGA molecules by hydrolysation (28, 29). 3-PGA is then transformed by phosphoglycerate kinase (PGK) and glyceraldehyde 3-phosphate dehydrogenase (GAPDH) in energy-intense reactions into glyceraldehyde 3-phosphate (GAP). Along the pentose phosphate pathway (PPP), GAP is transformed into ribulose 5-phosphate (Ru5P), which is then phosphorylated by the phosphoribulokinase (PRK) to RuBP (30) (Figure 4, purple arrows). At this point, the cycle restarts to fix more CO_2. RuBisCO is one of the most abundant enzymes on earth and is the protein that fixes the principal amount of CO_2 on earth (31). Besides the carboxylation activity, it also accepts O_2 as a substrate and produces 3-PGA and one 2-phosphoglycolate (2-PG) (32). The arising 2-PG is returned to the metabolism in a multiple-step mechanism called photorespiration (Figure 4, rose arrows). To prevent the oxygenation reaction of RuBisCO, cyanobacteria evolved a mechanism called carbon concentration mechanism (CCM) for a more efficient CO_2 fixation. The CCM in cyanobacteria comprises two parts: an HCO_3^-/CO_2-uptake system and a microcompartment called carboxysomes. *Synechocystis* possesses five membrane-bound complexes responsible for the uptake of HCO_3^-. The two thylakoid-located NDH-I_3 and NDH-I_4 convert free available CO_2 into HCO_3^-, whereas the three cytoplasmatic transporters BCT1, SbtA

and BicA directly transport HCO_3^- into the cell (33, 34). The enriched HCO_3^- then diffuses into the polyhedral-shaped carboxysomes. These structures encapsulate RuBisCO to protect it from oxygen. Additionally, the carboxysomes contain the carbonic anhydrase (CA), which converts HCO_3^- to CO_2, ensuring a high partial pressure of CO_2 close to the RuBisCO (35–37). The carboxysomes are built up by several shell proteins that exclude O_2 from the inside and enable the transfer of either HCO_3^-, Ru5P or 3-PGA (38, 39).

2.2.2 *Pentose-Phosphate-*, *Embden–Meyerhof–Parnas-* & *Entner-Doudoroff* Pathway

The PPP can be split into an oxidative (OPP) and a non-oxidative part (40)Besides the regeneration of RuBP in the CBB cycle via the non-oxidative PP, cyanobacteria use the OPP to supply NADPH as a reductive co-substrate and precursor for biosynthesis processes. Thereby, the OPP has a vital role in mobilising glycogen in the awakening of dormancy, e.g. chlorosis (41). In the OPP, glucose-6-P (G6P), primary from glycogen degradation, is transformed in two steps catalysed by Glucose-6-phosphate dehydrogenase (Zwf) and 6-Phosphogluconolactonase (Pgl) to 6-phosphogluconate (6PG). In the third step, 6PG is reduced to Ru5P (42–44). During these three steps, two NADPH molecules are formed. In the non-oxidative part, the transaldolase (Ta) and the transketolase (Tk) in interconversion steps in form C_3-, C_4-, C_5-, C_6- and C_7- sugars, which are used in nucleotide, vitamin or aromatic amino acid synthesis (45).The final product, Glc-6P, can be oxidised again by entering a new round of OPP reaction.

The EMP pathway in cyanobacteria occurs especially during starving situations or dark periods, where less NADPH and no biosynthetic precursors are required (46) (Figure 4, green arrows). In this pathway, G6P is isomerised to fructose-6-phosphate (F6P) by the G6P isomerase (Pgi), followed by phosphorylation to Fructose-1,6-bisphosphate (FBP) catalysed by the phosphofructokinase (Pfk). Subsequently, the aldolase splits the FBP into GAP and dihydroxy acetone phosphate (DHAP), which is isomerised by the triosephosphate isomerase (Tim), into GAP. The GAPDH and PGK are forming 3-PGA with simultaneous production of ATP and NADPH (47). In contrast, during resuscitation of deficiency adaptation, the EMP has only a minor role (41)

The ED pathway shares the Zwf and the Pgl with the OPP. At the point of 6PG, this pathway requires the fewest enzymes to gain the intermediary triose phosphates. 6PG is hydrolysed by phosphogluconate dehydratase (Edd) to 2-keto-3-deoxy-6-

phosphogluconate (KDPG). This C_6-body is directly split into 3-PGA and GAP (48). The key enzyme, KDPG aldolase (Eda), catalyses this reaction and is consistently present among cyanobacteria (49). A recently published study by Evans *et al.* 2024 revealed that no catalytical active products of Edd exist, evidencing an incomplete ED pathway in cyanobacteria. They also suggest that Eda, which is important in some growth situations, acts as an alternative for other aldolase reactions due to their promiscuity to substrates.

The processing of carbon reaches the point where 3-PGA is formed. At this point, it is decided whether the 3-PGA is directed in the CBB for RuBP regeneration or toward the lower glycolysis or carbon storage. In this regard, the 2,3-bisphosphate-independent phosphoglycerate mutase (iPGAM) is a decisive factor. iPGAM transforms 3-PGA to 2-phosphoglycerate (2-PGA) directed toward lower metabolic routes.

2.2.3 Carbon Storage & Glycogen metabolism

Throughout diurnal growth and some nutritional depletion periods, cyanobacteria store fixed carbon, mainly in form of glycogen. This polymer is well suited for this purpose because of the high energy and carbon storage per volume and the ability to mobilise monomers rapidly (50). It was proven that the PPP fuels glycogen biosynthesis in cyanobacteria (51, 52). Several studies have reviewed phosphoglucomutase (Pgm) as the key enzyme in the transition between the anabolic and katabolic routes (53, 54). Pgm catalyses the interconversion of G6P to glucose-1-phosphate (G1P), which is important for the initial step in glycogen formation. *Synechocystis* contains two isoenzymes*,* Pgm1 (sll0726) and Pgm2 (slr1334). The Pgm1 conducts 97 % of this activity and is, therefore, more critical in glycogen formation. Then, G1P adenylyltransferase (GlgC), activated by 3-PGA, adenylates G1P to ADP-Glucose (ADP-Glc), which is used by the glycogen synthase (GlgA). GlgA adds glucose with an α-1,4-glucosidic bond to the glycan chain, while the branching enzyme (GlgB) linkages an α-1,4-oligosaccharide to the polymer via an α-1,6-glucosidic bond, resulting in the branched glycogen. When glycogen is needed, the debranching enzyme (GlgX) and the glycogen phosphorylase (GlgP) mobilise the carbon by releasing G1P again, which is then redirected into the metabolism by Pgm (55–57) (Figure 4, orange arrows).

Some cyanobacteria, such as *Synechocystis,* are also able to produce another carbon polymer, polyhydroxybutyrate (PHB). This polymer is majorly produced during nitrogen deficiency periods for an as-yet-unknown reason (46, 58). In two steps, two molecules of Acetyl-CoA are reduced to 3-hydroxybutyryl-CoA (3-HB-CoA) by the acetyl-CoA acetyltransferase (PhaA) and acetoacetyl-CoA reductase (PhaB). The heterodimeric PHB synthase (PhaEC) then polymerises 3-HB-CoA to PHB (Figure 4, yellow arrows) (59, 60). The hydrophobic PHB is encapsulated into a hydrophilic protein shell. This microcompartment is also described as a carbonosome (61). PHB has similar properties to polypropylene and can be used as a natural alternative to petroleum-based plastics.

2.2.4 Krebs Cycle

When cyanobacteria are in an optimal environment, a significant proportion of 3-PGA is directed into the *Krebs* cycle, also known as TCA cycle. Here, the iPGAM, enolase (Eno), and pyruvate dehydrogenase (PDH) transform 3-PGA via PEP, pyruvate to acetyl-CoA, which is then condensed by the citrate synthase (GltA) with oxaloacetate (OAA) to citrate. In cyanobacteria, the TCA cycle primarily serves as a supplier of precursors for further biosynthesis, such as amino acids. Unlike most bacteria, cyanobacteria do not possess a 2-OG dehydrogenase (Kdg). They replace this enzyme with the 2-OG decarboxylase (2-OGDC), which splits 2-OG to succinic semialdehyde (SSA) instead of succinyl-CoA. Cyanobacteria also bypasses the Kdg reaction by the GABA shunt. Here, the 2-OG is aminased to Glutamate and transformed into γ-amino-butyric acid (GABA). The shunt is completed via transamination of GABA with 2-OG to SSA again. The TCA cycle of cyanobacteria is closed by the succinate-semialdehyde dehydrogenase, performing the reaction from SSA to succinate (62, 63). 2-OG is also the terminal acceptor of ammonium assimilation via the GS-GOGAT cycle, and thereby, the TCA cycle plays a pivotal role in the transition between carbon and nitrogen metabolism (64). The further reactions in the TCA cycle are equal to those of other bacteria (Figure 4, yellow circle). The PEP carboxylase (PepC) also plays an vital role in the TCA cycle. When the Krebs cycle is running out of intermediates, PepC refills the cycle in an anaplerotic synthesis of oxaloacetate (OAA) by the carboxylation of PEP and is therefore responsible for 50 % of the carbon intake of the TCA (65, 66). PepC is the secondary CO_2-fixing enzyme in cyanobacteria, responsible for up to 20 % of total fixed CO_2 (67).

2.2.5 Fatty Acid metabolism

The availability of fatty acids (FA) is crucial for forming membranes. Therefore, a significant proportion of fixed carbon is also directed into the synthesis of FA. Cyanobacteria have an equal FA synthesis to other bacteria. Intriguingly, cyanobacteria lack the FA degradation cycle β-oxidation (68, 69).

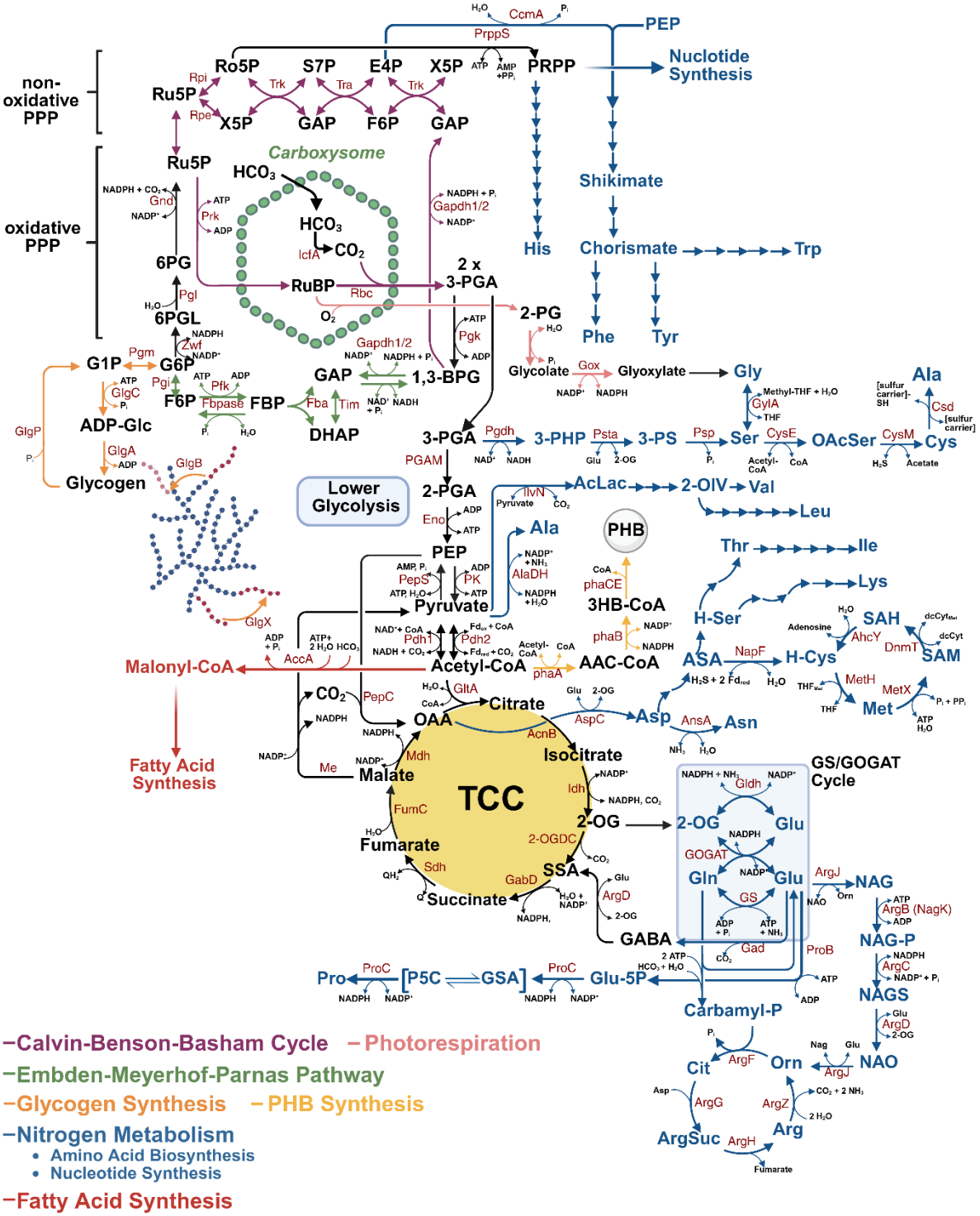

Figure 4 – Primary metabolic routes in cyanobacteria focused on glycolytic- and AA metabolism. Red text: Short names of enzymes based on gene names and aberrations of enzymes. Created with biorender.com

2.3 Nitrogen Metabolism

Nitrogenous compounds are essential in all living organisms. They serve as building blocks for proteins, nucleotides, and vitamins. Most cyanobacteria can form these required compounds on their own. For this, the cyanobacteria use primary ammonium for incorporation into their metabolism. To gain ammonium, combined nitrogen sources, such as ammonium itself, nitrate, nitrite or urea, are taken up into the cell by special transporters (70–72). Due to the high availability of nitrate in natural habitats, cyanobacteria often use NO_3^- as the nitrogen source, which they reduce to NH_3 in energy-consuming reactions (73). The ATP-binding cassette (ABC-) transporter NrtABCD is the uptake system for the nitrogen source nitrate. Once transported into the cell, the nitrate is reduced by the nitrate reductase to nitrite. The nitrite reductase subsequently reduces nitrite$^-$ to ammonium. The reduction is fueled by electrons from ferredoxin, which is reduced by the PSI. Urea is taken up by the ABC-transporter UrtABCD and degraded to ammonium via a Ni^{2+}-dependent urease. When NH_3 is available, the previously described uptake systems are repressed, and mainly NH_3 is taken up by the ammonium permease Amt1(64). Ammonium is primarily incorporated into the metabolism by the interplay of glutamine synthetase (GS) and glutamate-2-oxoglutarate aminotransferase (GOGAT), which use the TCC intermediate 2-OG as acceptor for ammonium. First, GS catalyses the ATP-dependent amination of the γ-carboxyl residue of glutamate to form glutamine. In the second step, the GOGAT transfers this γ-amino group onto the α-oxo group of 2-OG, resulting in two glutamate molecules. The GS is directly regulated via the inactivating factors IF7 and IF17 encoded by *gifA* and *gifB* (74). The expression of these genes is mediated by NtcA, which prevents an overflowing activity of GS during nitrogen repletion (75). A third enzyme, the glutamate dehydrogenase (GLDH), only becomes important during high nitrogen availability. GLDH directly adds ammonium to the oxo-group of 2-OG to form glutamate in an NADPH-dependent reaction. Glutamate is then used as a donor of the amino group in many transamination reactions to synthesise nitrogen-containing compounds.

2.3.1 Biosynthesis of Nitrogen-containing Compounds

Cyanobacteria can synthesise all essential nitrogen-containing metabolites that they require for their homeostasis. Many biosynthetic pathways for amino acids in cyanobacteria are similar to those of other bacteria, such as *Escherichia coli*. *Synechocystis* contains half as many functional genes as *E. coli* and requires fewer

enzymes to synthesise some amino acids (76). In the arginine pathway, in *Synechocystis*, the ArgA reaction is exchanged by the ArgJ, which catalyses the acetylation of glutamate via N-acetyl-ornithine instead of acetyl CoA (77). In this process, ornithine is released, resulting also in the replacement of the ArgE reaction. Another step where cyanobacteria only require a single enzyme is the transformation of tetrahydrodipicolinate to L,L-diaminopimelate in the lysine synthesis (76). Serine, in turn, can be synthesised via two different pathways in cyanobacteria. In the light-independent phosphoserine pathwy, 3-PGA is transformed in three steps to serine. In photorespiration, the 2-phosphoglycolate is recovered to glycine and further to serine. In addition to protein biosynthesis, some amino acids are incorporated into unique compounds, such as iron-sulfur-clusters and co-factors. Mainly, glutamate plays an extraordinary role in synthesising chlorophyll and glutathione (78, 79). Besides carbon storage, cyanobacteria also store nitrogen. For this purpose, cyanobacteria produce cyanophycin (CP). CP is a non-ribosomal peptide consisting of Arg and Asp monomers, which are connected via α- and β-amid bounds. A cyanophycin synthetase catalyses this polymerisation. Cyanobacteria produce CP in high-nitrogen environments while adapting to metabolic changes (80–82). Another essential synthesis is that of nucleotides. ATP and NAD(P)H are essential transmitters of energy and electrons, and all nucleotides are the information-providing building blocks of DNA and RNA. Due to the high similarity to *E. coli*, nucleotide synthesis is a less studied topic in cyanobacteriology. Purine and pyrimidine synthesis depend on the phosphoribosyl pyrophosphate synthetase (PRPPS) reaction, which catalyses the reaction of Ro5P to PRPP (76).

2.3.2 Adaptation to Nitrogen Availability

In natural habitats, the availability of combined nitrogen is subject to fluctuations, which can lead to nitrogen deficiency. To cope with this deficiency of combined nitrogen sources, various cyanobacteria evolved different mechanisms to maintain their viability. Cyanobacteria can be split into two groups. First, diazotrophs can use nitrogen gas (N_2) as nitrogen source, and second, the non-diazotrophs which are dependent on combined nitrogen sources. Diazotrophic species like *Anabaena variabilis* or *Cyanothece aeroginosa* possess a nitrogenase for the fixation of molecular nitrogen in periods of low availability of combined nitrogen sources (83). Multicellular diazotrophs such as *A. variabilis* evolved specialised N_2-fixing cells called *heterocysts* to enable the high-energy-consuming and O_2-sensitive reaction of the nitrogenase (84, 85). Unlike *Anabaena*, the genus *Cyanothece* performs the

nitrogenase reaction in dark phases when O_2-generation is low (86). Non-diazotrophic organisms are unable to fix N_2 and have evolved a mechanism to survive nitrogen depletion called chlorosis. Instead of N_2 fixation, they reorganise their metabolism to reach a dormant state with low metabolic activity. This physiological reprogramming is induced by sensing increasing terminal ammonium acceptor 2-OG. This activates a cascade of different survival mechanisms. Initially, they start to degrade the major light-harvesting phycobilisomes and the thylakoid, resulting in a colour change from blue-green to yellowish (Figure 5). They also immediately undergo a last cell division and start accumulating glycogen, which can reach up to 60 % of the cell dry weight (87). In total, the majority of the metabolic activity is reduced to a minimum, and only ~0.1 % of the photosynthetic capacity is maintained during chlorosis. This allows them to survive for several months in periods of low nitrogen availability (88–90). Some cyanobacteria, like *Synechocystis,* also produce PHB during chlorosis. In prolonged nitrogen deficiency, the polymer is formed fueled by the slight degradation of glycogen (46). Glycogen is also degraded, but more rapidly, when cyanobacteria resuscitate from the dormant state. In the first resuscitation phase, cyanobacteria require high levels of ATP, which they acquire via specialised sodium-dependent ATP synthetases (91). Further, they gain their energy by the degradation of glycogen and the oxidation of released G6P until they reach the second phase, where the photosynthetic machinery is recovered. In the course of resuscitation, the cells rebuild their internal structure, and overflowing nitrogen amounts are temporarily stored as cyanophycin (89).

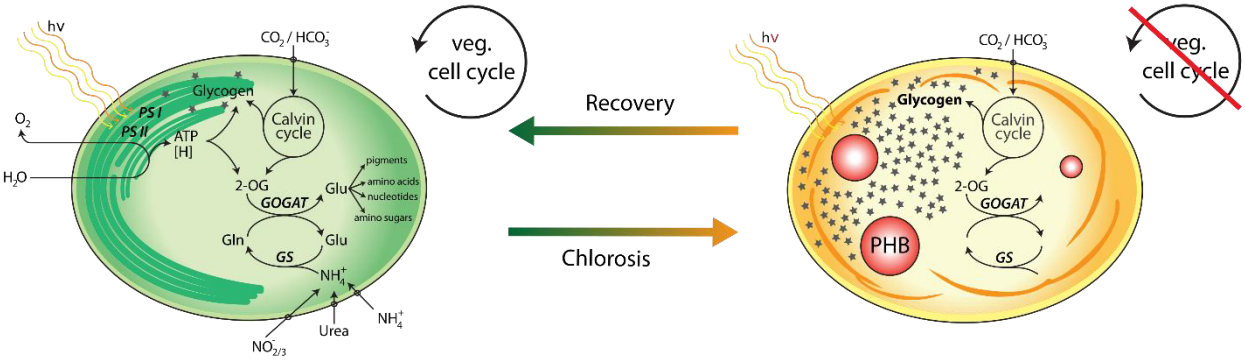

Figure 5 – Schematic overview of chlorosis and the resuscitation from chlorosis (adapted from Klotz et al., 2016)

3 C/N-balancing

The majority of all structures and mechanisms in living cells consist of carbon. The absence of carbon sources consequently leads to a stop of growth. As described before, nitrogen compounds are pivotal in almost all processes in metabolism. Accordingly, the metabolism of carbon and nitrogen must be strictly balanced. Cyanobacteria maintain the C/N balance with a sophisticated regulation system based on signal transduction protein P_{II}. (92)

3.1 The P_{II} Signal Transduction Protein

P_{II} proteins, encoded mainly by *glnB* and *glnK*, are present in a wide range of organisms, such as bacteria, archaea and plants (93, 94). They act as a status reporter for the energy- and C/N-status (95). All P_{II} proteins share a typical core structure formed by three equal subunits of the gene product. A cylindric structure of antiparallel β-sheets shapes P_{II}'s inner core, surrounded by six α-helices on the surface (two of each P_{II} subunit). Also, each monomer exposes a B-loop, C-loop and T-loop to the surface (Figure 6 A). The loops are crucial for binding the sensory molecules ADP, ATP and 2-OG (96). Some plant P_{II}, such as *Arabidopsis thaliana*, also possess a fourth Q-loop for interacting with glutamine (97). The B-and-C-loop interacts with the phosphate moiety of ADP and ATP, while the core structure and the T-loop are involved in the adenosine binding. 2-OG only binds when simultaneously Mg^{2+} and ATP are bound (96, 98). The interactions result in conformational changes of the T-loop, resulting in a shift in P_{II}'s binding capabilities to their target proteins (99) (Figure 6 B).

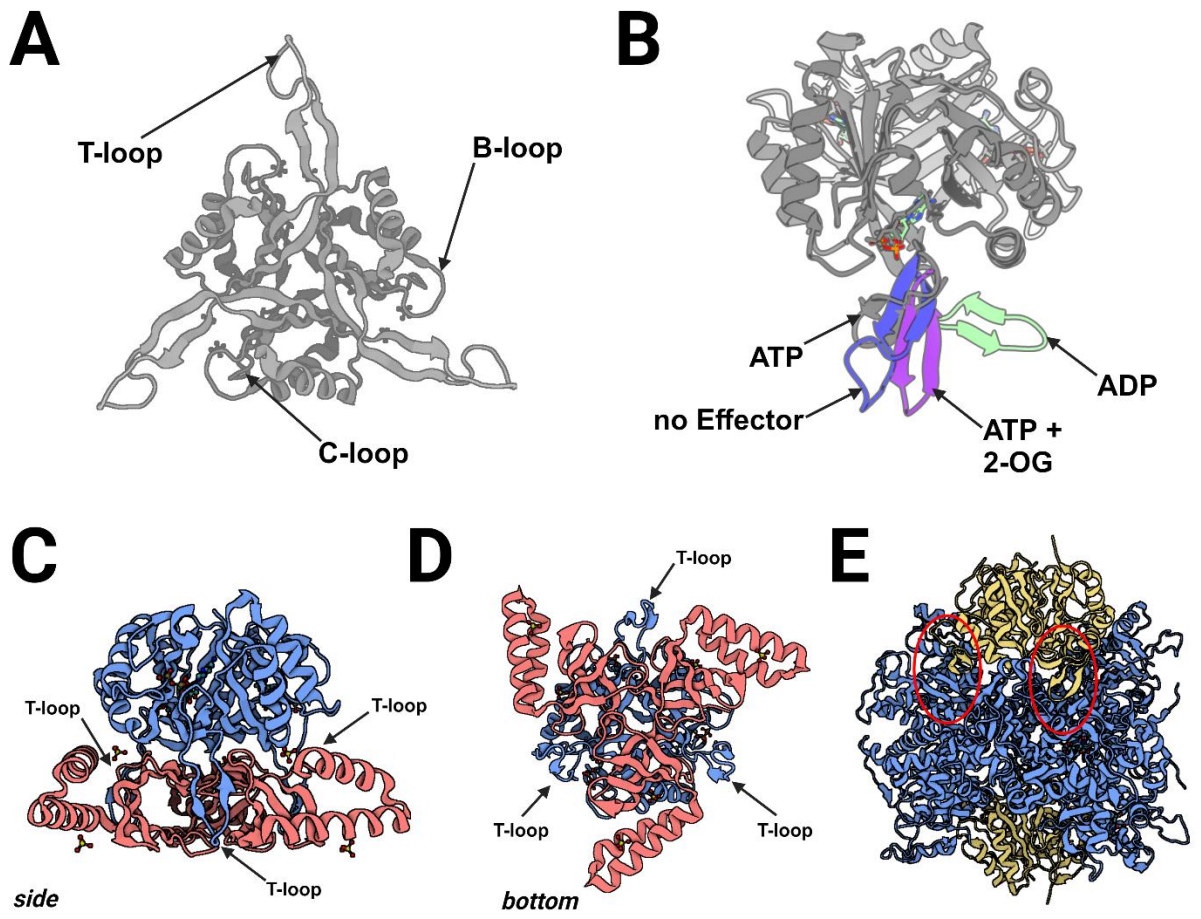

Figure 6 – Structure of P_{II} protein and interaction with binding partners. (**A**) The general structure of P_{II} with B-, C- and T-loop which are crucial for effector binding. PDB: 1QY7 (*Synechococcus* sp. PCC 7942) (**B**) Conformation of T-loop during binding of different effector molecules. No Effector (blue) = PDB: 1QY7; ADP (mint) = PDB: 4C3K (*Synechococcus elongatus*); ATP (grey) = PDB: 4CO1 (*Azospirillum brasilense* GlnZ); ATP + 2-OG (purple) = PDB: 3TA2 (GlnK3, *Archaeoglobus fulgidis*). (**C**) Side view of P_{II}-PipX complex (**D**) bottom view of P_{II}-PipX complex. P_{II} has grabs around the three PipX monomers. (**E**) Side view of P_{II}-NAGK complex. The red cycle focuses on the T-loop, which reaches inside the contact surface with NAGK. Created with biorender.com

When no effector molecule is bound, the T-loop has an opened structure, while the binding of ADP causes a closing of the T-loop (Figure 6 B) (100). This closing supports the binding of some interacting proteins, such as the P_{II} interacting protein X (PipX), by stabilising a grab-like structure around the interactor (Figure 6 C & D). In contrast, this conformation cannot bind N-actyl glutamate kinase (NAGK) (101). Due to the binding of ATP-$Mg^{2+,}$ the T-loop adopts another conformation, which allows different interactions with other binding partners, such as NAGK. In the case of NAGK, two P_{II}-trimers interact with a hexamer of NAGK. A stack of two trimers forms the NAGK hexamer. At the top and the bottom, each P_{II}-trimer

interacts with NAGK. Now, the T-loops of P_{II} reach into the contact surface with NAGK (102). The interaction of P_{II} with ATP and Mg^{2+} enables the binding of 2-OG. With 2-OG, the T-loop adopts an opened conformation again, further preventing the binding of many interacting partners (99).

Besides changes due to effector binding, P_{II} proteins are modified by post-translational modifications (PTM) depending on their nutritional status. In many bacteria, P_{II} is modified by uridylation or adenylation (103). In *E. coli,* the GlnB is uridylylated in low nitrogen availability (104). Under similar conditions, in cyanobacteria, the P_{II} is modified by phosphorylation, which sometimes adjusts its binding ability. The T-loop of cyanobacteria contains a unique serine residue (S49) for phosphorylation, close to the Y51, the uridylation site in *E. coli* (105, 106). The S49 is sometimes important in binding P_{II} targets, which is prevented by this phosphorylation, e.g. the interaction with NAGK (107). Another PTM detected in cyanobacterial P_{II} is the nitration of Y51 in the P_{II} of *Nostoc* sp. PCC 7120 (108). King *et al.* 2022 newly discovered another PTM in cyanobacterial P_{II} (109). In dependence on CO_2, the P_{II} gets carboxylated at a special lysine residue K73, preventing interaction with ATP.

3.1 The Regulating Network of P_{II}

The conformational flexibility induced by ATP, ADP, and 2-OG and the ability for PTM's make the P_{II} protein an ideal sensor molecule for regulating energy- and C/N-balancing. The P_{II} controls several metabolic routes and the uptake of nitrogen sources by direct protein-protein interaction with enzymes related to the target metabolism or indirectly through interaction with secondary mediating proteins (Figure 7). P_{II} prevents nitrate and nitrite uptake in an ammonium-rich environment by inhibiting the NrtABCD system (110). P_{II} also blocks ammonium uptake if its concentrations are too high (111). P_{II} regulates the activity of PepC, which plays an essential role in the transition between carbon and nitrogen metabolism. In the case of the well-balanced proportion of carbon and nitrogen, PepC maintains a high availability of intermediates of the Krebs cycle, which are crucial for the biosynthesis of amino acids (66). P_{II} binds PepC during this time and slightly increases its activity to ensure a high level of the amino acid precursors. This activation is modulated via ADP, 2-OG, or the phosphorylation of the T-loop of P_{II}. While ADP prevents the binding, and the phosphorylation only diminishes the binding to PepC, 2-OG only affects the mediation of the inhibition of PepC (112). P_{II}

also regulates the input into the Krebs cycle by inhibiting the first step of fatty acid synthesis. P_{II} binds to the biotin carboxyl carrier protein of the acetyl-CoA carboxylase (AccA) in an ATP-dependent manner and slows down its activity (113). This ensures appropriate levels of acetyl-CoA, which are directed to the citric acid cycle. Another enzyme P_{II} regulates is the N-acetyl glutamate kinase, the key enzyme in the synthesis of arginine and the associated cyanophycin (114). This direct regulation of nitrogen-related synthesis serves two purposes - preventing allosteric feedback inhibition by the terminal product of the related arginine pathway and activating NAGK (115, 116). More recently, the P_{II} interacting regulator of arginine synthesis (PirA) was discovered as a secondary regulatory protein of the NAGK (117). PirA sequestrates the P_{II} in an ADP-dependent manner during periods of high ammonium availability and abolishes the effects of P_{II} on NAGK. P_{II} also regulates the uptake of nitrogen sources by inhibiting the ammonium, nitrate, and urea transporters in nitrogen-rich conditions (111). The most prominent example of indirect regulation via P_{II} is the induction of nitrogen fixation in diazotroph and chlorosis in non-diazotroph cyanobacteria caused by the deficiency of combined nitrogen sources. In times of optimal energy- and C/N conditions, P_{II} binds PipX, as previously described. When GS-GOGAT no longer has sufficient ammonium to generate Glu, the concentration of the acceptor 2-OG increases. P_{II} senses the rise in 2-OG, and due to the conformational change of $P_{II,}$ PipX is released. Consequently, PipX binds to the global nitrogen regulator NtcA and acts as its co-activator (118). The 2-OG enhances the binding between PipX and NtcA and has a double function in the induction to the nitrogen acclimation mechanism (119). NtcA belongs to the transcription factors of the group of catabolite repressor proteins and affects up to 80 low-nitrogen acclimation genes in *Synechocystis* (120, 121). Two of those are *gifA* and *gifB*, the genes of GS inactivating factors IF7 and IF17, which are getting repressed by NtcA (122). Simultaneously, NtcA activates the expression of GS and the nitrogen uptake systems as a last resort to get nitrogen sources (123). In addition, this prepares the cells for rising nitrogen availability, which allows a rapid awakening of the dormancy.

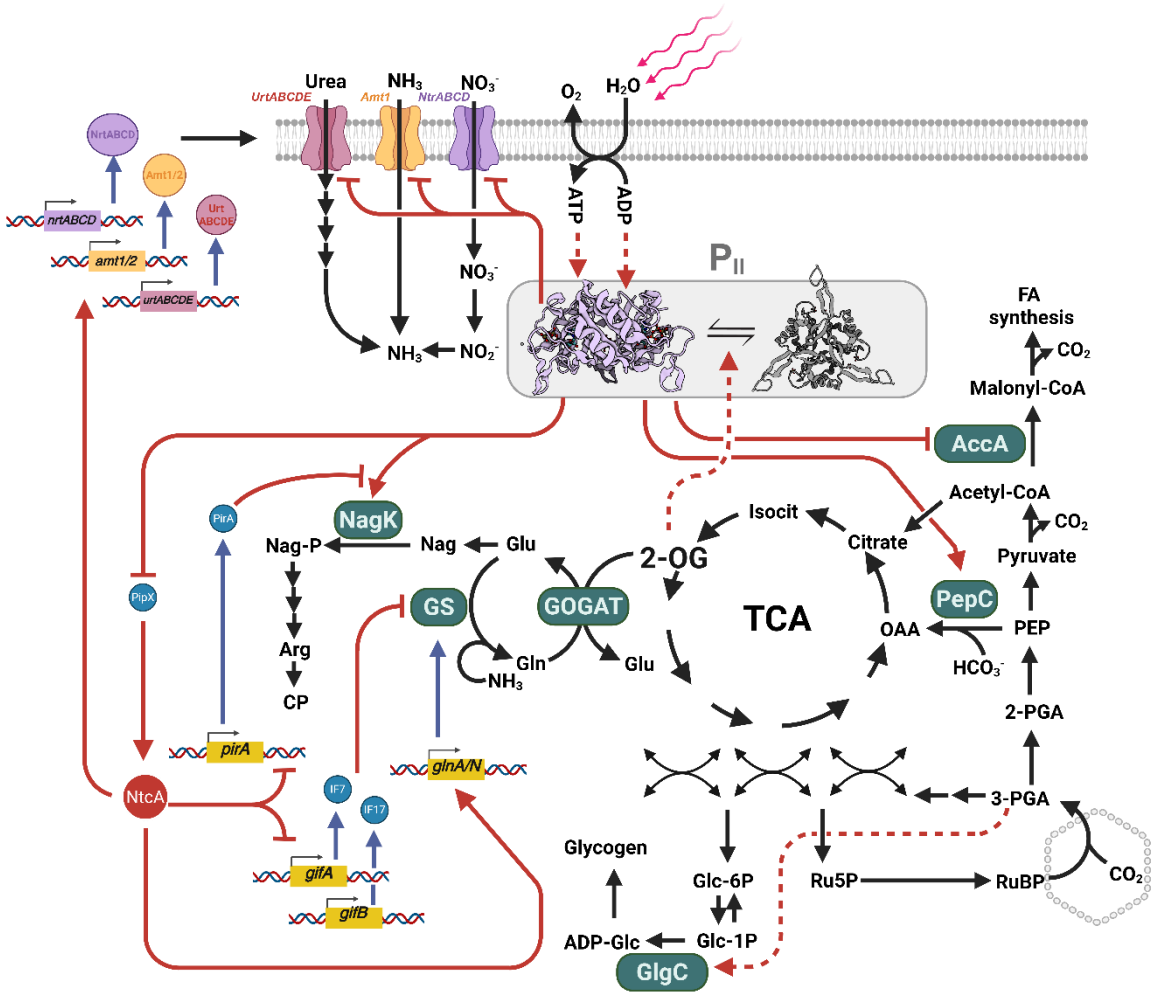

Figure 7 – Regulatory network of P_{II} in *Synechocystis* sp. PCC 6803 – When energy and nitrogen are highly available, sensed by ATP and ADP, and the interaction with 2-OG is missing, P_{II} adopts conformations that benefit the binding of their targets. P_{II} mitigates the FA synthesis by inhibiting AccA, enabling a higher acetyl-CoA level for the Krebs cycle. Furthermore, it enhances the PepC activity for an anaplerotic feeding of the Krebs cycle. Simultaneously, it slows down the nitrogen uptake to prevent ammonium levels in the cytoplasm that are too high. PII also activates NAGK. High ammonium levels mediate the expression of PirA, which prevents the NAGK activation by P_{II}. Also, IF7 and IF17 are expressed during high ammonium availability, mitigating the GS reaction. The complex formation of PipX and P_{II} prevents the activation of NtcA. Low levels of nitrogen sources result in the accumulation of 2-OG. AccA, PepC, NAGK and PipX are released from P_{II}. PipX then activates NtcA, which induces the nitrogen acclimation genes, including the nitrogen uptake systems and the GS. NtcA also inhibits the expression of IF7/17 and PirA. Arrow = activation, Flat ends = inhibition, dotted = metabolite inductions, dark blue arrows = expression. Created with bioren-der.com

4 Research Questions

The P_{II} protein in cyanobacteria is a vital regulator that processes several metabolic switches. However, not every interactions involving P_{II} is fully understood and is still elusive. For instance, the PamA membrane protein was detected in 2005 as a P_{II} interactor, but its function has not been fully clarified yet (124). It was expected that P_{II} influences not only carbon metabolism during vegetative but also during nitrogen-starving situations. In several studies, one special gene product, Sll0944, was often detected concerning nitrogen starvation and P_{II} interaction. (111, 125, 126). A potential candidate for P_{II} involvement in carbon metabolism during chlorosis and to extend knowledge of the P_{II} regulatory network.

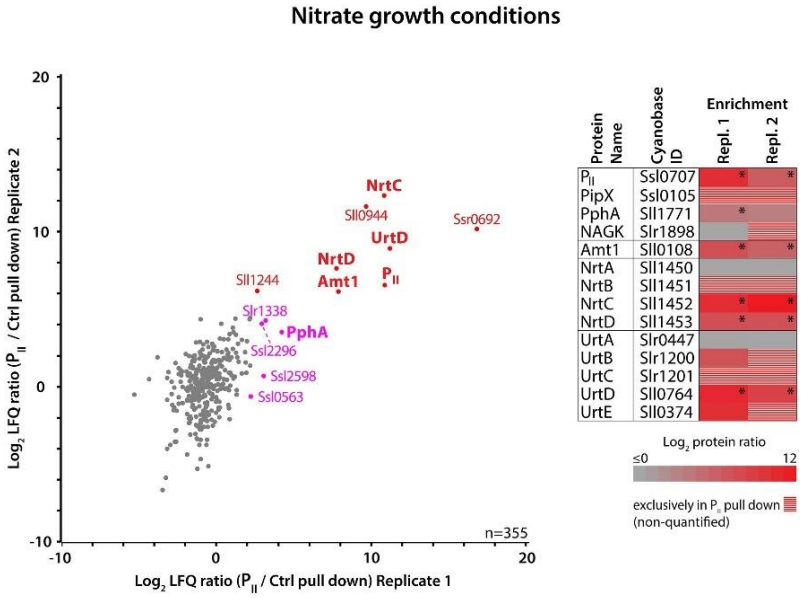

Figure 8 – α-Flag immunoprecipitation with Flag-tagged P_{II} from nitrate-grown cells. (111)

Preliminary unpublished data additionally detected an imbalance in carbon metabolism during chlorosis. This work deals with the investigation of the function of the Sll0944 protein. The emphasis was placed on the four sections:

1. Investigation of P_{II} interactions
2. Detection of possible interaction metabolic important enzymes
3. Molecular regulation of binding partners
4. Investigation of the structure of Sll0944 with and without their interacting partners

II Results

1 Detecting the Physiological Role of PirC

The main results of the following publications are summarised in the section.
Publication 1

> **Tim Orthwein,** Jörg Scholl, Phillip Spät, Stefan Lucius, Moritz Koch, Boris Macek, Martin Hagemann and Karl Forchhammer
>
> *"The novel PII-interactor PirC identifies phosphoglycerate mutase as the key control point of carbon storage metabolism in cyanobacteria."*
>
> PNAS February 9, 2021, 118 (6)
>
> https://doi.org/10.1073/pnas.2019988118

In this publication, the Sll0944 protein was detected as a regulator of carbon metabolism modulated by P_{II} and was named the **P**$_{II}$ **i**nteracting **r**egulator of **C**arbon Metabolism (PirC).

This section also includes additional non-published results (marked with *) related to this thesis's topic.

1.1 PirC is an exclusive protein of cyanobacteria

To gain more information about PirC regarding expression and potential binding partners, *in-silico* analyses, such as multiple sequence alignment (MSA) and gene neighbourhood analysis, were done. The analyses revealed that PirC is only present in Cyanobacteria. Each PirC protein contains the DUF1830 (Domain of Unknown function). The comparison of 53 different *pirC* genes revealed a dependence on nitrogen starvation. The NtcA-binding site 5'-GTN$_{10}$AC-3' was present before the *pirC* gene in each cyanobacterium. 67 % of the genes are in direct neighbouring to a noncanonical transfer RNA acetyltransferase. Synechocystis is upstream of the glgA1 gene that encodes the glycogen-synthase, which is important in glycogen formation during chlorosis (Publication 1, Fig. S1)

1.2 The role of PirC in the phosphorylation of P_{II}*

During adaptation to N-depletion, *Synechocystis* bleaches from bluish-green to yellowish according to the degradation of the phycobilisomes. This could be an effect of a change in the phosphorylation of the P_{II}. To check if PirC plays a crucial role in the phosphorylation of $P_{II,}$ a Native PAGE of WT and Δ*pirC* cultures with nitrate or ammonium as nitrogen source and two cultures with nitrogen or phosphate-depletion were conducted. The cultures were disrupted, and the protein

content was separated via non-denaturating Native PAGE and blotted on a PVDF membrane. There are four types of phosphorylated P_{II}. First, the non-phosphorylated and these, where one, two or three monomers of the trimeric P_{II} are phosphorylated. According to the negative charge of the phosphates, the four types of P_{II} run at different lengths through the polyacrylamide gel. After the transfer onto a membrane, the P_{II} proteins were visualised by detecting them with anti-P_{II} antibodies (Figure 9).

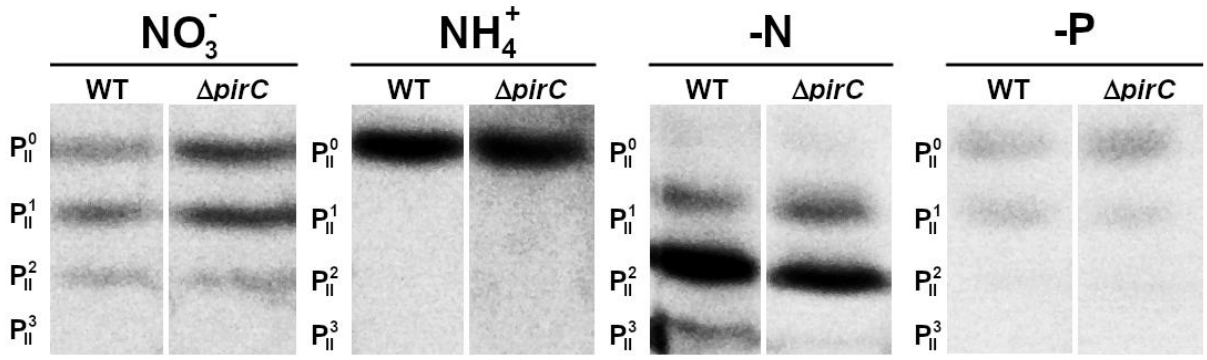

Figure 9 - P_{II} phosphorylation status in WT and Δsll0944 during growth with nitrate (NO_3^-); Ammonia (NH_3) and during depletion of nitrogen (N) and phosphate (P)

Under every condition, P_{II} was detected. During growth with nitrate, there is no difference in the phosphorylation between the WT and Δ*pirC.* The non-phosphorylated and one or two times phosphorylated P_{II} are seen. Only the phosphate-free P_{II} is present in the WT and Δ*pirC* in the ammonium samples*.* Under nitrogen depletion, the three types of phosphorylated P_{II} exist in both strains. Under phosphate depletion, both strains contain the same P_{II} phosphorylation variants with non-, one- or two-phosphorylated monomers.

1.3 PirC binds to P_{II} in a T-loop-specific manner

In previous studies, PirC was detected as a P_{II} binding partner. To elucidate the molecular dynamics of this binding, Biolayer interferometry (BLI) experiments were conducted. The BLI revealed a T-loop-dependent binding of PirC. PirC showed an enhanced binding affinity to P_{II} when ADP (K_D = 14.06 ± 0.74 nM) or ATP (K_D = 37.29 ± 2.49 nM) was added to the assay. Furthermore, the results showed inhibition of this binding via 2-OG addition (IC_{50} = 124.4 ± 1.1 µM) (Publication 1, Fig. 1).

1.4 PirC deletion lowers glycogen- and increases PHB levels

A *Synechocystis* strain with a deleted PirC gene (Δ*pirC)* was investigated during growth with sufficient nutrition and according to the interaction with P_{II} to nitrogen depletion under a day-night regime. This should give evidence of the potential functions of PirC in the physiology of *Synechocystis*. The deletion showed no disadvantage compared to the WT. When the cells were shifted to a nitrogen-poor medium, the Δ*pirC* lacked in the initial doubling of chlorosis. Furthermore, the mutant could not form as much glycogen as the WT. In contrast, the Δ*pirC* produced twice as much PHB than the WT. The reintroduction of the pirC also proved the effects, and *Synechocystis* regained the behaviour of the WT (Publication 1, Fig 2)

1.5 The iPGAM was detected as an active binding partner of PirC

Co-immunoprecipitation of *Synechocystis* with a PirC fused to mCitrine was performed to detect active PirC binding partners. The analysis revealed the product of *slr1945*, which encodes the 2,3-bisphosphoglycerate-independent phosphoglycerate mutase (iPGAM), as a binding partner of PirC (Publication 1, Fig. S6, Fig. S7). The effect of PirC on the iPGAM activity was tested using an enzymatic assay. The experiments showed PirC inhibiting iPGAM. (Publication 1, Fig. 3 A). A further assay where the interplay with P_{II} was tested showed that the inhibition of iPGAM was revised in the presence of $P_{II,}$ and 2-OG again prevented this effect (Publication 1, Fig. 3 B). BLI experiments also detected an influence of the enzyme substrates on PirC's binding ability (Publication 1, Fig. 3 C, D & E)

1.6 iPGAM inhibition leads to a metabolic switch

The enzymatic assay results showed an *in vitro* inhibition of iPGAM, leading to the assumption that PirC affects the glycolytic pathways *in vivo*. This was checked by detecting the metabolite contents during an ongoing nitrogen depletion over 24 h using WT and the ΔpirC culture. It was shown that the 3-PGA concentration accumulated over 24 h of chlorosis in the WT, while the content in ΔpirC stayed low. In contrast, the ΔpirC accumulated 14 times more pyruvate than the WT.

2 Molecular Regulation of iPGAM

Publication 3

> **Tim Orthwein**, Phillipp Fink, Janette T. Alford, Nathalie Becker & Karl Forchhammer
>
> *„Structural elements of cyanobacterial co-factor-independent phosphoglycerate mutase that mediate regulation by PirC"*

It was shown that PirC regulates the carbon-/nitrogen homeostasis in cyanobacteria tuned by the nitrogen regulator protein P_{II}. Besides the interaction with P_{II}, the iPGAM interaction is also crucial in understanding the regulation dynamics. Based on the exclusiveness of the iPGAM inhibition by a unique protein in cyanobacteria, the iPGAM of *Synechocystis* was analysed in terms of emerging specialities.

2.1 iPGAM of cyanobacteria have particular sub-structure

First, the iPGAM sequence of *Synechocystis* was analysed by a phylogenetic and multiple sequence alignment (MSA) to get more information on cyanobacterial iPGAMs. It was shown that the cyanobacterial iPGAM exclusively evolved compared to other species (Publication 3, Figure 1). Early red algae and cyanobacteria split from other bacterial iPGAMs in the phylogenetic tree, indicating a distinguished evolution in cyanobacteria. In particular, an MSA revealed two sequences that only exist in the cyanobacterial iPGAMs. An inner structure and an extended C-terminus with conserved amino acids in sequence (detected by SeqLogo of an alignment with 644 different cyanobacterial PGAMs).

2.2 Structure Prediction of iPGAM

To see if the segments are important structural elements, the structure of the iPGAM was predicted using AlphaFold and SWISS-MODEL. The prediction showed the typical separation in phosphatase- and transferase-domain with an in-between substrate binding cleft. The inner cyanobacterial segment was predicted as the inner loop segment (called a loop) and a random coil of the C-Terminus. The loop segment is directly connected to the catalytic centre via a ten amino acid long ß-strand. The loop contains an inner hydrogen bond between highly conserved glutamate (E468) and lysine (K473) residue (Publication 3, Figure 2)

2.3 Mass photometry indicates a 1:3 stochiometry of iPGAM-PirC

Mass photometry was conducted to detect the stochiometry of the iPGAM-PirC complex. The analysis of iPGAM indicated a monomer, and the PirC was detected mainly as a hexamer but with signals of even higher oligomeric species. The combination of the complex attested to a potential stoichiometry of one iPGAM with three PirC monomers.

2.4 Structure Prediction of iPGAM

The structure of the iPGAM-PirC complex was predicted with AlphaFold to get information on potential interaction which can mediate the inhibition. It revealed three independent binding sites for PirC. One in the binding cleft and another one concerning the loop structure. A conserved tyrosine (Y39) from PirC forms a hydrogen bond with the K473 of iPGAM and prevents the E468-K473 hydrogen bond. The third predicted binding site showed no specialised interaction with iPGAM.

2.5 The iPGAM variants have changed affinities to PirC and changed inhibitory effects

To detect the effect of the variants on the binding and the inhibitory effect of PirC, BLI measurements and a coupled enzymatic assay were conducted with purified proteins of created strep-iPGAM variants lacking the sub-structures (iPGAM-Δloop, -ΔCT & -ΔloopΔCT). The detected K_D values of iPGAM-WT (378.4 ± 50.3 nM) iPGAM-Δloop (203.2 ± 45.04 nM), iPGAM-ΔCT (113.6 ± 18.3 nM) & iPGAM-ΔloopΔCT (233.4 ± 45.3 nM) show an enhanced affinity of PirC to the iPGAM. The activity of both loop-free iPGAMs is drastically reduced compared to the WT, while the PGAM-ΔCT has double the maximum activity. Despite the stronger binding of PirC, the inhibitory concentration (IC_{50}) of PirC of iPGAM-ΔCT is 10 times higher than in the WT. The IC_{50} of the two other variants are close to the WT (Publication 3, Table 2, Figure 5).

2.6 The iPGAM variants influence the metabolism during chlorosis

To test the effect of the different variants on the physiology of *Synechocystis*, strains with exchanged iPGAM with iPGAM-Δloop -ΔCT & -ΔloopΔCT were created. The ΔPirC strain was used as a control for an uninfluenced iPGAM. The variants were tested on the effect of general laboratory conditions with nitrate and ammonia. No differences between all strains were detected. Furthermore, an nitrogen depletion experiment was conducted to see the influence of the iPGAMs in

chlorosis. The ΔPirC had a lack of initial doubling in chlorosis. The iPGAM-ΔCT & -ΔloopΔCT strains produced similar amounts of PHB to the ΔPirC strain but had no missing doubling at the beginning of chlorosis. The iPGAM-Δloop showed no significant differences to the WT and ΔPirC. (Publication 3, Figure 6).

3 Investigation of potential binding Partners of PirC and PGAM

Th following sections, 3 and 4, only contain unpublished results.

3.1 Co-Immunoprecipitation using anti-PirC antibodies

Co-immunoprecipitation (CoIP) using the GFP-Trap beads and mCitrine-PirC as bait revealed the iPGAM as an active target in cyanobacterial metabolism. There is the possibility of additional binding partners. To test this, another co-immunoprecipitation experiment was conducted. In this case, antibodies against the native protein were used to trap the PirC and detect novel binding partners. As control and to detect putative binding partners during growth, the CoIP was conducted with vegetative growing cultures in continuous light. This analysis was done with WT and cells containing the loop-free iPGAM (Δloop) variant to detect differences from the native iPGAM. The samples were prepared and analysed as described in III Material and Methods of Additional Results. The enrichment of proteins co-precipitated in the sample was compared against the same experiment using a control antibody (TnrA protein from *Bacillus subtilis*). The results of the experiments were depicted in a dot plot, x-axis: log2 of the LFQ intensity ratio of the sample against control, y-axis log10 of the overall intensities. The results of the experiment using the WT cells are shown in Figure 10.

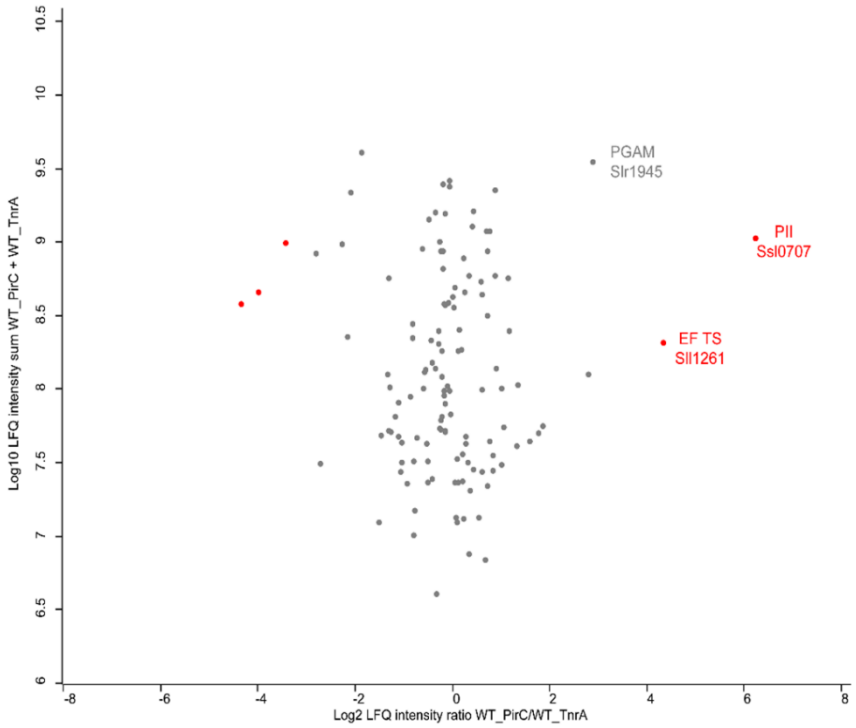

Figure 10 - Co-immunoprecipitation of vegetative-grown WT cells using α-PirC as a trapping molecule. Each point represents the log2 ratio of protein enrichment in the PirC antibody sample to the control (TnrA AB) against the log10 of the total enrichment. Each point depicts the mean of independent triplicates.

As expected, the most abundant protein in the sample is P_{II}. A second protein which was highly abundant in the sample enrichment was the Ssl1261. This protein is annotated as the elongation factor (EF) TS, which catalyses the release of GDP from the EF-TS (127). Surprisingly, iPGAM was also found to have higher contents in the sample.

The same experiment was repeated using vegetative growing cells of Δloop (Figure 11).

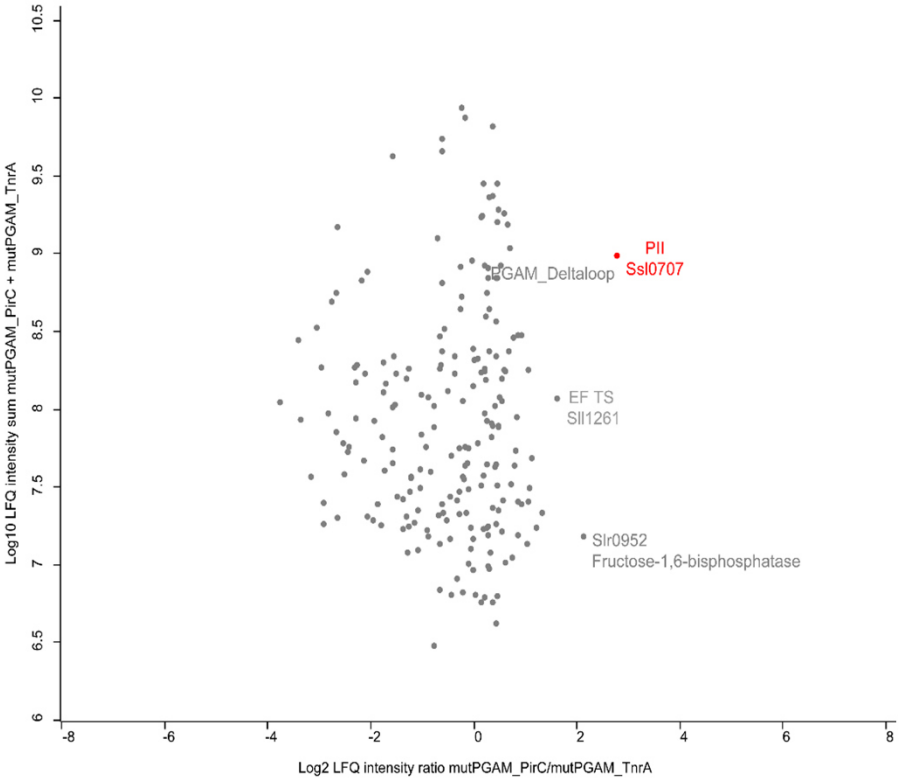

Figure 11 - Co-immunoprecipitation of vegetative-grown Δloop cells using α-PirC as a trapping molecule. Each point represents the log2 ratio of protein enrichment in the PirC antibody sample to the control (TnrA antibody) against the log10 of the total enrichment. Each point depicts the mean of independent triplicates.

A similar outcome mainly was detected as in the WT, except for the intensities. P_{II} was again the most abundant protein, and the EF TS protein was detected in higher amounts but with a much lower ratio than the WT. Additionally to the WT, with a log2 ratio of around 2, the Fructose-1,6-bisphosphate was detected.

As detected in previous studies, PirC is mainly bound by P_{II} in a nutrition-rich environment and is more exposed during nitrogen starvation. The CoIP was also conducted with cells from a nitrogen-depleted culture. The graph in Figure 12 shows the results of an experiment with the WT cells.

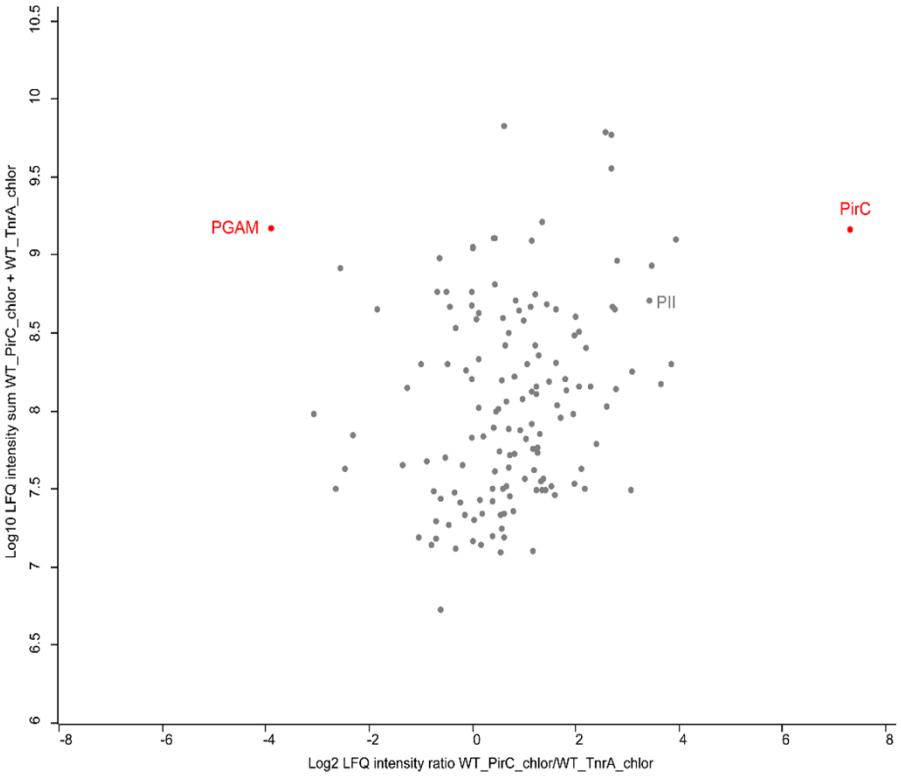

Figure 12 - Co-immunoprecipitation of n-depleted WT cells using α-PirC as a trapping molecule. Each point represents the log2 ratio of protein enrichment in the PirC antibody sample to the control (TnrA AB) against the log10 of the total enrichment. Each point depicts the mean of independent triplicates.

Unlike expected, the iPGAM was highly underrepresented in the sample precipitation, and the only noticeable abundant protein was the bait protein PirC itself. As the vegetative sample, P_{II} could be detected as slightly enriched but with lower intensities. The same experiment conducted with iPGAM-Δloop is shown in Figure 13.

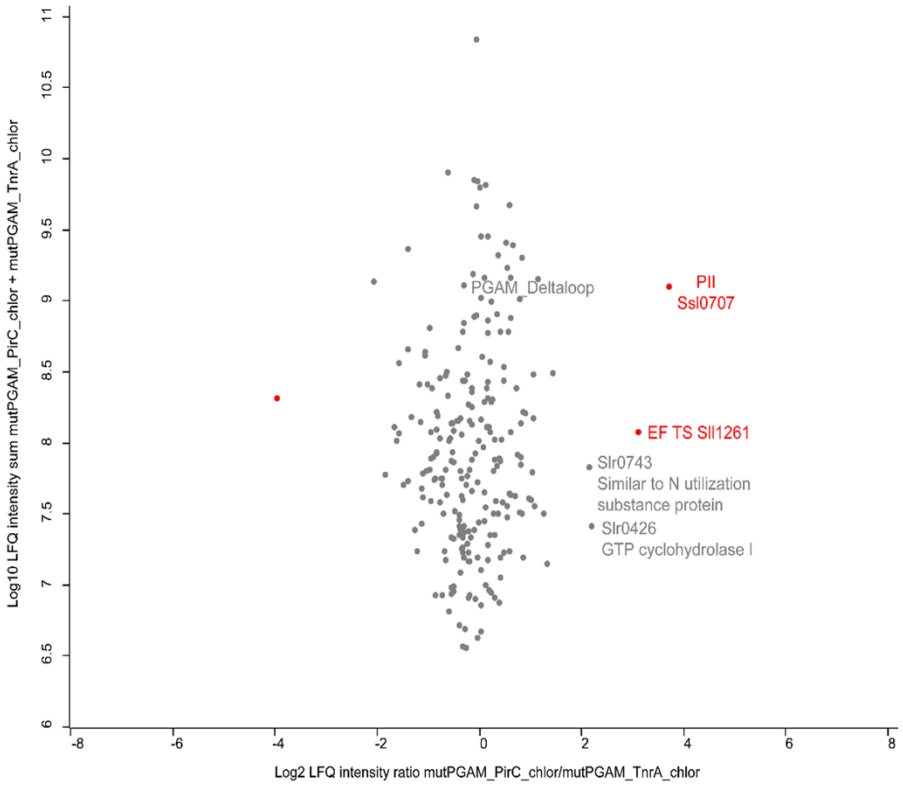

Figure 13 - Co-immunoprecipitation of n-depleted Δloop cells using α-PirC as a trapping molecule. Each point represents the log2 ratio of protein enrichment in the PirC antibody sample to the control (TnrA AB) against the log10 of the total enrichment. Each point depicts the mean of independent triplicates.

Again, P_{II} was the most abundant protein. In this sample, the EF-TS protein could also be detected in higher amounts than in the control. In slightly higher amounts, the Slr0743 and the Slr0426 were detected. The Slr0743 is annotated as NusA protein, a part of the rRNA transcription and antitermination complex (128)The Slr0426 protein, annotated as GTP cyclohydrolase I, hydrolyses GTP to dihydro-neopterin triphosphate, the initial intermediate in the synthesis of tetrahydrofolate (129).

A disadvantage of relative quantitative analysis against a control is the loss of proteins exclusively available in the sample's enrichment (deviation with zero is not allowed). Due to this fact, proteins solely enriched in the sample were also analysed. For the analysis, all exclusive proteins found in the measurements of vegetative (+ N) or N-depleted cells (- N) were considered and filtered to detect potential hits. The threshold was set to a minimum of LFQ of $1 \cdot 10^8$. Only proteins detected in WT and the Δloop of each growth background were used. Results are shown in Figure 14.

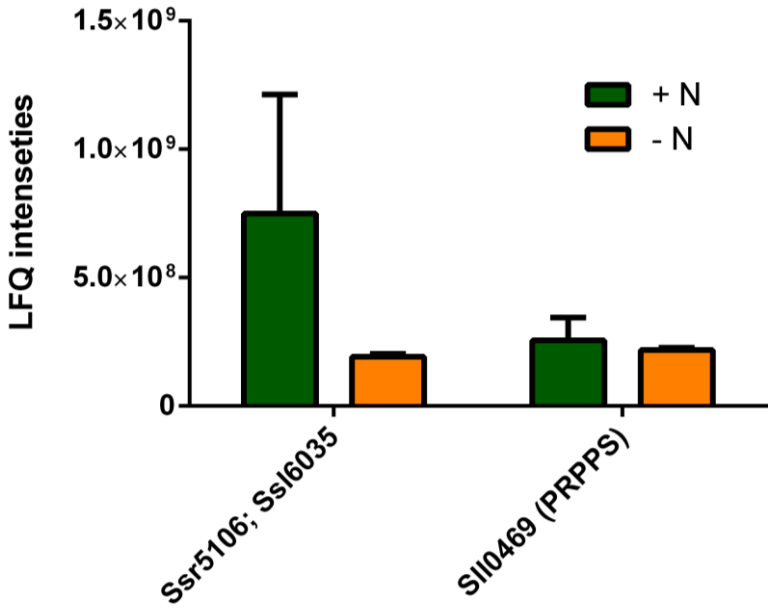

Figure 14 – Exclusively detected proteins in the α-PirC sample. Green: proteins detected in vegetative-grown cells. Orange: proteins detected in chlorotic cells (24 h nitrogen depletion).

The analysis mentioned above revealed two proteins exclusively enriched in the sample. First, the proteins Ssr5106 and Ssl6035 are encoded by similar genes but located on either pSYSM or pSYSX, the naturally occurring plasmid in Synechocystis. Both genes are located upstream of the gene encoding the partitioning protein ParA (130). The protein is four times more enriched in the vegetative-grown sample than in the nitrogen-depleted sample. Second, the Sll0469 was enriched in identical amounts in the vegetative and nitrogen-depleted samples. Sll0469 is the phosphoribosyl pyrophosphate synthase, which is crucial in nucleotide synthesis (76).

3.1.1 Measuring the potential PRPPS-PirC interaction

Osanai *et al*. 2014 (125) have shown that the PRPP content and some further intermediates are drastically reduced during the first 24 h of N-depletion. Since PRPPS was detected in the CoIP results, we assumed a role for PirC in regulating PRPPS. An inhibition of PRPPS would cause a shift in PRPP content due to lower activity. BLI measurement and enzyme assay with a purified strep-tagged PRPPS enzyme and a His-tagged PirC were conducted to investigate the relation of PirC with PRPPS (BLI not shown, Figure 15).

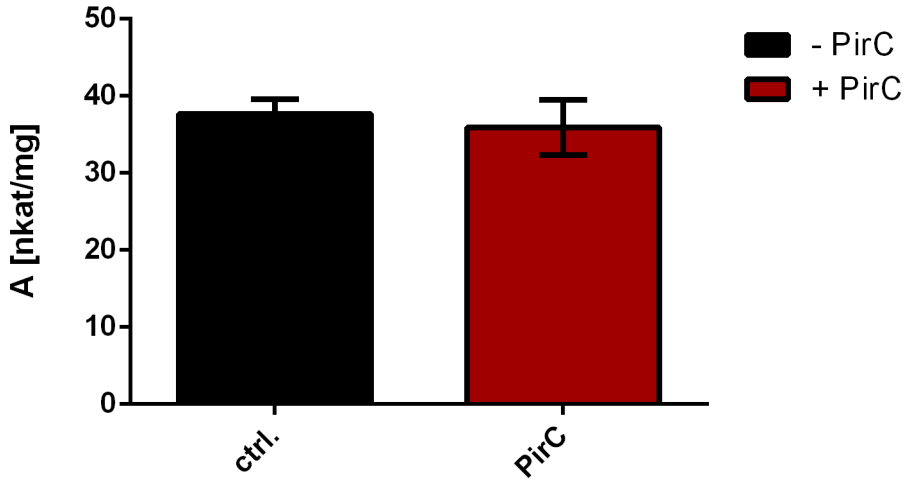

Figure 15 – PirC-PRPPS binding and activity of PRPPS. (**A**) Representavtive graph of PirC-PRPPS BLI measurement. (**B**) PGAM assay with 0.1 mM Ru5P

In the BLI measurement, the his-tagged PirC was immobilised on the surface of NTA sensors and dipped in an analyte solution of 3000 nM PRPPS. No binding between the PirC and the PRPPS with this experimental design could be detected. Also, in the enzyme assay, no influence of PirC on the PRPPS reaction could be detected (Figure 15).

3.2 Co-Immunoprecipitation using anti-iPGAM antibodies

The importance of the iPGAM in cyanobacterial chlorosis makes them another important target. To reveal further binding partners or a prevention of binding due to the loss of the loop, a CoIP was also done using an α-iPGAM antibody to use the iPGAM as a bait. The procedure was repeated as described above in section 3.1. The analysis with the WT cells is reflected in the dot plot depicted in Figure 16.

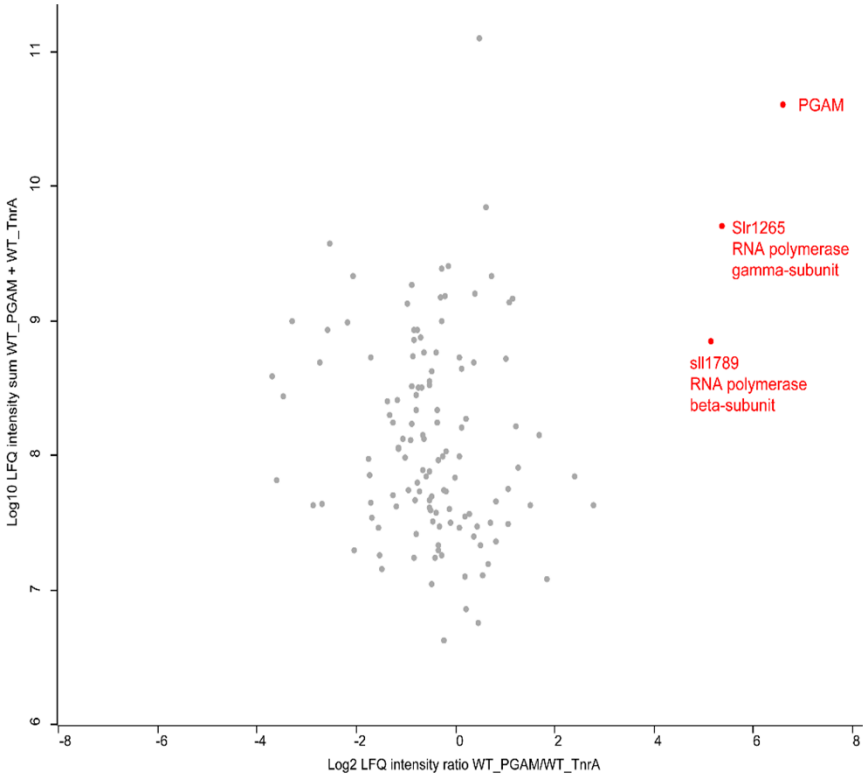

Figure 16 - Co-immunoprecipitation of vegetative-grown WT cells using α-iPGAM as a trapping molecule. Each point represents the log2 ratio of protein enrichment in the PGAM antibody sample to the control (TnrA AB) against the log10 of the total enrichment. Each point depicts the mean of independent triplicates.

In this enrichment, the products of *slr1245* and *sll1789* were found with a log2 fold of around 5. They are annotated as RNA polymerase gamma-subunit and RNA polymerase beta-subunit. Both are also annotated as DNA-directed RNA polymerase (RNAP) subunit beta' (beta prime) or *rpoC1* and *rpoC2.* These subunits are the largest subunits of the RNAP (131). In cyanobacteria and chloroplasts, the beta' is split in rpoC1 and rpoC2. Both possess parts of the catalytic site of the RNAP (132).

As expected, the iPGAM was the most abundant protein in the CoIP. The same experiment was conducted with the loop-free variant strain, resulting, in Figure 17.

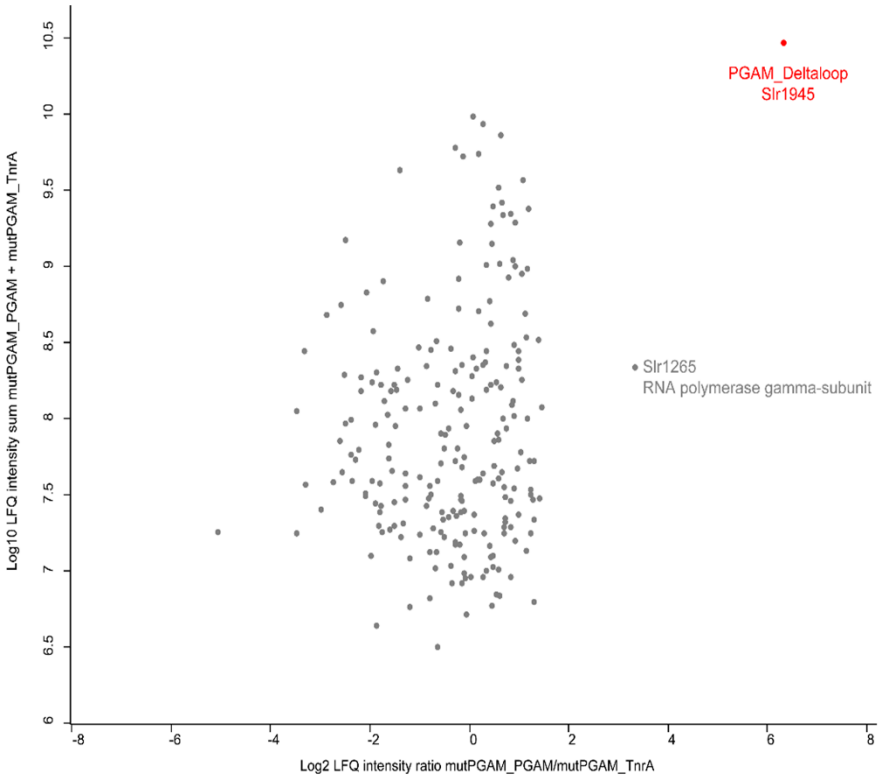

Figure 17 - Co-immunoprecipitation of vegetative-grown ΔIoop cells using α-iPGAM as a trapping molecule. Each point represents the log2 ratio of protein enrichment in the iPGAM antibody sample to the control (TnrA AB) against the log10 of the total enrichment. Each point depicts the mean of independent triplicates.

Again, the slr1265 was found in the analysis. Except for this protein, no other proteins have a higher log2 fold above 2, indicating no further interactors were found. As expected, the bait protein iPGAM was highly enriched. The experiments were repeated with nitrogen-depleted cells to detect possible differences between vegetative growth and chlorosis. The results are shown in Figure 18.

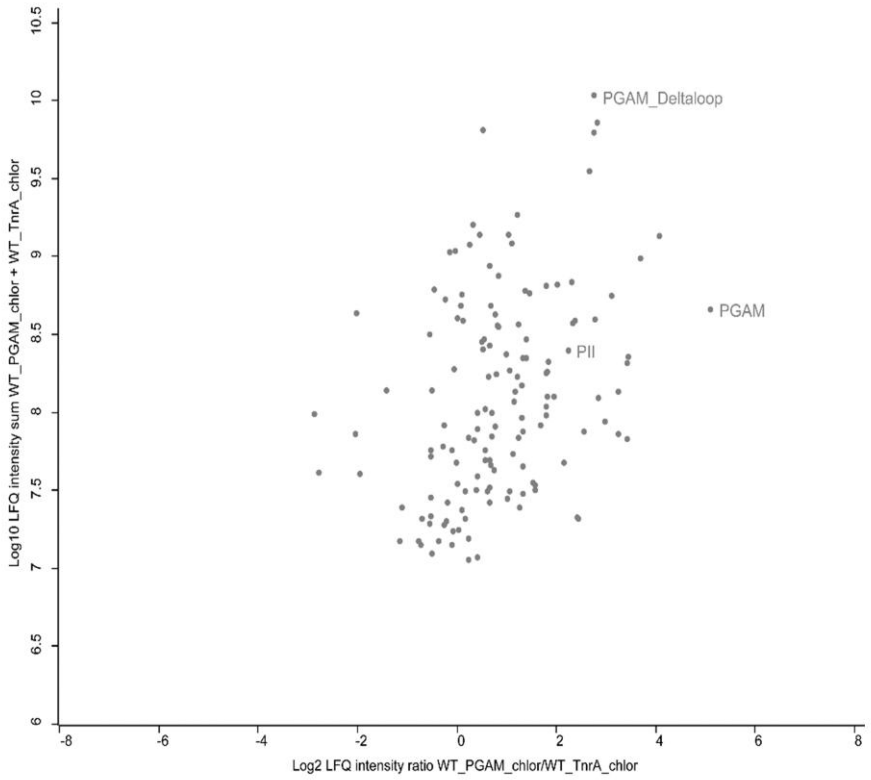

Figure 18 - Co-immunoprecipitation of n-depleted WT cells using α-iPGAM as a trapping molecule. Each point represents the log2 ratio of protein enrichment in the PirC antibody sample to the control (TnrA AB) against the log10 of the total enrichment. Each point depicts the mean of independent triplicates.

Again, the most abundant protein is the iPGAM itself. Unusually, the PGAM-∆loop appeared in the analysis. Possibly, a misanalysis of the natural iPGAM, which shares 97.5 % identity with the PGAM-∆loop. Interestingly, the RNAP subunits found under vegetative growth are not enriched with nitrogen-depleted WT cells, and no exceptional proteins are enriched in this analysis. In the last CoIP experiment, the ∆loop strain was used. The results are shown in Figure 19

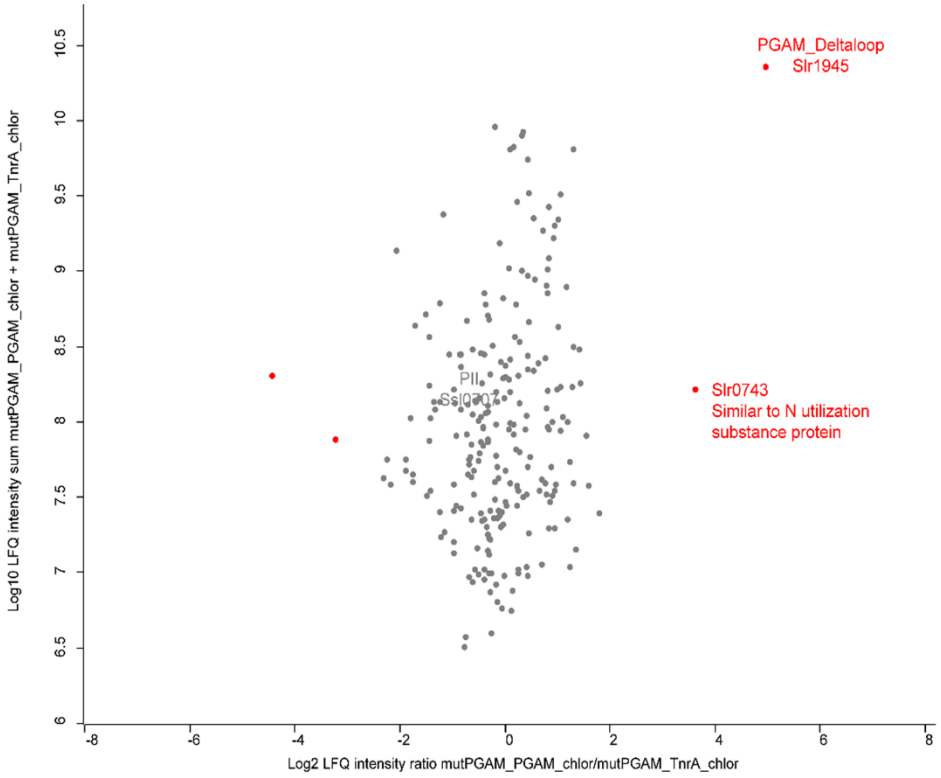

Figure 19 - Co-immunoprecipitation of n-depleted Δloop cells using α-PirC as a trapping molecule. Each point represents the log2 ratio of protein enrichment in the PirC antibody sample to the control (TnrA AB) against the log10 of the total enrichment. Each point depicts the mean of independent triplicates.

In this analysis, the iPGAM without the loop was the most detected protein in the sample. In addition, the Slr743, a NusA protein, was highly enriched. NusA is a termination/antitermination protein of the transcription. Furthermore, Cohen *et al.* 2010 (133) and Li *et al*. 2013 (134) detected chaperone function and relation to cellular DNA damage coordination (135).

4 Structure of PirC and their complexes

4.1 The structure of PirC

The three-dimensional structures help to understand the function of proteins. Experiments in the lab conducted by Jörg Scholl (136) show purified PirC elutes very early in an SEC experiment. Moreover, it elutes in a broad peak where no primary oligomerisation state is detectable. Attempts to crystalise PirC-P_{II} complexes were unsuccessful, possibly because of the described aggregation. Alphafold predictions of different oligomers (one to 12) were also unsuccessful.

4.2 The complex of PirC and P_{II}

P_{II} often binds to other trimeric structures. One popular example is the binding with the NAGK. The key enzyme in the synthesis of arginine forms a dimer of trimers, and two P_{II} trimers bind to the top and the bottom of this structure (102). Another example is the binding of the nitrogen starvation co-inducer protein PipX. The P_{II} trimer binds three individual PipX proteins. In both cases, the T-loop is strictly involved in this interaction (101). ATP or ADP enhances, and 2-OG inhibits, the binding of P_{II}. This also applies to the interaction of P_{II} and PirC. Attempts to crystalise PirC-P_{II} complexes were not successful. According to that, an AlphaFold prediction was made with the assumption of a trimer-monomer- (Figure 20) and a trimer-trimer complex (Figure 21).

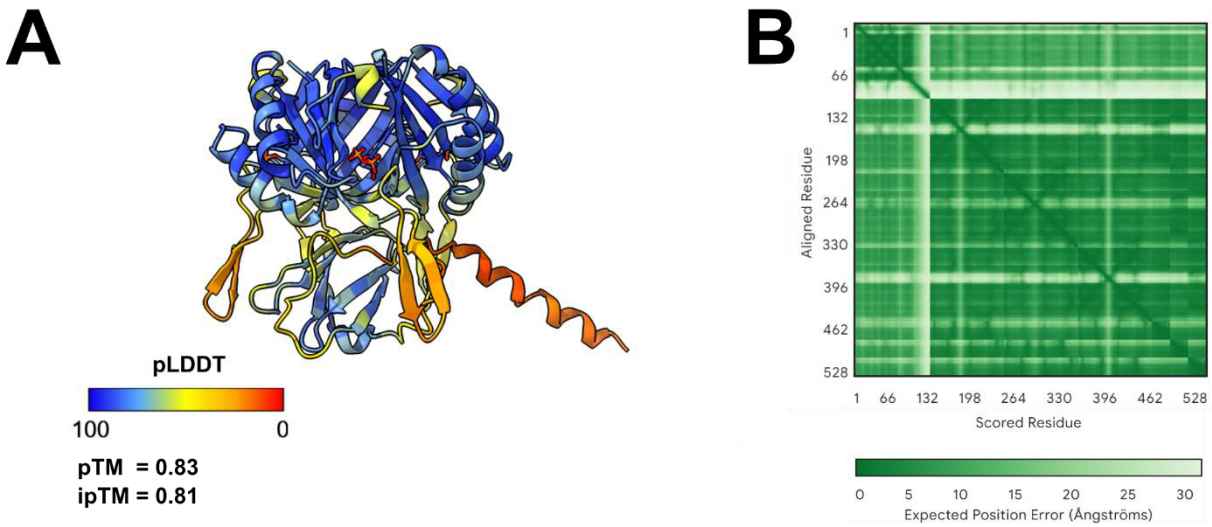

Figure 20 – Alphafold prediction of a P_{II}-PirC monomer complex. (**A**) Cartoon representation of P_{II}-PirC with pTM and iptM score. (**B**) Predicted aligned error graph of the complex.

The core structure of P_{II} was predicted with high confidence (blue colouring of the structure). The Predicted aligned error (PAE, Figure 20 B) graph also proves high

confidence in the P_{II} core structure (residues 130-528). Only the T-loop's prediction quality was lower (orange colouring), also visible as three light lines in the PAE (vertically and horizontally, residues 198, 264, 396). An overlay of the P_{II} structures of this prediction and the PipX-bonded P_{II} revealed an almost identical structure of P_{II} of *Anabaena* sp. binding to three PipX molecules (PDB:3N5B). In contrast, the PAE (from 0-116) and the pLDTT colouring indicate lower confidence in the PirC structure. The predicted β-sheet of the DUF1830 (domain of unknown function) has the highest confidence in the PirC structure. The lowest quality is at the C-terminus of PirC with a predicted α-helix. The overall prediction quality scores (pTM & ipTM) are above the good quality threshold. However, based on the recurring structural phenomenons of P_{II} binding to trimeric or three individual monomers, an alphafold prediction of a 3:3 stochiometry of P_{II} with PirC was conducted (Figure 21).

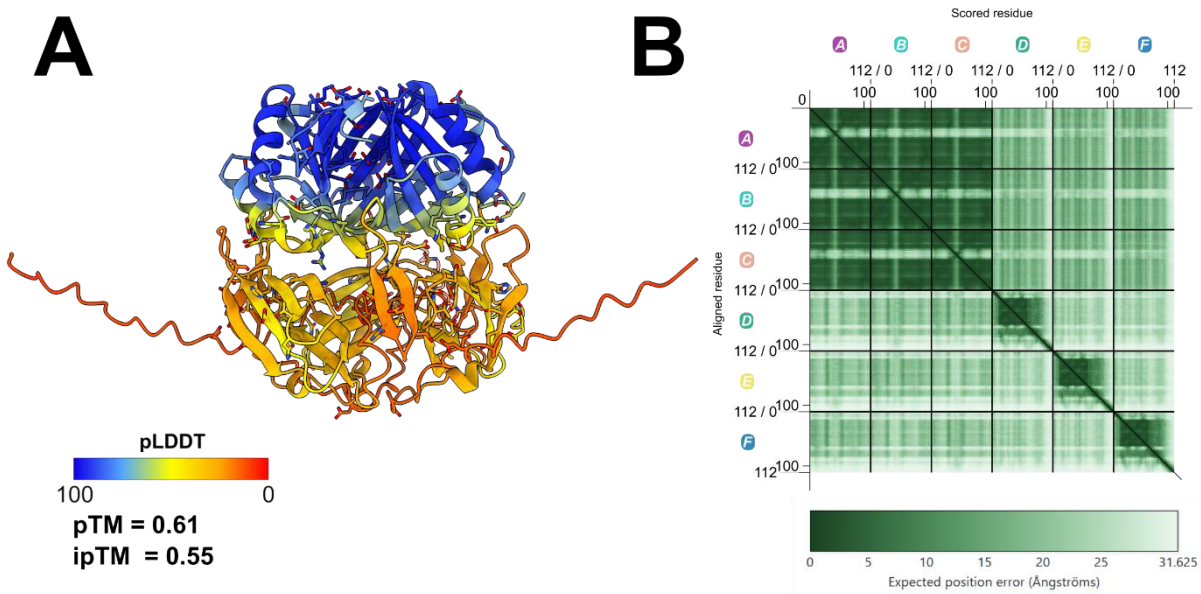

Figure 21 - Alphafold prediction of a P_{II}-PirC trimer complex. (**A**) Cartoon representation of P_{II}-PirC with pTM and ipTM score. (**B**) Predicted aligned error graph of the complex.

According to the calculated pTM and ipTM, this prediction is of lower quality than the P_{II}-PirC monomeric structure. Again, the highest confidence is calculated in the P_{II}-core structure. An overlay of P_{II} prediction with the P_{II} which binds to PipX (same as mentioned above) is similar to the prediction of P_{II} binding to one PirC. The PAE again refers to acceptable confidence in the core area of PirC, while the outer surface is less accurate. This is consistent with the structure's depicted pLDDT.

The involvement of the T-loop in the binding of PirC suggests the potential effect of PTM in the binding, such as phosphorylation of the S49. To test this, BLI

measurements were conducted with P_{II} and a variant mimicking the S49 phosphorylation (S49E). The preliminary resulting binding curves are shown in Figure 22.

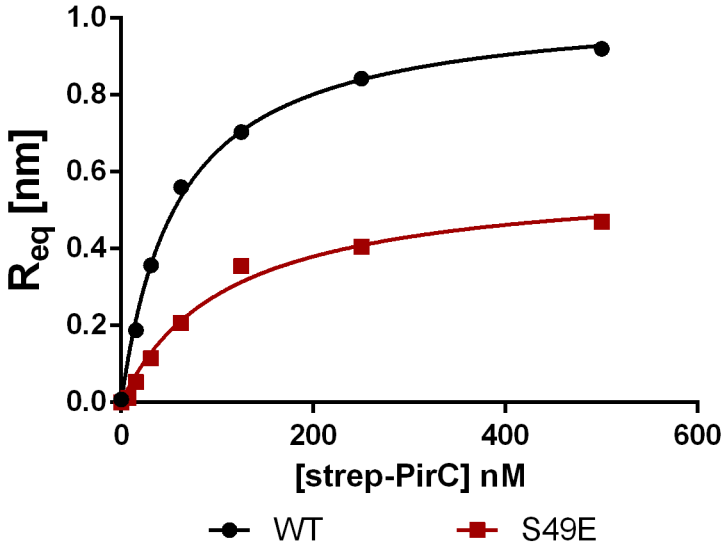

Figure 22 - Binding of P_{II} or P_{II}(S49E) with PirC in the presence of 2 mM ATP. Single measurement of P_{II} variants as bait and strep-PirC as analytes.

The variant that contains glutamate at the position of S49 has a lower binding than WT P_{II}. The maximal binding is strongly reduced, and an estimation of the K_D indicates a reduced affinity to PirC due to a low K_D.

III Material and Methods of Additional Results

1 Native Page and Western blot

The influence of P_{II}'s phosphorylation status was detected via native polyacrylamide gel electrophoresis, followed by western blot detection of P_{II} using α-P_{II} antibodies. Depending on the nutrition availability, the P_{II} trimer inside the *Synechocystis* can exist in four different phosphorylated variants, without any phosphorylation and with one, two or three phosphorylated P_{II} monomers. According to this, the P_{II} runs through an SDS-free polyacrylamide gel at different distances: the more phosphorylated monomers, the further P_{II} runs through the gel. To detect the P_{II} phosphorylation inside *Synechocystis,* the cells were cultivated under nitrogen-rich and nitrogen-poor conditions. During N-depleted conditions, the P_{II} is phosphorylated, while it is non-phosphorylated during high N availability.

2.1 Native PAGE

15 ml of a *Synechocystis* culture - cultivated in different conditions - was harvested and lysed in 250 ml lysis buffer (50 mM Tris-HCl pH 7.4, 5 mM EDTA) using glass beads and a shaking homogeniser. The soluble and the insoluble part were separated via centrifugation. The soluble crude cell extract was used for the native page. It was mixed with ultrapure water and 2x loading buffer (25 mM Tris-HCl, 50 mM potassium phosphate buffer pH 7.4, 2.5 mM $MgCl_2$, 2.5 mM DTT, 0.5 mM EDTA, 25 mM KCl, 1 mM benzamidine hydrochloride and 8 mg · ml^{-1} BSA) to a protein concentration of 10 µg/15 µl. This mixture was then loaded on an SDS-free polyacrylamide gel (Stacking gel: 5 % polyacrylamide, 125 mM Tris-HCl pH 6.8, 0.15 % NP-40, 1 % APS, 0.1 % TEMED; resolving Gel: 8 % polyacrylamide, 125 mM Tris-HCl pH 8.8, 0.15 % NP-40, 1 % APS, 0.1 % TEMED). The electrophoresis was then performed at a constant current of 30 mA and a maximum of 200 V until the dye front reached the bottom of the gel.

2.2 Western Blot

The separated proteins inside the gels were then blotted on a PVDF membrane with a semi-dry western blot. The native PAG was placed on an activated PVDF membrane (soaking in 100 % methanol for 30 sec) and assembled through two filter paper layers above and below the gel membrane sandwich. The blotting

sandwich was placed on the anode and covered with the cathode. The proteins were transferred for 30 min at a constant voltage of 30 V.

2.3 Immunodetection

The membrane was incubated with anti-P_{II} (α-P_{II}) antibodies to visualise fixed P_{II}. First, to block free protein binding capacities, the membrane was incubated for 16 h with blocking buffer (50 mM Tris/HCl pH 7.4, 150 mM NaCl, 1 % (v/v) Tween20, 5 % no-fat milk powder). The excess blocking buffer was removed by three-time membrane-washing with 5 ml washing buffer (Tris/HCl pH 7.4, 150 mM NaCl, 1 % (v/v) Tween20). The membrane was then incubated with the specific antibody α-P_{II}. Here, the antiserum was diluted $\frac{1}{2500}$ in 5ml dilution buffer (Tris/HCl pH 7.4, 150 mM NaCl, 0.1 % (v/v) Tween20) and added to the membrane. After 2 hours of incubation, the membrane was washed again three times. To visualise bound α-P_{II}, the membrane was incubated for 1 h with a dilution buffer containing the detection antibody in a $\frac{1}{5000}$ dilution. The detection antibody is coupled to a horseradish peroxidase. After a third washing step, the membrane was developed with the BM Chemilumineszenz-Western-Blot-Substrat (POD) of Roche (Basel, Switzerland) according to the manufacturer's protocol.

2 Co-immunoprecipitation using target-specific antibodies

Another co-immunoprecipitation experiment was conducted to determine other binding proteins of PirC or PGAM. In this case, specific antibodies (AB) against the PirC protein and the PGAM were used as bait.

2.1 Sampling of vegetative and N-depleted cultures

Synechocystis sp. PCC 6803 was inoculated in 1000 mL batch cultures at OD_{750}=0.2 and propagated at 28 °C and 40 µmol photons m^{-2} s^{-1} in BG_{11} medium, supplemented with 5 mM $NaHCO_3$ and 5 mM HEPES. Cultures were stirred at 120 rpm and bubbled with ambient air. Samples (400 ml at vegetative nitrate conditions) were taken at OD_{750}=0.6, and subsequently, the remaining culture was shifted to a nitrogen depletion medium. After 6 h incubation, a further 600 mL sample was taken. Cells were pelleted by centrifugation with 5000 x g for 10 min. The supernatant was discarded, and the cell pellet was suspended in 2 mL of a detergent-free lysis buffer (100 mM TRIS (pH 7.5), 100 mM KCl, 1 mM $MgCl_2$, 1 mM DTT, 0.5 mM EDTA, and additionally for N-depleted samples with 2 mM ATP

and 2-OG) and transferred into a two 1.5 mL sealed screw cap tube. Glass beads with a diameter of 0.1 mm were added and cells were disrupted with a FastPrep®-24 Ribolyser with the following settings: five cycles with 6.5 $m*s^{-1}$ for of 30 sec; each cycle followed by a 5 min break; constantly at 4 °C. The samples were centrifuged with 16.000 x g for 5 min at 4 °C to pellet cell debris. The clear cell extract was carefully transferred into a fresh 1.5 mL tube at 4 °C. Protein concentrations in crude protein extracts were quantified by Bradford assay.

2.2 Immunoprecipitation

For antibody binding of the PirC- (α-PirC), iPGAM-specific (α-iPGAM), and control pull-down (TnrA), each 150 µL of a well-resuspended Protein G magnetic beads slurry was aliquoted, washed twice with 1 ml of the lysis buffer and subsequently incubated for 15 min at RT under agitation on an orbital shaker with 15 µL of either the *Synechocystis* antisera (produced in rabbit) or an unspecific *B. subtilis* TnrA antiserum (produced in rabbit). Coupled beads were rewashed and incubated with 2 mg crude protein extract at previous coupling conditions. After three washing steps, protein elution was performed in two consecutive steps, with each 60 µL of a 200 mM glycine buffer at pH 2.5. Eluate fractions were combined and stored at - 80 °C.

Sample preparation

Samples were lyophilised and resuspended in 100 µL denaturation buffer. The sample pH was adjusted to 8 by adding 12 µL 1M Tris/base (pH 11). The sample was reduced and alkylated by adding 1 mM DTT and 5.5 mM IAA and incubation for at least 60 min at RT in the dark while shaking. To pre-digest the proteins, 50 µL of the sample was incubated with 0.5 µg Lys-C for 3 h at RT shaking. The pre-digest mixture was then diluted with 200 µl 20 mM ABC buffer (pH 8.0) and 0.5 µg trypsin was added. This mixture was incubated overnight at RT while shaking. After the incubation, 10 % (v/v) TFA was added to adjust the pH to 2.5. Ultimately, 100 µl of the digested protein mixture was cleaned via **st**op-**a**nd-**g**o **e**xtraction (STAGE) using C18-clean-up tips.

2.3 LC-MS measurement

The measurement of the peptides was conducted as described in publication 1.

3 Biolayer interferometry using Octet K2

All additional BLI measurements were conducted as described in publication 2.

4 Phosphoribosyl pyrophosphate synthase assay

An enzymatic assay was performed to test if the PRPPS is a target of PirC. Here, the assay was prepared as described in the protocol provided by Sigma Aldrich (https://www.sigmaaldrich.com/deepweb/assets/sigmaaldrich/marketing/global/documents/165/895/phosphoribpyrosyn.pdf, last access: 24/07/10). This protocol is based on and used by Gudas *et al.* 1978 (137). For measuring the activity of the PRPPS of T-lymphoma cells of mice. The conversion of ribose 5-phosphate with ATP to Phosphoribosyl pyrophosphate and AMP is coupled to myokinase, pyruvate kinase (PK), and lactate dehydrogenase (LDH) reactions. The myokinase produces two ADP molecules from AMP and ATP. The releasing ADP is then coupled to the PK reaction to produce pyruvate, which is then reduced with NADH to lactate by LDH. The decreasing NADH concentration was measured spectrophotometrically at λ = 340 nm. The assay was conducted at 30 °C, and the volume was reduced to 250 µl. All assays were done on a 96-well plate and measured in a Biotek Epoch 2 plate reader (Agilent, Santa Clara, USA). To test the effect of PirC, 400 nM of a strep-tagged PirC was added to the assay mixture.

5 Protein structure prediction via AlphaFold

Some protein structure predictions were performed to get structural information on PirC and its complex with P_{II}. In 2020, Jumper et al. Published in Nature is a novel, outstanding protein structure prediction algorithm called AlphaFold. AlphaFold is an artificial intelligence (AI)-based neural network that predicts protein structure based only on the amino acid sequence close to experimental accuracy (136). In 2023, DeepMind published a newer version (AlphaFold3) capable of predicting multimeric complexes and some ligands, shown in Table 1 (137). AlphaFold3 can be used at alphafoldserver.com.

Table 1 – List of predictable ligands in AlphaFold3.

Type of ligands	Molecules possible
Nucleic acids	DNA, RNA
Ions	Ca^{2+}, Cl^{-}, Co^{2+}, Cu^{2+}, Fe^{3+}, K^{+}, Mg^{2+}, Mn^{2+}, Na^{+}, Zn^{2+}
Molecules	AMP, ADP, ATP, GDP, GTP, FAD, NAD, NADP, NADPH, Heme, Heme C, Palmitic acid, oleic acid, myristic acid, citric acid, chlorophyll A, chlorophyll B, bacteriochlorophyll A, bacteriochlorophyll B

Quality assessment of predictions

The accuracy of the AlphaFold predictions can be divided into three confidence metrics.

1. The **pLDTT** (predicted Local Distance Difference Test) is a scale ranging from zero to 100 and derived from LDDT, which is a superposition-free score that evaluates the local distance differences of all atoms in a modelled polymer (138). Values above 80 indicate high confidence, while values below 50 indicate low confidence (139).
2. The **PAE** (Predicted aligned error) graph displays the confidence of the relative positions and orientation of the prediction (140). The darker the position in the graph, the lower the expected position error.
3. The two scores derived from the template modelling (TM) score, predicted TM, and interface predicted TM (**pTM** & **ipTM**) measure the protein's overall accuracy (141, 142). pTM values above 0.5 indicate a good prediction of the structure. ipTM values above 0.8 represent a good prediction of a complex. Predictions with values below 0.6 are failed predictions. Values between 0.6 – 0.8 refer to predictions that can be true.

IV Discussion

1 Physiological function of PirC

The variety of pathways in cyanobacteria, all dependent on the fixation of CO_2, are strictly regulated to maintain the optimal proportion of cellular structures, enzymes, nucleic acids and metabolic intermediates. In natural habitats, cyanobacteria must cope with several stresses, such as oxygenic toxification and energy- and nutrition limitations. Due to approximately three billion years of existence, cyanobacteria evolved sophisticated mechanisms to overcome many stressful situations. One of the most important mechanisms is the regulatory network based on the nitrogen regulatory protein P_{II}. In times of well-balanced nutrient availability, P_{II} ensures the optimal distribution of carbon- and nitrogen via activation of PepC and attenuation of ACCase. In nitrogen limitation, P_{II}'s regulation of these metabolic key points is terminated. P_{II} activates the nitrogen acclimation genes via the release of PipX, which further activates the nitrogen regulator transcription factor NtcA (118). In diazotrophs, NtcA then activates the genes that prepare the cells for the fixation of atmospheric nitrogen, whereas, in non-diazotrophs, chlorosis is initiated. A crucial component in the differentiation to this dormant state is the accurate distribution of newly fixed carbon. In the chlorosis process, newly fixed CO_2 is initially stored in glycogen. The subsequent slow degradation of the glycogen during prolonged chlorosis is also regulated. This work detected the Sll0944 protein, which we named PirC, as part of the P_{II} regulatory network with a critical role in the direction of carbon flux during nitrogen depletion. As with many other P_{II} interactors, the PirC is bound in T-loop dependence, as proven by binding experiments with the typical binding partners of P_{II}, ADP, ATP, and 2-OG. In the presence of ADP or ATP, P_{II} binds to PirC with a similar affinity to PipX (143). 2-OG prevents 50 % of the binding of PirC in concentrations close to the K_D of the third 2-OG binding site in P_{II} (144) (Publication 1, Figure 1). This referred to an involvement in nitrogen-induced chlorosis. Experiments with a strain lacking the expression of PirC (ΔPirC) also revealed a lack of glycogen synthesis. Furthermore, the degradation of glycogen drastically increased, and the PHB levels reached double as high as in the WT after 35 days of chlorosis (Publication 1, Figure 2). The detection of iPGAM (Slr1945) as an active binding partner, which PirC inhibits, declared its effect on physiology (Publication 1, Figure 3). The iPGAM connects the upper and lower glycolytic routes, converting 3-PGA to 2-PGA. The iPGAM content in *Synechocystis* corresponds only to 10 % of the other important

mutase in carbon metabolism, Pgm1 (Sll0726) (compared via cyanoatlas (145)). This indicates the iPGAM requires strong and strict regulation. The strong binding of PirC by P_{II} in the presence of the energy sensor molecules keeps the iPGAM in a non-inhibited state during high access to carbon and nitrogen. This guarantees a balanced distribution of newly fixed carbon to the synthesis of amino acids via the Krebs cycle and feeding the CBB with 3-PGA. In turn, the vast dissociation of PirC from $P_{II,}$ even with the small quantities of 2-OG, permits a rapid inhibition of the iPGAM. Truly, this switches the direction of carbon backward to carbon storage during chlorosis. This hypothesised regulation was underpinned by the detection of metabolites during chlorosis of WT and Δ*pirC* (Publication 1, Fig. 4). The Δ*pirC* accumulated pyruvate, a stable downstream intermediate of the iPGAM reaction, in concentrations 14-fold higher than in the WT after 48 hours of nitrogen depletion. Pyruvate is the intermediate directly converted to acetyl-CoA, which serves as a precursor of PHB synthesis. This increases the formation of PHB. Not only did the PHB content rise in Δ*pirC*, but additionally, the levels of citrate/isocitrate were approximately 30 % higher than in the WT. Also, malate levels reached higher levels in Δ*pirC.* Furthermore, 2-OG levels decreased in the WT after the initial increase caused the absence of ammonia. Conversely, the 2-OG levels stayed the same in the PirC deletion mutant. This is another proof of the disturbed flux of carbon during the absence of PirC. At the same time, the WT, where the iPGAM is regularly inhibited by PirC, showed a two-times elevated 3-PGA concentration to the Δ*pirC*. 3-PGA serves as a potent allosteric activator of GlgC, the enzyme that catalyses the initial step of glycogen synthesis. In *Synechocystis*, GlgC is activated by 3-PGA to a remarkable extent of 1630 % (146). As a result, the slightest increase in 3-PGA content activates the GlgC reaction. While the 3-PGA dropped in Δ*pirC,* glycogen synthesis also stalled due to the less activated glgC by 3-PGA. Based on these results, a model of how PirC regulates carbon metabolism is proposed (Figure 23). PirC extends the P_{II} regulatory network significantly. It evidences a direct influence of P_{II} in the regulation of carbon metabolism, especially during nitrogen starvation. During sufficient nutritional availability, when ADP or ATP levels are high and 2-OG levels are low, P_{II} ensures a balanced distribution of freshly incorporated CO_2 by binding to the iPGAM inhibitor PirC. Besides the regeneration of 3-PGA in the PPP to RuBP, iPGAM converts significant amounts of 3-PGA to 2-PGA. This is further directed into the lower glycolysis, feeding the Krebs cycle to generate precursors for other biosynthesis. When nitrogen levels decrease, 2-

OG levels increase. P_{II} releases the PirC that inhibits the iPGAM. As a result, 3-PGA levels slightly accumulate and activate GlgC. Thereby, glycogen is synthesised in high amounts. During long-term chlorosis, PirC still reduces the iPGAM, thereby balancing the glycogen degradation. This keeps sufficient energy levels needed for the residual metabolism in the dormant state of chlorosis (147).

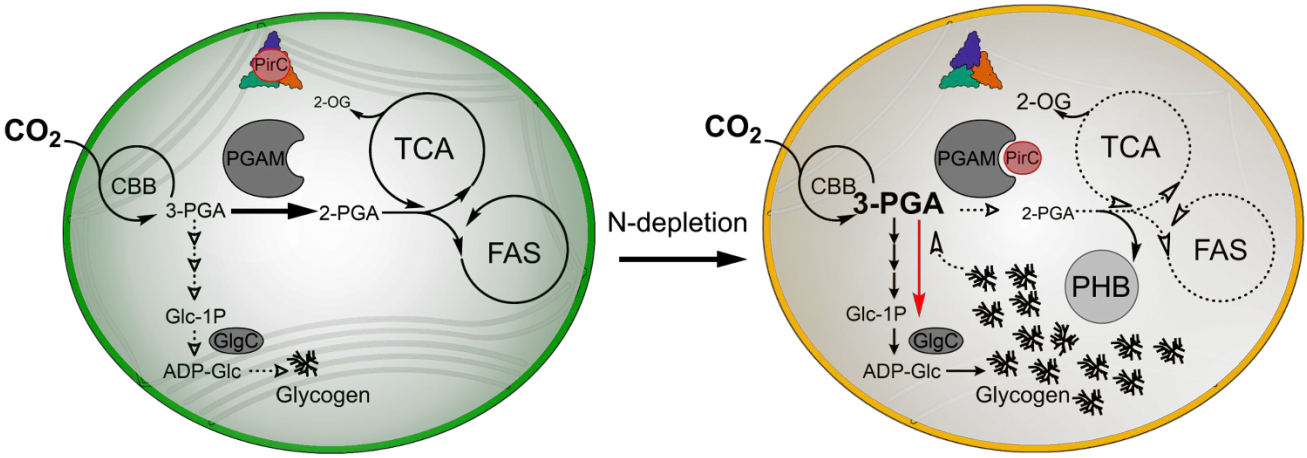

Figure 23 – Model of how PirC regulates the carbon metabolism in the switch between vegetative growth and nitrogen-induced chlorosis. P_{II} binds PirC in dependence on ATP and ADP. 2-OG levels are low.

The reported results still leave questions unanswered. The Δ*pirC*, with the lack of initial doubling, has an additional disadvantage in chlorosis. The abolished iPGAM inhibition and the accompanying lack of synthesising glycogen cannot answer this open question. Also, the increased levels of PHB cannot declare the missing division at the beginning of adaptation. In Publication 3, it is shown that elevated PHB concentration does not necessarily lead to a lack in the initial doubling during chlorosis. It is assumed that PirC interacts with further proteins, leading to division. A good candidate would have been the PRPPS, exclusively detected in the CoIP with α-PirC antibodies as bait in the sample. PRPPS is the entry point of R5P into the synthesis of nucleotides, especially of purines. A pyrophosphate moiety of ATP is transferred onto the C1 of R5P, forming PRPP. Without regulation of this synthesis during chlorosis, nucleotides like ATP, $NAD(P)^+$ and other building blocks of the nucleic acids would overflow and influence the physiology negatively. Osanai *et al.* 2014 detected a drop in PRPP levels in one day of nitrogen depletion down to one-tenth compared to the non-starved cells (125). An inhibition of PRPPS by PirC could cause a harsh decrease in PRPP levels. The BLI measurement showed no interaction between PirC and PRPPS with the performed experimental design. As well, the

PirC did not affect the enzymatic activity of PRPPS. Due to the results, the mechanism which allows the doubling at the beginning of the chlorosis is still elusive.

Publication 1 and Koch et al. 2020 revealed a supporting effect on the PHB synthesis when the cells are cultivated in a day/night regime. Since PHB is only produced during chlorosis, this effect is assumed to depend on glycogen synthesis. A transcriptomic analysis of the important glycogen genes in *Synechocystis*, *glgA1*, *glgC*, and *glgP2*, as well as the *pirC* and *glnB*, confirmed diurnal relations (Figure 24).

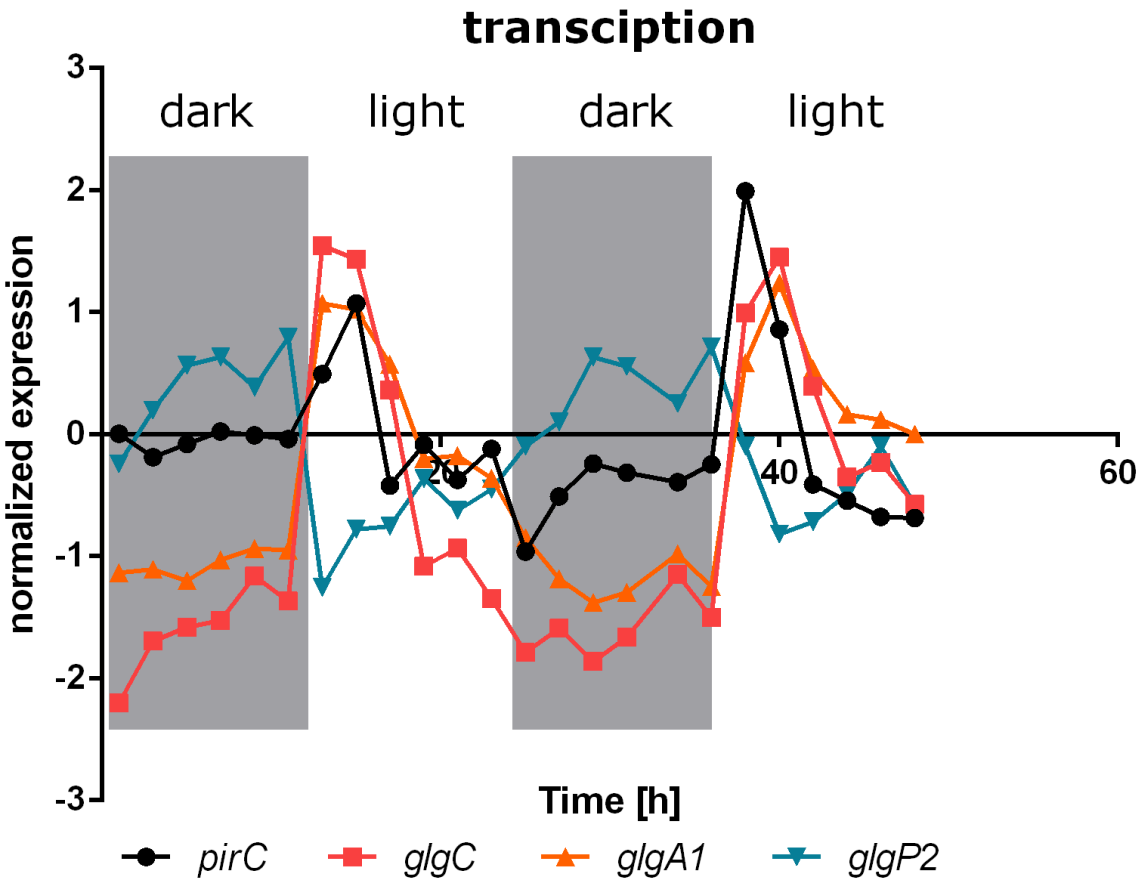

Figure 24 – Transcription of PirC, GlgA1, GlgC and GlgP2 during diurnal growth. Data derived from Saha et al. 2016 (148). Two days, starting with a 12-hour dark phase, are shown in a day/night regime. Grey background: dark phase; white background: light phase

Synechocystis produces glycogen in day phases to prepare for energy generation via glycogen degradation at night (57). In agreement, the anabolic genes *glgC* & *glgA1* are upregulated in light phases, and the catabolic gene *glgP2* is upregulated within the dark phase. Simultaneously, the *pirC* is upregulated, matching with the anabolic enzymes and indicating a regulating function of PirC in daily growth. PirC

inhibits the iPGAM and directs the flux into carbon storage. The rising P_{II} levels moderate the inhibition to prevent an imbalance of metabolites. This iPGAM inhibition also promotes the regeneration of RuBP through 3-PGA. Furthermore, this effect also supports glycogen formation during chlorosis. As shown in the Δ*pirC*, the loss of PirC leads to further enhanced glycogen degradation, resulting in higher PHB levels. The suggested mechanism is based on assumptions and poorly significant databases and has to be tested experimentally.

The results of this work, mainly of Publication 1, revealed potentially only one part of the physiological function of PirC. However, there is evidence of further interaction partners of PirC. CoIP experiments did not deliver the appropriate results for PirC's further binding partners. Proximity labelling with PirC fused to a promiscuous biotin ligase, as described by Banon *et al.* 2018, could reveal potential PirC binding partners. Banon *et al.* 2018 developed TurboID or miniTurbo via directed evolution, which ensures a rapid and easy-to-use proximity labelling assay (149). Proteins that interact with the PirC fusion protein get biotinylated. The biotinylated protein can then be immobilised with streptavidin beads and analysed via MS, similar to the procedure described in the "2 Co-immunoprecipitation using target-specific antibodies" section.

The role of PirC in other types of cyanobacteria

Obviously, PirC contributes to other nitrogen adaptation mechanisms due to its existence in cyanobacteria of all sections. In A. variabilis, PirC could be a key player in the heterocyst formation. In heterocysts, exopolysaccharides are needed to protect the oxygen-sensitive nitrogenase from oxygen. The inhibition of iPGAM of A. variabilis could promote this synthesis. In the unicellular nitrogen assimilating C. aeroginosa, the regulation by PirC could contribute to the nitrogen fixation. Here, glycogen is essential to produce the energy for the nitrogenase reaction at night (86). No experiments regarding PirC regulation were ever conducted with another organism. These speculations have low informative value. Answering these questions is an exciting topic for future investigations.

2 Molecular regulation of iPGAM

Phosphoglycerate mutase (PGAM) enzymes are important in all living organisms. It connects the upper and lower part of the glycolytic metabolism by converting 3-PGA into 2-PGA and vice versa. There are two different types of PGAMs in terms of their catalysing mechanism. Vertebrates primarily contain the 2,3-bisphosphoglycerate-dependent PGAM (dPGAM), which essentially requires the phosphorylation of a particular histidine residue by 2,3-bisphosphoglycerate to perform the catalysis (150). Other than that, most bacteria contain a co-factor-independent PGAM (iPGAM). Here, the interconversion is catalysed via the phosphorylation of a unique serine residue by 3- or 2-PGA, forming a phosphate-free intermediate and retransfer the phosphate onto the glycerate basis. For the reaction, manganese plays an essential role in the coordination of the phosphoglycerate. Therefore, the reaction is very pH sensitive. In the genus of *Bacillota* (*Firmicutes*), this effect is used to regulate the iPGAM during spore differentiation. During the differentiation, the pH increases, and the iPGAM is inhibited. Consequently, 3-PGA accumulates up to 0.3 % of the cell dry weight, preparing the bacteria for a rapid germination (151).

Other than this, the iPGAM of cyanobacteria is regulated via protein-protein interaction with PirC, as shown previously. The PirC exclusively appears in cyanobacteria and contains a conserved core annotated as domain of unknown function 1830 (DUF1830). In all cases, the DUF1830 is predicted as an intertwined structure of three β-sheet, with AlphaFold (https://alphafold.ebi.ac.uk/). The exclusivity of PirC in cyanobacteria and its ability to interact with the iPGAM indicates the potential for specialities in cyanobacterial iPGAM. Phylogenetic analysis showed that the cyanobacterial- and algae split very early from the other iPGAMs in evolution (Publication 3, Figure 1). In comparison, chlorotic iPGAM of higher plants deviate strongly from the cyanobacterial iPGAM. Furthermore, MSA with hundreds of iPGAM sequences and a structure prediction with *Synechocystis* iPGAM revealed unique cyanobacterial elements in the iPGAM. An internal loop structure and an extended C-terminus (Publication 3, Figure 2). The start of the phylogenetic tree seems to be the point of endosymbiotic engulfment of cyanobacteria. From there, the different conditions lead to a different evolution of iPGAMs. Whereas the future chloroplast obtained a novel genetic spectrum for regulating iPGAMs through the plant genome, cyanobacteria only depend on its genetic material. For instance, adaptation to nitrogen deficiency is not required for the chloroplast because

the mechanisms of the surrounding plant take over this task. Endosymbiotic cyanobacteria possibly also possessed the iPGAM harbouring the loop and the extended CT, but they were exchanged with the cytosolic or mitochondrial iPGAM of the plant ancestor. The gene responsible for the resulting outdated PirC was removed. On the other hand, red algae retained more regulatory mechanisms of the engulfed cyanobacteria, and the evolution splits from cyanobacteria later and with a slightly different mechanism.. MSA showed remaining sequence identities of algae iPGAM with the cyanobacterial ones, but they also lost the PirC over time. The phylogenetic tree of iPGAM clearly distinguishes between α-cyanobacteria and β-cyanobacteria. The classification into α-cyanobacteria and β-cyanobacteria is based on the containing carboxysomes. The α-cyanobacteria contain α-carboxysomes, which include the A1 type RuBisCO, whereas β-carboxysomes contain a RuBisCO of the 1B type. Also, they have distinct organisation in gene regulation, assembling and composition (152, 153). Nevertheless, both groups possess an iPGAM containing the loop and C-Terminus. The surprisingly close phylogenetic relation between iPGAM and carboxysomes may suggest a functional relation since the product released from RuBisCO is the substrate of iPGAM.

The AlphaFold- and a SWISS-MODEL prediction of the iPGAM of *Synechocystis* mainly showed the typical structure of iPGAM, described for many other iPGAMs. It consists of two domains with different functions in the iPGAM reaction. First, the phosphatase domain for the dephosphorylation of the substrate and second, the phosphotransferase domain for the rephosphorylation at the new position. The domains are separated by a cleft. The binding of the substrate induces a flipping of the enzyme, resulting in a closure of this cleft, which is essential for catalysing the reaction (154). The AlphaFold elucidated an important feature within the loop structure. The two highly conserved amino acids, glutamate 468 and lysine 473 form a hydrogen bond. The loop is directly connected to the His 457 over a ten amino acid long β-strand. His 457 is a coordinating residue, an essential required manganese ion. Intriguingly, the hydrogen bond of the two residues within the loop adopts the iPGAM in a conformation favouring manganese binding. Enzyme assays with the iPGAM variant without the loop showed a ten-fold lower affinity for manganese and a strongly reduced activity. Apparently, the loop keeps the catalytic centre in a position, which is also beneficial for performing the overall reaction. The loop also acts as a mediator of the PirC inhibition. The AlphaFold prediction of the iPGAM-PirC complex, which was empirically proved to be a 1:3 complex

of iPGAM compared to PirC, also detected a hydrogen bond between the tyrosine 39 residue of PirC and the lysine 473. This interaction disrupts the stabilising hydrogen bond of glutamate 468 and lysine 473 and changes the affinity to the substrate. The loop-free iPGAM had a disturbed K_m inhibition and mainly only a reduced maximal activity. In contrast, the extended C-Terminus has an intrinsic inhibitory effect, further enhanced by the binding of PirC. Deleting the C-Terminus in iPGAM (iPGAM-ΔCT) increased activity strongly. Furthermore, the inhibitory effect of PirC was drastically reduced, but the binding was increased. Here, ten times higher amounts of PirC are needed to reach 50 % inhibition of the enzyme. Moreover, the inhibited iPGAM-ΔCT still has a higher maximal activity than the non-inhibited iPGAM-WT. Primarily, the K_m of the substrate was changed with increased PirC levels. This C-terminal extension may decrease the v_{max} of the reaction by hindering the closure of the two domains. The binding of PirC augments the inhibitory effect on catalysis. The bending of the C-Terminus in the inhibitory position is thermodynamically adverse, resulting in impaired PirC binding. The iPGAM-ΔloopΔCT showed compensatory effects. Once again, the deletion of the C-Terminus increased the activity compared to the iPGAM-Δloop. The change also resulted in catalytic efficiency between iPGAM-Δloop and iPGAM-ΔCT. However, the C-Terminus truncation could not compensate for the Δloop decrease. One important binding site was predicted in the cleft between the iPGAM domains. A binding of PirC at this position can mediate both changes in activity. In this case, PirC is able to block the binding of the substrate, which would lead to elevated K_m. The flip into the catalytic conformation of phosphatase and transferase domain will also be disturbed if the substrate has already entered the catalytic centre. Without this ability, the v_{max} drops. The PirC binding within the cleft is possibly mainly responsible for inhibiting the iPGAM-ΔloopΔCT.

The effects on the biochemistry of the iPGAM also influence the physiology of Synechocystis. The experiments with strains containing the different iPGAM variants revealed a strong influence of the C-Terminus free variants on the PHB production within the cells in chlorosis (Publication 3, Figure 6). The strain expressing the iPGAM-ΔCT had a similar amount of PHB as the ΔpirCs previously shown as a PHBoverproducing strain. At the same time, the strain iPGAM-ΔCT produced a lot more glycogen than the ΔpirC during chlorosis. The degradation slightly increased in iPGAM-ΔCT, compared to the WT, but remained higher glycogen levels as the

ΔpirC. The final cell division at the beginning of the chlorosis was not impaired, reinforcing the idea of additional functions of PirC. It is shown that the elevated flux toward lower glycolysis, caused by the increased iPGAM activity, increases the production of PHB during the chlorosis. More precursors for the PHB synthesis are provided through higher activity, which drives the formation of PHB. This moderate fueling of the PHB synthesis is sufficient for efficient production and does not waste the precursors, which in the ΔpirC are further directed into the Krebs cycle. Potentially, this creates an accumulation of TCA intermediates, as shown in Publication 1, Figure 4. Here, the ΔpirC strain accumulated citrate/isocitrate and 2-OG levels were kept high. Additionally, the iPGAM-ΔloopΔCT strain had similar PHB levels as the iPGAM-ΔCT. Indeed, this makes no sense in the first view except if the loop or the C-terminus has promiscuous functions or other mechanisms in Synechocystis that can rapidly compensate for the disadvantages. Further investigations, including metabolic or proteomic analyses, are required for clarification.

3 PirC-P_{II} interaction

The newly discovered PirC is the first P_{II}-interacting protein, directly influencing an enzyme after dissociation from the P_{II} complex. Besides the investigation with the active PirC partner iPGAM, the investigation of the molecular interaction with P_{II} is of great importance. The elucidation of the structure of the complex of P_{II} and PirC helps to understand how ADP and ATP influence the interaction. Furthermore, it can show if the PTM of the P_{II} can further change the binding abilities of PirC. Publication 1 demonstrated very well the T-loop depending binding of PirC. In the presence of both energy mediator molecules ADP and ATP, PirC's binding is enhanced. Also, 2-OG interferes with this interaction and ensures the release of PirC. However, this measurement alone could not clarify which amino acid residues of P_{II} and PirC are involved in the binding. The T-loop of P_{II} contains a serine residue, which is phosphorylated in-vivo and fine-tunes the interaction between P_{II} and its binding partners. Since attempts to elucidate the P_{II}-PirC structure via Xray crystallography failed, several P_{II}-PirC structure predictions with different stoichiometric ratios were conducted. Until then, experiments only suggested a ratio of one P_{II} trimer with one PirC protein (136). First, a prediction of this complex was made. The prediction resulted in an accurate prediction regarding the confidence values of Alphafold predictions. The structure verified the role of the T-loop, and a grabbing-like structure was predicted. A closer look at the T-loop (via hydrogen bond and contact analysis) showed no special and constantly occurring interactions between the T-loop and the PirC protein. Only partly hydrogen bonds with the amino acid backbone were seen. P_{II} binds to multimeric protein, which fits the number of T-loops of a P_{II} trimer. Concerning this, a prediction was made with three PirC monomers. This prediction also confirmed the T-loop-dependent binding of PirC. Here, the contacts analysis shows an increased volume of contacts between the T-loop of P_{II} and PirC (Figure 25 A). Additionally, the hydrogen bonds analysis of the P_{II}-PirC interaction indicates specific interactions between the Tloop and the PirC (Figure 25). This confirms the pivotal role of the T-loop in the interaction with PirC.

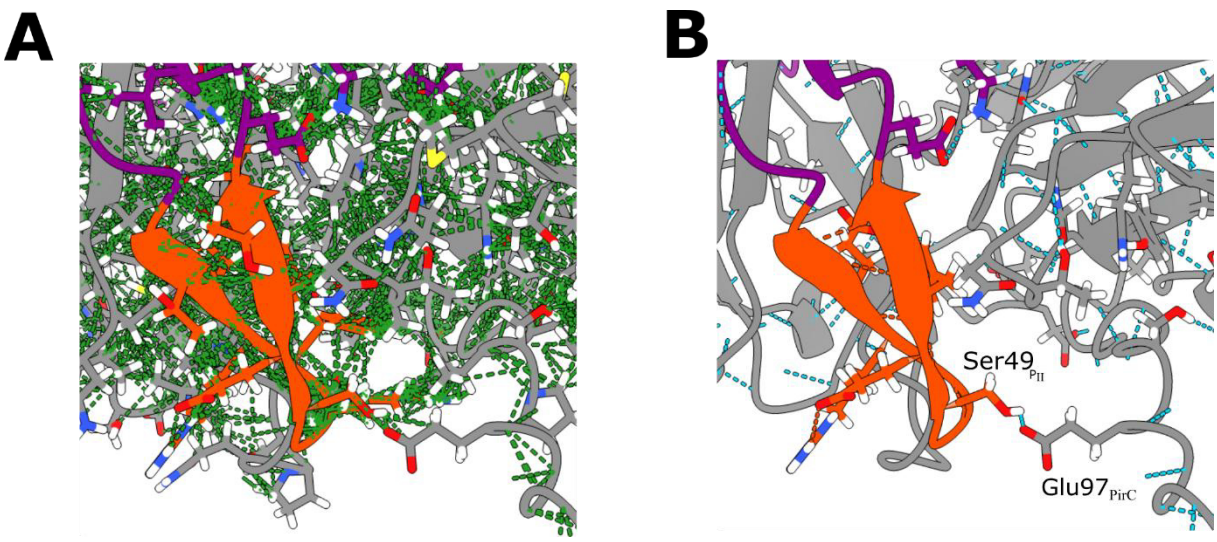

Figure 25 – Interaction of P_{II} (Purple; T-loop: orange) with PirC (grey). (**A**) hydrogen bond between P_{II}'s S49 and the E97 of PirC. (**B**) Contacts of P_{II} and PirC. Contacts: green; Hydrogen bond: cyan. Analysed and created with ChimeraX 1.8 and illustrated with Inkscape 1.3.

Interestingly, the hydrogen of the OH group of the specific serine 49 residue, where P_{II} can be phosphorylated, forms a hydrogen bond with the oxygen of the glutamate 97 of PirC. This indicates a potential significance of the phosphorylation in the PirC regulation. The phosphorylation of the T-loop would decrease PirC binding, resulting in increased inhibition of iPGAM. In high ammonium availability, P_{II} is completely dephosphorylated (156) (Figure 9). At this time, the vast incorporation of ammonium is crucial for an efficient distribution of nitrogen. The non-phosphorylated P_{II} strongly binds to PirC. The iPGAM is not inhibited and directs high amounts of 3-PGA toward the Krebs cycle, where 2-OG for the ammonium incorporation is formed. P_{II} is partially phosphorylated if the Synechocystis grows in a nitrate-rich environment (106) (Figure 9). The cells must balance the energy usage between the reduction of nitrate to ammonium and its incorporation. A phosphorylated P_{II} would release some PirC, leading to a stalled influx toward lower glycolysis by inhibiting iPGAM, which preserves energy for ammonium reduction. For this, it would be interesting to know in which stoichiometry the PirC-P_{II} complex is formed and if P_{II} can bind individual PirC molecules. The preliminary binding assay of PirC binding with P_{II}(WT) or P_{II}(S49E) confirms the involvement of the S49 in the PirC binding. P_II(S49E) is a mutated variant of P_{II} where the S49 is exchanged by glutamate. Glutamate mimics a potential phosphorylation at this position.

It is shown that the phosphomimicry variant S49E has a lower binding to PirC. Both kinetic parameters are impaired with the exchange of serine to glutamate. However, further verification of the result is required.

Not only the effect of the S49 phosphorylation is an interesting modification to be tested. Furthermore, investigating other P_{II} variants could provide information for a deeper understanding of the PirC-P_{II} interaction. Variants with impaired binding capacities of ADP and ATP or 2-OG are attractive targets to test the interaction with PirC. The novelty discovered carboxylation of P_{II}, where ATP binding is inhibited in times of high CO_2, could uncover further regulation mechanisms of PirC. Suppose the carboxylation induces a decrease in PirC binding. In that case, the release of PirC will result in an inhibition of iPGAM and an elevated flux into the regeneration of Ru5P and glycogen synthesis. Nevertheless, the results already gained about PirC help expand the knowledge about the PII regulatory network and the transition in carbon metabolism between vegetative growth and the differentiation into a dormant chlorotic cell.

Extension of the regulatory network of P_{II}

PirC has a significant impact on the regulation of carbon metabolism within cyanobacteria. It switches the flux from lower glycolysis toward carbon storage during nitrogen starvation. Not only the primarily discovered function but also the secondary effects influence carbon metabolism and balance the distribution of freshly fixed CO_2 through the cell. The interaction with the P_{II} controls the impact of PirC by protein-protein interaction. This adds another component to the P_{II} regulatory network (Figure 26).

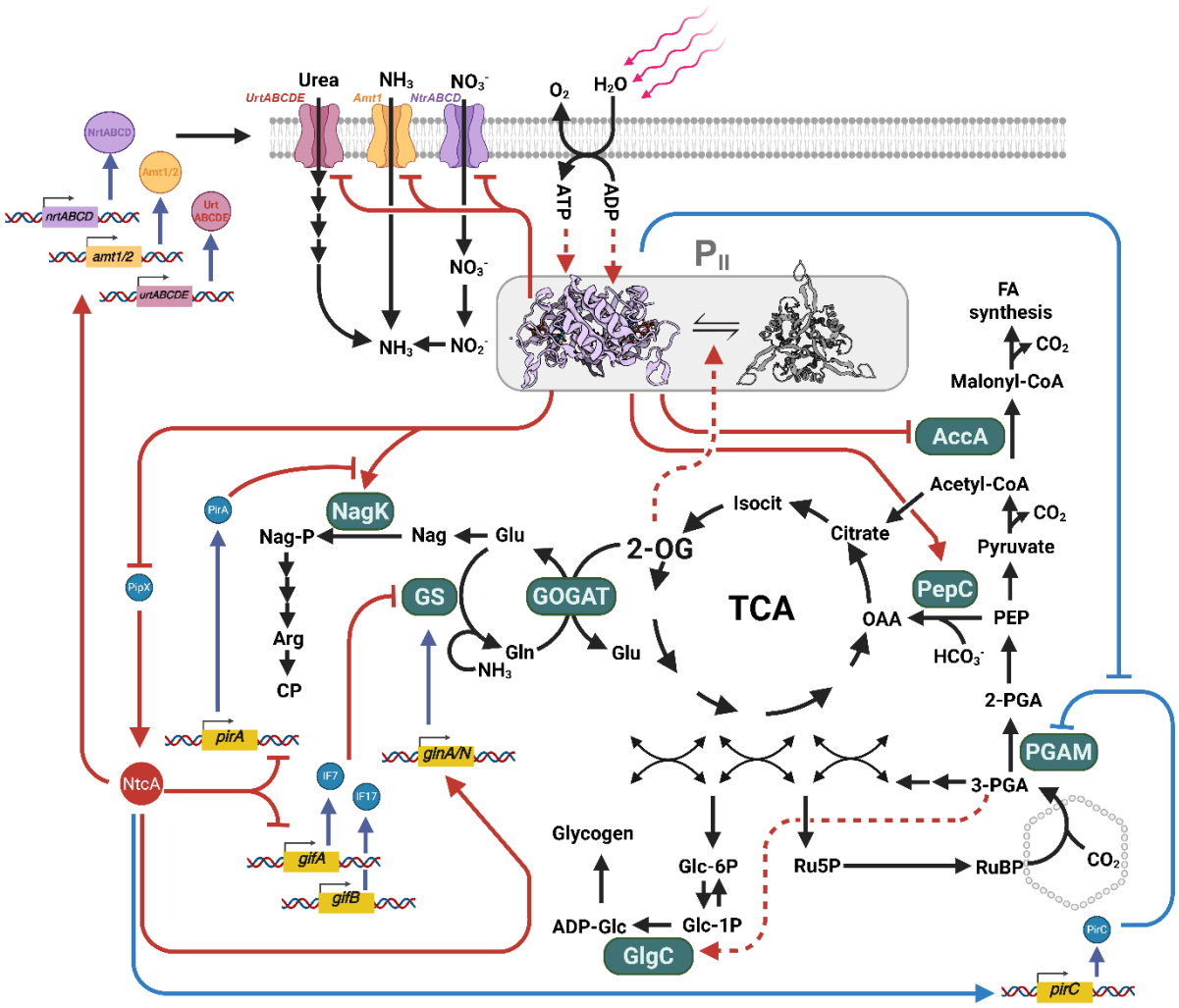

Figure 26 – Regulatory network of P_{II} in Synechocystis sp. PCC 6803 extended with the PirC interaction. PirC is moderately expressed during high ATP and ADP accompanying nutrient availability. P_{II} binds PirC and prevents its actions. In times of low availability of combined nitrogen sources, the nitrogen assimilation genes are activated by the P_{II}-PipX-NtcA cascade. Also, the expression of PirC is activated. In high 2-OG concentrations, P_{II} releases PirC, and those inactivate the iPGAM. The flux is directed toward glycogen synthesis. Arrow = activation, Flat ends = inhibition, dotted = metabolite inductions, dark blue arrows = expression, light blue – newly discovered interactions which are PirC related.

During growth in an environment with sufficient nutrient supply, P_{II} regulates the uptake of nitrogen sources by mitigating their uptake systems. Furthermore, it ensures appropriate levels of amino acid precursors by activating PepC and inhibiting the ACCase. P_{II} also stimulates arginine formation by activating NAGK. In turn, PirA prevents the activation when ammonium levels rise. Simultaneously, the PipX binding prevents NtcA activation. As a result, the GS is expressed in moderate amounts, and its inhibiting factors IF7/IF17 keep the activity balanced. Now, we also know that P_{II} regulates the distribution of fixed carbon dependent on the PirC

binding. The freshly fixed CO_2 resulting in 3-PGA is directed partially into the lower glycolysis via the iPGAM reaction. In times of high nitrate levels, when P_{II} also exists in phosphorylated states, PirC could be released and bind to iPGAM. This, in turn, preserves energy for nitrate reduction because nitrogen incorporation is lowered due to lower precursor amounts. Combined with alternating light conditions, where PirC is also expressed at higher levels, it would stimulate glycogen synthesis. The rise of 2-OG, accompanied by nitrogen depletion, results in a solid switch in P_{II} regulations. The interactions with PepC, ACCase, NAGK, and PipX have been cancelled. The latter induces the activation of NtcA. PirA and IF7/IF17 expression is inhibited. The expression of GS and the nitrogen source uptake systems is stimulated. Also, the PirC expression is elevated, and the iPGAM is inhibited. Carbon is then primarily directed toward glycogen synthesis

4 The novel *Synechocystis* strains as chassis for developing production strains.

The manipulation of the regulatory function of carbon metabolism plays a vital role in the development of biotechnologically relevant production strains. This work alters the understanding of manipulating carbon metabolism in Synechocystis to produce economically valuable products. As mentioned before, our working group creates a strain called PPT1, which can produce PHB up to approximately 60 % of its cell dry weight (80 % with acetate feeding) based on the results acquired in this work. The ΔpirC strain was improved by introducing the *phaA* and *phaB* genes of *Cupriavidus necator*. However, there are a variety of disadvantages to this strain. The strain required a long time to achieve high PHB levels. However, the biggest issue of the PPT1 is the loss of biomass when the PHB synthesis is induced by nitrogen depletion. Here, the lack of PirC causes an impaired chlorosis response with impaired final cell division. One solution to this problem would be the prevention of the interaction with the known target of PirC. This problem is solved using the iPGAM-ΔCT. With this strain, it is possible to produce the same amount of PHB in the cell without losing biomass. A strain with iPGAM-ΔCT and the phaA and phaB genes would result not only in an increase in the amount in the cell but also in the yield of PHB by 100 %. An adjustable induction of the PirC could additionally lead to a controlled glycogen turnover. Overexpressing PirC, as Muro-Pastor et al. 2020 did (155), lead to an overproduction of glycogen, which can be used to fuel the PHB synthesis in a way where the degradation of glycogen is adjusted to an ideal level for the PHB-producing enzymes. This could also result in higher PHB without

the addition of acetate. It is shown that PirC is attractive for manipulating the physiology of Synechocystis to create a biotechnological chassis for PHB production. However, still, there is a lot of work to do to achieve sufficient production rates. This also applies to research that deals with the sustainable production of metabolic-derived compounds, like succinate, lactate, or isoprenoids.

5 Conclusion

This work expands knowledge about the regulatory network of P_{II} and sheds light on the function of the novel discovered P_{II} interacting regulator of carbon metabolism. PirC orchestrates the distribution of freshly fixed CO_2 via mutual exclusive interaction with P_{II} or iPGAM. It impressively underlines the importance of P_{II} in the regulation of cyanobacterial metabolism. The results highlight the relevance of the iPGAM reaction in the physiology of cyanobacteria. The evolution of iPGAM amazingly correlates with carboxysomes, suggesting a functional relation, and demonstrates the central role of nitrogen and carbon metabolism in the evolution of cyanobacteria. Nevertheless, there are still open questions to clarify. The elucidation of the structure of PirC and its complexes with iPGAM and P_{II} is still being uncovered, and some of the structure predictions do not provide sufficient quality. Some results indicated more interaction partners for PirC, which should be investigated to complete the knowledge of PirC's function. Detailed insights have been obtained from PirC, but PirC remains an exciting topic in the study of cyanobacterial metabolism. Beyond that, it is an outstanding target for creating cyanobacterial strains that help produce chemicals for a sustainable future.

References

1. Rippka E, Deruelles J, Waterbury NB. 1979. Generic Assignments, Strain Histories and Properties of Pure Cultures of Cyanobacteria. Journal of General MicrobioZogy 111:1–61.

2. Rasmussen B, Fletcher IR, Brocks JJ, Kilburn MR. 2008. Reassessing the first appearance of eukaryotes and cyanobacteria. Nature 455:1101–1104.

3. Ikeuchi M, Tabata S. 2001. Synechocystis sp. PCC 6803 - A useful tool in the study of the genetics of cyanobacteria. Photosynth Res 70:73–83.

4. Grigorieva G, Shestakov S. 1982. Transformation in the cyanobacterium Synechocystis sp. 6803. FEMS Microbiol Lett 13:367–370.

5. Glatz A, Vass I, Los DA, Vigh L. 1999. The Synechocystis model of stress: from molecular chaperones to membranes. Plant Physiology and Biochemistry 37:1–12.

6. Wang Y, Lv X, Ji X-J, Ji B, Satta A, Esquirol L, Ebert BE. 2023. Current Metabolic Engineering Strategies for Photosynthetic Bioproduction in Cyanobacteria. Microorganisms 2023, Vol 11, Page 455 11:455.

7. Holland HD. 1999. When did the Earth's atmosphere become oxic? A Reply.

8. Jablonsky J, Papacek S, Hagemann M. 2016. Different strategies of metabolic regulation in cyanobacteria: from transcriptional to biochemical control. Sci Rep 6.

9. Zahra Z, Choo DH, Lee H, Parveen A. 2020. Cyanobacteria: Review of Current Potentials and Applications. Environments 2020, Vol 7, Page 13 7:13.

10. Renger G, Renger T. 2008. Photosystem II: The machinery of photosynthetic water splitting. Photosynthesis Research 2008 98:1 98:53–80.

11. Hervás M, Navarro JA, De La Rosa MA. 2003. Electron transfer between membrane complexes and soluble proteins in photosynthesis. Acc Chem Res 36:798–805.

12. Shevela D, Kern JF, Govindjee G, Messinger J. 2023. Solar energy conversion by photosystem II: principles and structures. Photosynthesis Research 2023 156:3 156:279–307.

13. Broser M, Gabdulkhakov A, Kern J, Guskov A, Müh F, Saenger W, Zouni A. 2010. Crystal structure of monomeric photosystem II from Thermosynechococcus elongatus at 3.6-Å resolution. Journal of Biological Chemistry 285:26255–26262.

14. Baniulis D, Yamashita E, Whitelegge JP, Zatsman AI, Hendrich MP, Hasan SS, Ryan CM, Cramer WA. 2009. Structure-function, stability, and chemical

modification of the cyanobacterial cytochrome b6f complex from Nostoc sp. PCC 7120. Journal of Biological Chemistry 284:9861–9869.

15. Inoue T, Sugawara H, Hamanaka S, Tsukui H, Suzuki E, Kohzuma T, Kai Y. 1999. Crystal structure determinations of oxidized and reduced plastocyanin from the cyanobacterium Synechococcus sp. PCC 7942. Biochemistry 38:6063–6069.

16. Jordan P, Fromme P, Witt HT, Klukas O, Saenger W, Krauß N. 2001. Three-dimensional structure of cyanobaoterial photosystem I at 2.5 Å resolution. Nature 411:909–917.

17. Morales R, Kachalova G, Vellieux F, Charon MH, Frey M. 2000. Crystallographic studies of the interaction between the ferredoxin-NADP+ reductase and ferredoxin from the cyanobacterium Anabaena: Looking for the elusive ferredoxin molecule. Acta Crystallogr D Biol Crystallogr 56:1408–1412.

18. Stadnichuk IN, Tropin I V. 2017. Phycobiliproteins: Structure, functions and biotechnological applications. Appl Biochem Microbiol 53:1–10.

19. Stadnichuk IN. 1995. Phycobiliproteins: Determination of chromophore composition and content. Phytochemical Analysis 6:281–288.

20. Garcia-Pichel F. 2009. Cyanobacteria. Encyclopedia of Microbiology, Third Edition 107–124.

21. Brown JS. 1969. Absorption and Fluorescence of Chlorophyll a in Particle Fractions from Different Plants. Biophys J 9:1542–1552.

22. Mullineaux CW. 2014. Co-existence of photosynthetic and respiratory activities in cyanobacterial thylakoid membranes. Biochimica et Biophysica Acta (BBA) - Bioenergetics 1837:503–511.

23. Lea-Smith DJ, Ross N, Zori M, Bendall DS, Dennis JS, Scott SA, Smith AG, Howe CJ. 2013. Thylakoid Terminal Oxidases Are Essential for the Cyanobacterium Synechocystis sp. PCC 6803 to Survive Rapidly Changing Light Intensities. Plant Physiol 162:484–495.

24. Peschek GA, Obinger C, Paumann M. 2004. The respiratory chain of blue-green algae (cyanobacteria). Physiol Plant 120:358–369.

25. Howitt CA, Vermaas WFJ. 1998. Quinol and cytochrome oxidases in the cyanobacterium Synechocystis sp. PCC 6803. Biochemistry 37:17944–17951.

26. Cooley JW, Vermaas WFJ. 2001. Succinate Dehydrogenase and Other Respiratory Pathways in Thylakoid Membranes of Synechocystis sp. Strain PCC 6803: Capacity Comparisons and Physiological Function. J Bacteriol 183:4251–4258.

27. Ohkawa H, Sonoda M, Shibata M, Ogawa T. 2001. Localization of NAD(P)H dehydrogenase in the cyanobacterium Synechocystis sp. Strain PCC 6803. J Bacteriol 183:4938–4939.

28. Andersson I, Backlund A. 2008. Structure and function of Rubisco. Plant Physiology and Biochemistry 46:275–291.

29. Pierce J, Lorimer GH, Reddy GS. 1986. Kinetic Mechanism of Ribulosebisphosphate Carboxylase: Evidence for an Ordered, Sequential Reaction. Biochemistry 25:1636–1644.

30. Clapero V, Arrivault S, Stitt M. 2024. Natural variation in metabolism of the Calvin-Benson cycle. Semin Cell Dev Biol 155:23–36.

31. Erb TJ, Zarzycki J. 2018. A short history of RubisCO: the rise and fall (?) of Nature's predominant CO2 fixing enzyme. Curr Opin Biotechnol 49:100–107.

32. Tolbert NE. 1997. THE C2 OXIDATIVE PHOTOSYNTHETIC CARBON CYCLE. Annu Rev Plant Physiol Plant Mol Biol 48:1–25.

33. Han X, Sun N, Xu M, Mi H. 2017. Co-ordination of NDH and Cup proteins in CO2 uptake in cyanobacterium Synechocystis sp. PCC 6803. J Exp Bot 68:3869–3877.

34. Sun N, Han X, Xu M, Kaplan A, Espie GS, Mi H. 2019. A thylakoid-located carbonic anhydrase regulates CO2 uptake in the cyanobacterium Synechocystis sp. PCC 6803. New Phytologist 222:206–217.

35. Price GD, Pengelly JJL, Forster B, Du J, Whitney SM, Von Caemmerer S, Badger MR, Howitt SM, Evans JR. 2013. The cyanobacterial CCM as a source of genes for improving photosynthetic CO2 fixation in crop species. J Exp Bot 64:753–768.

36. Badger MR, Badger DP, Price MR, Badger MR, Price GD. 1992. The CO2concentrating mechanism in cyanobactiria and microalgae. Physiol Plant 84:606–615.

37. Kerfeld CA, Melnicki MR. 2016. Assembly, function and evolution of cyanobacterial carboxysomes. Curr Opin Plant Biol 31:66–75.

38. Klein MG, Zwart P, Bagby SC, Cai F, Chisholm SW, Heinhorst S, Cannon GC, Kerfeld CA. 2009. Identification and Structural Analysis of a Novel Carboxysome Shell Protein with Implications for Metabolite Transport. J Mol Biol 392:319–333.

39. Marcus Y, Berry JA, Pierce J. 1992. Photosynthesis and photorespiration in a mutant of the cyanobacterium Synechocystis PCC 6803 lacking carboxysomes. Planta 187:511–516.

40. Stincone A, Prigione A, Cramer T, Wamelink MMC, Campbell K, Cheung E, Olin-Sandoval V, Grüning NM, Krüger A, Tauqeer Alam M, Keller MA, Breitenbach M, Brindle KM, Rabinowitz JD, Ralser M. 2015. The return of metabolism:

biochemistry and physiology of the pentose phosphate pathway. Biol Rev Camb Philos Soc 90:927.

41. Doello S, Klotz A, Makowka A, Gutekunst K, Forchhammer K. 2018. A Specific Glycogen Mobilization Strategy Enables Rapid Awakening of Dormant Cyanobacteria from Chlorosis. Plant Physiol 177:594–603.

42. GLASER L, BROWN DH. 1955. PURIFICATION AND PROPERTIES OF d-GLUCOSE-6-PHOSPHATE DEHYDROGENASE. Journal of Biological Chemistry 216:67–79.

43. Synthesis G, Subbarow Y, Gortner RA, Hausberger FX, Neuenschwander-Lemmer N, Lineweaver H, Burke D, Ostern P, Herbert D, Holmes E, Tuerkischer E, Wertheimer E. 1951. Direct oxidation of glucose-6-phosphate, 6-phosphogluconate and pentose-5-phosphates by enzymes of animal origin. Biochemical Journal 50:81.

44. Kawada M, Kagawa Y, Takiguchi H, Shimazono N. 1962. Purification of 6-phosphogluconolactonase from rat liver and yeast; its separation from gluconolactonase. Biochim Biophys Acta 57:404–407.

45. Rashida Z, Laxman S. 2021. The pentose phosphate pathway and organization of metabolic networks enabling growth programs. Curr Opin Syst Biol 28:100390.

46. Koch M, Doello S, Gutekunst K, Forchhammer K. 2019. PHB is Produced from Glycogen Turn-over during Nitrogen Starvation in Synechocystis sp. PCC 6803. Int J Mol Sci 20.

47. Slonczewski JL; FJW. 2017. Microbiology - an Evolving Science, 4th ed. W.W.Norton, NewYork.

48. Conway T. 1992. The Entner-Doudoroff pathway: history, physiology and molecular biology. FEMS Microbiol Rev 9:1–27.

49. Chen X, Schreiber K, Appel J, Makowka A, Fähnrich B, Roettger M, Hajirezaei MR, Sönnichsen FD, Schönheit P, Martin WF, Gutekunst K. 2016. The Entner-Doudoroff pathway is an overlooked glycolytic route in cyanobacteria and plants. Proc Natl Acad Sci U S A 113:5441–5446.

50. Colpaert M, Chabi M, Cenci U, Colleoni C. 2020. Storage Polysaccharides in Prokaryotes: Glycogen, Granulose, and Starch-Like Granules 177–210.

51. Shimmori Y, Kanesaki Y, Nozawa M, Yoshikawa H, Ehira S. 2018. Transcriptional Activation of Glycogen Catabolism and the Oxidative Pentose Phosphate Pathway by NrrA Facilitates Cell Survival Under Nitrogen Starvation in the Cyanobacterium Synechococcus sp. Strain PCC 7002. Plant Cell Physiol 59:1225–1233.

52. Shinde S, Zhang X, Singapuri SP, Kalra I, Liu X, Morgan-Kiss RM, Wang X. 2020. Glycogen Metabolism Supports Photosynthesis Start through the Oxidative Pentose Phosphate Pathway in Cyanobacteria. Plant Physiol 182:507.

53. Ortega-Martínez P, Roldán M, Díaz-Troya S, Florencio FJ. 2023. Stress response requires an efficient connection between glycogen and central carbon metabolism by phosphoglucomutases in cyanobacteria. J Exp Bot 74:1532–1550.

54. Doello S, Forchhammer K. 2023. Phosphoglucomutase comes into the spotlight. J Exp Bot 74:1293.

55. Preiss J. 1984. Bacterial glycogen synthesis and its regulation. Annu Rev Microbiol 38:419–458.

56. Klotz A, Forchhammer K. 2017. Glycogen, a Major Player for Bacterial Survival and Awakening from Dormancy. Future Microbiol 12:101–104.

57. Lehmann M, Wöber G. 1976. Accumulation, mobilization and turn-over of glycogen in the blue-green bacterium Anacystis nidulans. Arch Microbiol 111:93–97.

58. Osanai T, Oikawa A, Shirai T, Kuwahara A, Iijima H, Tanaka K, Ikeuchi M, Kondo A, Saito K, Hirai MY. 2014. Capillary electrophoresis-mass spectrometry reveals the distribution of carbon metabolites during nitrogen starvation in Synechocystis sp. PCC 6803. Environ Microbiol 16:512–524.

59. Khetkorn W, Incharoensakdi A, Lindblad P, Jantaro S. 2016. Enhancement of poly-3-hydroxybutyrate production in Synechocystis sp. PCC 6803 by overexpression of its native biosynthetic genes. Bioresour Technol 214:761–768.

60. Sudesh K, Taguchi K, Doi Y. 2002. Effect of increased PHA synthase activity on polyhydroxyalkanoates biosynthesis in Synechocystis sp. PCC6803. Int J Biol Macromol 30:97–104.

61. Jendrossek D. 2009. Polyhydroxyalkanoate granules are complex subcellular organelles (carbonosomes). J Bacteriol 191:3195–3202.

62. Zhang S, Bryant DA. 2011. The tricarboxylic acid cycle in cyanobacteria. Science (1979) 334:1551–1553.

63. Steinhauser D, Fernie AR, Araújo WL. 2012. Unusual cyanobacterial TCA cycles: Not broken just different. Trends Plant Sci 17:503–509.

64. Flores E, Herrero A. 2005. Nitrogen assimilation and nitrogen control in cyanobacteria. Biochem Soc Trans 33:164–167.

65. Izui K, Matsumura H, Furumoto T, Kai Y. 2004. Phosphoenolpyruvate carboxylase: A new era of structural biology. Annu Rev Plant Biol 55:69–84.

References

66. Cousins AB, Baroli I, Badger MR, Ivakov A, Lea PJ, Leegood RC, Von Caemmerer S. 2007. The Role of Phosphoenolpyruvate Carboxylase during C4 Photosynthetic Isotope Exchange and Stomatal Conductance. Plant Physiol 145:1006–1017.

67. COLEMAN JR, COLMAN B. 1981. Photosynthetic carbon assimilation in the blue-green alga Coccochloris peniocystis. Plant Cell Environ 4:285–290.

68. Leão PN, Martins TP, Abt K, Reis JPA, Figueiredo S, Castelo-Branco R, Freitas S. 2023. Incorporation and modification of fatty acids in cyanobacterial natural products biosynthesis. Chem Commun (Camb) 59:4436.

69. Figueiredo SAC, Preto M, Moreira G, Martins TP, Abt K, Melo A, Vasconcelos VM, Leão PN. 2021. Discovery of Cyanobacterial Natural Products Containing Fatty Acid Residues**. Angewandte Chemie International Edition 60:10064–10072.

70. Valladares A, Montesinos M, … AH-M, 2002 undefined. 2002. An ABC-type, high-affinity urea permease identified in cyanobacteria. Wiley Online LibraryA Valladares, ML Montesinos, A Herrero, E FloresMolecular microbiology, 2002•Wiley Online Library 43:703–715.

71. Omata T, Andriesse X, Hirano A. 1993. Identification and characterization of a gene cluster involved in nitrate transport in the cyanobacterium Synechococcus sp. PCC7942. MGG Molecular & General Genetics 236:193–202.

72. Montesinos M, Muro-Pastor A, … AH-J of B, 1998 undefined. 1998. Ammonium/Methylammonium Permeases of a Cyanobacterium: IDENTIFICATION AND ANALYSIS OF THREE NITROGEN-REGULATEDamt GENES IN. ASBMB 273:31463–31470.

73. Flores E, Frías JE, Rubio LM, Herrero A. 2005. Photosynthetic nitrate assimilation in cyanobacteria. Photosynth Res 83:117–133.

74. García-Domínguez M, Reyes JC, Florencio FJ. 1999. Glutamine synthetase inactivation by protein-protein interaction. Proc Natl Acad Sci U S A 96:7161–7166.

75. Galmozzi C V., Fernández-Avila MJ, Reyes JC, Florencio FJ, Muro-Pastor MI. 2007. The ammonium-inactivated cyanobacterial glutamine synthetase I is reactivated in vivo by a mechanism involving proteolytic removal of its inactivating factors. Mol Microbiol 65:166–179.

76. Mills LA, McCormick AJ, Lea-Smith DJ. 2020. Current knowledge and recent advances in understanding metabolism of the model cyanobacterium Synechocystis sp. PCC 6803. Biosci Rep 40:20193325.

77. Sakanyan V, Charlier D, Legrain C, Kochikyan A, Mett I, Pierard A, Glansdorff N. 1993. Primary structure, partial purification and regulation of key enzymes of the acetyl cycle of arginine biosynthesis in Bacillus stearothermophilus: Dual function of ornithine acetyltransferase. J Gen Microbiol 139:393–402.

78. Willows RD. 2003. Biosynthesis of chlorophylls from protoporphyrin IX. Nat Prod Rep 20:327–341.

79. Meister A. 1988. On the discovery of glutathione. Trends Biochem Sci 13:185–188.

80. Allen MM. 1984. Cyanobacterial cell inclusions. Annu Rev Microbiol 38:1–25.

81. Watzer B, Forchhammer K. 2018. Cyanophycin: A Nitrogen-Rich Reserve PolymerCyanobacteria. InTech.

82. Flores E, Arévalo S, Burnat M. 2019. Cyanophycin and arginine metabolism in cyanobacteria. Algal Res 42:101577.

83. Kim J, Rees DC. 1994. Nitrogenase and Biological Nitrogen Fixation. Biochemistry 33:389–397.

84. Fay P, Stewart W, Walsby A, Nature GF-, 1968 undefined. Is the heterocyst the site of nitrogen fixation in blue-green algae? nature.comP Fay, WDP Stewart, AE Walsby, GE FoggNature, 1968•nature.com.

85. Peterson RB, Wolk CP. 1978. High recovery of nitrogenase activity and of 55Fe-labeled nitrogenase in heterocysts isolated from Anabaena variabilis. Proc Natl Acad Sci U S A 75:6271–6275.

86. Reddy KJ, Haskell JB, Sherman DM, Sherman LA. 1993. Unicellular, aerobic nitrogen-fixing cyanobacteria of the genus Cyanothece. J Bacteriol 175:1284–1292.

87. Klotz A, Forchhammer K. 2017. Glycogen, a major player for bacterial survival and awakening from dormancy. Future Microbiol 12:101–104.

88. Collier JL, Grossman AR. 1992. Chlorosis induced by nutrient deprivation in Synechococcus sp. strain PCC 7942: not all bleaching is the same. J Bacteriol 174:4718.

89. Klotz A, Georg J, Bučinská L, Watanabe S, Reimann V, Januszewski W, Sobotka R, Jendrossek D, Hess WR, Forchhammer K. 2016. Awakening of a Dormant Cyanobacterium from Nitrogen Chlorosis Reveals a Genetically Determined Program. Current Biology 26:2862–2872.

90. Sauer J, Schreiber U, Schmid R, Völker U, Forchhammer K. 2001. Nitrogen starvation-induced chlorosis in Synechococcus PCC 7942. Low-level photosynthesis as a mechanism of long-term survival. Plant Physiol 126:233–243.

91. Doello S, Burkhardt M, Forchhammer K. 2021. The essential role of sodium bioenergetics and ATP homeostasis in the developmental transitions of a cyanobacterium. Current Biology 31:1606-1615.e2.

92. Wolk CP. 1973. Physiology and cytological chemistry blue-green algae. Bacteriol Rev 37:32.

93. Huergo L, Chandra G, reviews MM-F microbiology, 2013 undefined. 2013. PII signal transduction proteins: nitrogen regulation and beyond. academic.oup.comLF Huergo, G Chandra, M MerrickFEMS microbiology reviews, 2013•academic.oup.com.

94. Leigh JA, Dodsworth JA. 2007. Nitrogen regulation in bacteria and archaea. Annu Rev Microbiol 61:349–377.

95. Zhang Y, Zhao JD. 2008. PII, the key regulator of nitrogen metabolism in the cyanobacteria. Sci China C Life Sci 51:1056–1065.

96. Forchhammer K. 2004. Global carbon/nitrogen control by PII signal transduction in cyanobacteria: from signals to targets. FEMS Microbiol Rev 28:319–333.

97. Selim KA, Ermilova E, Forchhammer K. 2020. From cyanobacteria to Archaeplastida: new evolutionary insights into PII signalling in the plant kingdom. New Phytologist 227:722–731.

98. Forchhammer K, Hedler A. 1997. Phosphoprotein PII from Cyanobacteria. Eur J Biochem 244:869–875.

99. Forchhammer K, Selim KA. 2020. Carbon/nitrogen homeostasis control in cyanobacteria. FEMS Microbiol Rev 44:33–53.

100. Forchhammer K, Selim KA, Huergo LF. 2022. New views on PII signaling: from nitrogen sensing to global metabolic control. Trends Microbiol 30:722–735.

101. Fokina O, Herrmann C, Forchhammer K. 2011. Signal-transduction protein PII from Synechococcus elongatus PCC 7942 senses low adenylate energy charge in vitro. Biochemical Journal 440:147–156.

102. Llácer JL, Contreras A, Forchhammer K, Marco-Marín C, Gil-Ortiz F, Maldonado R, Fita I, Rubio V. 2007. The crystal structure of the complex of PII and acetylglutamate kinase reveals how PII controls the storage of nitrogen as arginine. Proc Natl Acad Sci U S A 104:17644–17649.

103. Selim KA, Alva V. 2024. PII-like signaling proteins: a new paradigm in orchestrating cellular homeostasis. Curr Opin Microbiol 79:102453.

104. Atkinson MR, Kamberov ES, Weiss RL, Ninfa AJ. 1994. Reversible uridylylation of the Escherichia coli PII signal transduction protein regulates its ability to stimulate the dephosphorylation of the transcription factor nitrogen regulator I (NRI or NtrC). Journal of Biological Chemistry 269:28288–28293.

105. Forchhammer K, De Marsac NT. 1994. The PII protein in the cyanobacterium Synechococcus sp. strain PCC 7942 is modified by serine phosphorylation and signals the cellular N-status. J Bacteriol 176:84–91.

106. Forchhammer K, De Marsac NT. 1995. Functional analysis of the phosphoprotein PII (glnB gene product) in the cyanobacterium Synechococcus sp. strain PCC 7942. J Bacteriol 177:2033.

107. Burillo S, Luque I, Fuentes I, Contreras A. 2004. Interactions between the Nitrogen Signal Transduction Protein PII and N-Acetyl Glutamate Kinase in Organisms That Perform Oxygenic Photosynthesis. J Bacteriol 186:3346.

108. Zhang Y, Pu H, Wang Q, Cheng S, Zhao W, Zhang Y, Zhao J. 2007. PII is important in regulation of nitrogen metabolism but not required for heterocyst formation in the cyanobacterium Anabaena sp. PCC 7120. Journal of Biological Chemistry 282:33641–33648.

109. King DT, Zhu S, Hardie DB, Serrano-Negrón JE, Madden Z, Kolappan S, Vocadlo DJ. 2022. Chemoproteomic identification of CO2-dependent lysine carboxylation in proteins. Nature Chemical Biology 2022 18:7 18:782–791.

110. Lee HM, Flores E, Forchhammer K, Herrero A, Tandeau De Marsac N. 2000. Phosphorylation of the signal transducer PII protein and an additional effector are required for the PII-mediated regulation of nitrate and nitrite uptake in the cyanobacterium Synechococcus sp. PCC 7942. Eur J Biochem 267:591–600.

111. Watzer B, Spät P, Neumann N, Koch M, Sobotka R, MacEk B, Hennrich O, Forchhammer K. 2019. The signal transduction protein PII controls ammonium, nitrate and urea uptake in cyanobacteria. Front Microbiol 10:465012.

112. Scholl J, Dengler L, Bader L, Forchhammer K. 2020. Phosphoenolpyruvate carboxylase from the cyanobacterium Synechocystis sp. PCC 6803 is under global metabolic control by PII signaling. Mol Microbiol 114:292–307.

113. Hauf W, Schmid K, Gerhardt ECM, Huergo LF, Forchhammer K. 2016. Interaction of the nitrogen regulatory protein GlnB (PII) with biotin carboxyl carrier protein (BCCP) controls acetyl-Coa levels in the cyanobacterium synechocystis sp. PCC 6803. Front Microbiol 7:1700.

114. Heinrich A, Maheswaran M, Ruppert U, Forchhammer K. 2004. The Synechococcus elongatus PII signal transduction protein controls arginine synthesis by complex formation with N-acetyl-l-glutamate kinase. Mol Microbiol 52:1303–1314.

115. Maheswaran M, Urbanke C, Forchhammer K. 2004. Complex Formation and Catalytic Activation by the PII Signaling Protein of N-Acetyl-l-glutamate Kinase from Synechococcus elongatus Strain PCC 7942. Journal of Biological Chemistry 279:55202–55210.

116. Fokina O, Chellamuthu VR, Zeth K, Forchhammer K. 2010. A Novel Signal Transduction Protein PII Variant from Synechococcus elongatus PCC 7942 Indicates a Two-Step Process for NAGK–PII Complex Formation. J Mol Biol 399:410–421.

117. Bolay P, Rozbeh R, Isabel Muro-Pastor M, Timm S, Hagemann M, Florencio FJ, Forchhammer K, Klähn S. 2021. The novel pii-interacting protein pira controls flux into the cyanobacterial ornithine-ammonia cycle. mBio 12.

118. Espinosa J, Rodríguez-Mateos F, Salinas P, Lanza VF, Dixon R, De La Cruz F, Contreras A. 2014. PipX, the coactivator of NtcA, is a global regulator in cyanobacteria. Proc Natl Acad Sci U S A 111:E2423–E2430.

119. Vázquez-Bermúdez M, Herrero A, letters EF-F, 2002 undefined. 2002. 2-Oxoglutarate increases the binding affinity of the NtcA (nitrogen control) transcription factor for the Synechococcus glnA promoter. ElsevierMF Vázquez-Bermúdez, A Herrero, E FloresFEBS letters, 2002•Elsevier.

120. Vega-Palas MA, Flores E, Herrero A. 1992. NtcA, a global nitrogen regulator from the cyanobacterium Synechococcus that belongs to the Crp family of bacterial regulators. Mol Microbiol 6:1853–1859.

121. Giner-Lamia J, Robles-Rengel R, Hernández-Prieto MA, Isabel Muro-Pastor M, Florencio FJ, Futschik ME. 2017. Identification of the direct regulon of NtcA during early acclimation to nitrogen starvation in the cyanobacterium Synechocystis sp. PCC 6803. Nucleic Acids Res 45:11800–11820.

122. García-Domínguez M, Reyes JC, Florencio FJ. 2000. NtcA represses transcription of gifA and gifB, genes that encode inhibitors of glutamine synthetase type I from Synechocystis sp. PCC 6803. Mol Microbiol 35:1192–1201.

123. Giner-Lamia J, Robles-Rengel R, Hernández-Prieto MA, Isabel Muro-Pastor M, Florencio FJ, Futschik ME. 2017. Identification of the direct regulon of NtcA during early acclimation to nitrogen starvation in the cyanobacterium Synechocystis sp. PCC 6803. Nucleic Acids Res 45:11800–11820.

124. Osanai T, Sato S, Tabata S, Tanaka K. 2005. Identification of PamA as a PII-binding membrane protein important in nitrogen-related and sugar-catabolic gene expression in Synechocystis sp. PCC 6803. J Biol Chem 280:34684–34690.

125. Osanai T, Oikawa A, Iijima H, Kuwahara A, Asayama M, Tanaka K, Ikeuchi M, Saito K, Hirai MY. 2014. Metabolomic analysis reveals rewiring of Synechocystissp. PCC 6803 primary metabolism by ntcA overexpression. Environ Microbiol 16:3304–3317.

126. Giner-Lamia J, Robles-Rengel R, Hernández-Prieto MA, Isabel Muro-Pastor M, Florencio FJ, Futschik ME. 2017. Identification of the direct regulon of NtcA during early acclimation to nitrogen starvation in the cyanobacterium Synechocystis sp. PCC 6803. Nucleic Acids Res 45:11800–11820.

127. Kawashima T, Berthet-Colominas C, Wulff M, Cusack S, Leberman R. 1996. The structure of the Escherichia coli EF-Tu· EF-Ts complex at 2.5 Å resolution. Nature 1996 379:6565 379:511–518.

128. Huang YH, Hilal T, Loll B, Bürger J, Mielke T, Böttcher C, Said N, Wahl MC. 2020. Structure-Based Mechanisms of a Molecular RNA Polymerase/Chaperone Machine Required for Ribosome Biosynthesis. Mol Cell 79:1024-1036.e5.

129. Auerbach G, Herrmann A, Bracher A, Bader G, Gütlich M, Fischer M, Neukamm M, Garrido-Franco M, Richardson J, Nar H, Huber R, Bacher A. 2000. Zinc plays a key role in human and bacterial GTP cyclohydrolase I. Proc Natl Acad Sci U S A 97:13567–13572.

130. López-Maury L, Sánchez-Riego AM, Reyes JC, Florencio FJ. 2009. The Glutathione/Glutaredoxin System Is Essential for Arsenate Reduction in Synechocystis sp. Strain PCC 6803. J Bacteriol 191:3534.

131. Ovchinnikov YA, Monastyrskaya GS, Gubanov V V., Guryev SO, Salomatina IS, Shuvaeva TM, Lipkin VM, Sverdlov ED. 1982. The primary structure of E. coli RNA polymerase, Nucleotide sequence of the rpoC gene and amino acid sequence of the beta'-subunit. Nucleic Acids Res 10:4035–4044.

132. Bergsland KJ, Haselkorn R. 1991. Evolutionary relationships among eubacteria, cyanobacteria, and chloroplasts: evidence from the rpoC1 gene of Anabaena sp. strain PCC 7120. J Bacteriol 173:3446–3455.

133. Cohen SE, Lewis CA, Mooney RA, Kohanski MA, Collins JJ, Landick R, Walker GC. 2010. Roles for the transcription elongation factor NusA in both DNA repair and damage tolerance pathways in Escherichia coli. Proc Natl Acad Sci U S A 107:15517–15522.

134. Li K, Jiang T, Yu B, Wang L, Gao C, Ma C, Xu P, Ma Y. 2013. Escherichia coli transcription termination factor NusA: heat-induced oligomerization and chaperone activity. Scientific Reports 2013 3:1 3:1–9.

135. Srivastava A, Kumar A, Biswas S, Srivastava V, Rajaram H, Mishra Y. 2023. Cd-induced cytosolic proteome changes in the cyanobacterium Anabaena sp. PCC7120 are mediated by LexA as one of the regulatory proteins. Biochimica et Biophysica Acta (BBA) - Proteins and Proteomics 1871:140902.

136. Jörg Scholl. 2023. Identification and Characterization of Novel Interaction Partners of the Signaling Protein PII in the Cyanobacterium Synechocystis sp. PCC 6803. Dissertation. University of Tübingen, Tübingen.

137. Gudas LJ, Cohen A, Ullman B, Martin DW. 1978. Analysis of adenosine-mediated pyrimidine starvation using cultured wild-type and mutant mouse T-lymphoma cells. Somatic Cell Genet 4:201–219.

References

138. Mariani V, Biasini M, Barbato A, Schwede T. 2013. lDDT: a local superposition-free score for comparing protein structures and models using distance difference tests. Bioinformatics 29:2722–2728.

139. Guo HB, Perminov A, Bekele S, Kedziora G, Farajollahi S, Varaljay V, Hinkle K, Molinero V, Meister K, Hung C, Dennis P, Kelley-Loughnane N, Berry R. 2022. AlphaFold2 models indicate that protein sequence determines both structure and dynamics. Scientific Reports 2022 12:1 12:1–15.

140. Elfmann C, Stülke J. 2023. PAE viewer: a webserver for the interactive visualization of the predicted aligned error for multimer structure predictions and cross-links. Nucleic Acids Res 51:W404–W410.

141. Xu J, Zhang Y. 2010. How significant is a protein structure similarity with TM-score = 0.5? Bioinformatics 26:889–895.

142. Zhang Y, Skolnick J. 2004. Scoring function for automated assessment of protein structure template quality. Proteins: Structure, Function, and Bioinformatics 57:702–710.

143. Rozbeh R, Forchhammer K. 2021. Split NanoLuc technology allows quantitation of interactions between PII protein and its receptors with unprecedented sensitivity and reveals transient interactions. Scientific Reports 2021 11:1 11:1–13.

144. Ma CW, Lüddecke J, Forchhammer K, Zeng AP. 2014. Population shift of binding pocket size and dynamic correlation analysis shed new light on the anticooperative mechanism of PII protein. Proteins: Structure, Function, and Bioinformatics 82:1048–1059.

145. Wang J, Huang X, Ge H, Wang Y, Chen W, Zheng L, Huang C, Yang H, Li L, Sui N, Wang Y, Zhang Y, Lu D, Fang L, Xu W, Jiang Y, Huang F, Wang Y. 2022. The quantitative proteome atlas of a model cyanobacterium. Journal of Genetics and Genomics 49:96–108.

146. Iglesias AA, Kakefuda G, Preiss J. 1991. Regulatory and Structural Properties of the Cyanobacterial ADPglucose Pyrophosphorylases. Plant Physiol 97:1187–1195.

147. Greening C, Grinter R, Chiri E. 2019. Uncovering the Metabolic Strategies of the Dormant Microbial Majority: towards Integrative Approaches. mSystems 4.

148. Saha R, Liu D, Hoynes-O'Connor A, Liberton M, Yu J, Bhattacharyya-Pakrasi M, Balassy A, Zhang F, Moon TS, Maranas CD, Pakrasia HB. 2016. Diurnal Regulation of Cellular Processes in the Cyanobacterium Synechocystis sp. Strain PCC 6803: Insights from Transcriptomic, Fluxomic, and Physiological Analyses. mBio 7:e00464-16.

149. Branon TC, Bosch JA, Sanchez AD, Udeshi ND, Svinkina T, Carr SA, Feldman JL, Perrimon N, Ting AY. 2018. Efficient proximity labeling in living cells and organisms with TurboID. Nat Biotechnol 36:880.

150. Jedrzejas MJ, Chander M, Setlow P, Krishnasamy G. 2000. Structure and mechanism of action of a novel phosphoglycerate mutase from Bacillus stearothermophilus. EMBO J 19:1419.

151. Loshon CA, Setlow P. 1993. Levels of small molecules in dormant spores of *Sporosarcina* species and comparison with levels in spores of *Bacillus* and *Clostridium* species. Can J Microbiol 39:259–262.

152. MacCready JS, Tran L, Basalla JL, Hakim P, Vecchiarelli AG. 2021. The McdAB system positions α-carboxysomes in proteobacteria. Mol Microbiol 116:277–297.

153. Rae BD, Long BM, Badger MR, Price GD. 2013. Functions, Compositions, and Evolution of the Two Types of Carboxysomes: Polyhedral Microcompartments That Facilitate CO2 Fixation in Cyanobacteria and Some Proteobacteria. Microbiol Mol Biol Rev 77:357.

154. Roychowdhury A, Kundu A, Bose M, Gujar A, Mukherjee S, Das AK. 2015. Complete catalytic cycle of cofactor-independent phosphoglycerate mutase involves a spring-loaded mechanism. FEBS J 282:1097–1110.

155. Muro-Pastor MI, Cutillas-Farray Á, Pérez-Rodríguez L, Pérez-Saavedra J, Vega-De Armas A, Paredes A, Robles-Rengel R, Florencio FJ. 2020. CfrA, a Novel Carbon Flow Regulator, Adapts Carbon Metabolism to Nitrogen Deficiency in Cyanobacteria. Plant Physiol 184:1792–1810.

Appendix

Publication 1

The novel PII-interactor PirC identifies phosphoglycerate mutase as the key control point of carbon storage metabolism in cyanobacteria.

Tim Orthwein, Jörg Scholl, Phillip Spät, Stefan Lucius, Moritz Koch, Boris Macek, Martin Hagemann and Karl Forchhammer

Available at: https://doi.org/10.1073/pnas.2019988118

The novel P_{II}-interactor PirC identifies phosphoglycerate mutase as key control point of carbon storage metabolism in cyanobacteria

Tim Orthwein[a,1], Jörg Scholl[a,1], Philipp Spät[b,1], Stefan Lucius[c], Moritz Koch[a], Boris Macek[b], Martin Hagemann[c], and Karl Forchhammer[a,2]

[a]Interfaculty Institute of Microbiology and Infection Medicine, University of Tübingen, 72076 Tübingen, Germany; [b]Department of Quantitative Proteomics, University of Tübingen, 72076 Tübingen, Germany; and [c]Institute of Biological Sciences, Plant Physiology Department, University of Rostock, 18059 Rostock, Germany

Edited by Susan S. Golden, University of California San Diego, La Jolla, CA, and approved December 9, 2020 (received for review September 23, 2020)

Nitrogen limitation imposes a major transition in the lifestyle of nondiazotrophic cyanobacteria that is controlled by a complex interplay of regulatory factors involving the pervasive signal processor P_{II}. Immediately upon nitrogen limitation, newly fixed carbon is redirected toward glycogen synthesis. How the metabolic switch for diverting fixed carbon toward the synthesis of glycogen or of cellular building blocks is operated was so far poorly understood. Here, using the nondiazotrophic cyanobacterium *Synechocystis* sp. PCC 6803 as model system, we identified a novel P_{II} interactor, the product of the *sll0944* gene, which we named PirC. We show that PirC binds to and inhibits the activity of 2,3-phosphoglycerate–independent phosphoglycerate mutase (PGAM), the enzyme that deviates newly fixed CO_2 toward lower glycolysis. The binding of PirC to either P_{II} or PGAM is tuned by the metabolite 2-oxoglutarate (2-OG), which accumulates upon nitrogen starvation. In these conditions, the high levels of 2-OG dissociate the PirC–P_{II} complex to promote PirC binding to and inhibition of PGAM. Accordingly, a PirC-deficient mutant showed strongly reduced glycogen levels upon nitrogen deprivation, whereas polyhydroxybutyrate granules were overaccumulated compared to wild-type. Metabolome analysis revealed an imbalance in 3-phosphoglycerate to pyruvate levels in the *pirC* mutant, confirming that PirC controls the carbon flux in cyanobacteria via mutually exclusive interaction with either P_{II} or PGAM.

glycogen metabolism | polyhydroxybutyrate | cyanobacteria | nitrogen starvation | carbon flow

Cellular homeostasis relies on the capacity of living systems to adjust their metabolism in response to changes in the environment. Therefore, organisms must be able to sense the metabolic state and tune it in response to environmental fluctuations. It has been proposed that cyanobacteria do not extensively rely on direct environmental sensing but rather are primarily concerned about their internal metabolic state (1). This "introvert" lifestyle requires that they constantly and precisely monitor their intracellular milieu in order to detect imbalances caused by external perturbations. The maintenance of carbon/nitrogen (C/N) homeostasis is one of the most fundamental aspects of cellular physiology. For photoautotrophic organisms like cyanobacteria, it is essential to tightly interconnect CO_2 fixation and nitrogen assimilation. To fulfill this task, cyanobacteria use a sophisticated signaling network organized by the pervasive P_{II}-signaling protein. P_{II} proteins are fundamental for this task in most free-living prokaryotes and chloroplasts of green plants (2). They act as multitasking signal integrators, combining information on the metabolic C/N balance through interaction with the metabolite 2-oxoglutarate (2-OG) and on the cellular energy state by competitive adenosine triphosphate (ATP) or adenosine diphosphate (ADP) binding. 2-OG is ideally suited as a status reporter metabolite for C/N balance, as this tricarboxylic acid (TCA) cycle intermediate represents the precursor metabolite into which ammonia is incorporated through the nitrogen assimilatory reactions catalyzed by the glutamine-synthetase–glutamate-synthase (GS/GOGAT) cycle (3).

The interaction of P_{II} proteins with various effector molecules, the conformational changes that ensue from these interactions, and their perception by the targets have been elaborated in great detail [recently reviewed (3–6)]. The three intersubunit clefts of the trimeric P_{II} proteins contain intercommunicating effector-molecule–binding sites; ADP and ATP compete for occupying these sites, and binding of ATP, but not ADP, creates a coordination sphere for the effector 2-OG through a bridging Mg^{2+} ion. Depending on the effector molecules bound, the large and flexible target-binding loops (termed T-loops), protruding from the effector binding sites, can adopt specific conformations, allowing signal receptor proteins to read out the metabolic information through protein–protein interactions (5). A variety of key metabolic enzymes, transcription factors, and transport proteins use this signaling path to tune their activity in response to the metabolic state. P_{II} in its different conformations can directly interact with various target proteins such as the N-acetyl-L-glutamate kinase, catalyzing the committed step in arginine

Significance

In this work, we identified the regulatory mechanism of the key control point of cyanobacterial carbon metabolism, the glycolytic phosphoglycerate mutase (PGAM) reaction, converting 3-PGA into 2-PGA and thereby exporting organic carbon from the photosynthetic Calvin cycle. We show that PGAM activity is controlled by a small modulator protein PirC (product of *sll0944*), which inhibits the enzyme through protein–protein interaction. The availability of PirC for PGAM inhibition is controlled by the pervasive carbon/nitrogen balance regulator P_{II}, which sequesters PirC at low 2-oxoglutarate levels and releases it at high 2-oxoglutarate levels. PirC-mediated inhibition of PGAM triggers glycogen accumulation, and disrupting this regulation allows the redirection of carbon flux, a decisive requirement for transforming cyanobacteria into green factories.

Author contributions: K.F. designed research; T.O., J.S., P.S., S.L., and M.K. performed research; B.M. contributed new reagents/analytic tools; T.O., J.S., P.S., B.M., M.H., and K.F. analyzed data; and K.F. wrote the paper.

The authors declare no competing interest.

This article is a PNAS Direct Submission.

[1]T.O., J.S., and P.S. contributed equally to this work.

[2]To whom correspondence may be addressed. Email: karl.forchhammer@uni-tuebingen.de.

This article contains supporting information online at https://www.pnas.org/lookup/suppl/doi:10.1073/pnas.2019988118/-/DCSupplemental.

Published February 1, 2021.

biosynthesis (7, 8); the acetyl-CoA carboxylase, catalyzing the rate-limiting step in fatty acid biosynthesis (9); the phosphoenolpyruvate carboxylase, which catalyzes an anaplerotic carbon fixation (10); or the glutamine-dependent nicotinamide adenine dinucleotide (NAD^+) synthetase (11). Besides tuning the activity of enzymes, recent analyses revealed that, through direct protein–protein interaction, the abundant P_{II} proteins can also regulate transport activities, including an ensemble of nitrogen transporters such as the nitrate/nitrite transport system, the urea transport system, and the ammonium transporter (12).

A different mechanism underlies the ability of P_{II} proteins to modulate gene expression in response to different C/N ratios. In this case, the effect of P_{II} proteins is mediated through binding to a small signaling mediator protein called PipX (P_{II}-interacting protein X), which acts as a transcriptional coactivator of the global nitrogen control transcription factor NtcA. The latter controls a large regulon of about 80 genes (13). The mediator PipX swaps between P_{II}- and NtcA-bound states, thereby either tuning down or stimulating the activity of NtcA, respectively (6, 14). Partner swapping of PipX occurs in response to the effector molecule 2-OG and the ATP/ADP balance (14).

In a previous P_{II} protein interaction study, several putative P_{II} interactors of unknown function were identified (12). The most prominent hit was the product of the *sll0944* gene, a member of the NtcA regulon (11, 13). The *sll0944* gene product is annotated in Uniprot (https://www.uniprot.org/uniprot/P77971) as a protein of unknown function. Close homologs are widespread in the cyanobacterial phylum, pointing to an important function of this protein in the cyanobacterial metabolism. We previously observed that *sll0944* is up-regulated both at the transcriptional (15) and posttranscriptional (16) level during the response of the model cyanobacterium *Synechocystis* PCC 6803 (from now on termed *Synechocystis*) to nitrogen starvation. Following nitrogen depletion, the CO_2-fixation products are redirected toward glycogen synthesis, and, concomitantly, the phycobiliproteins and the entire photosynthetic machinery are proteolytically degraded, causing loss of pigments of the cells (referred as chlorosis) (15). Moreover, the carbon polymer polyhydroxybutyrate (PHB) slowly accumulates in granular structures, which are derived from glycogen turnover (17, 18). The metabolic activities decrease as the cells enter into a dormant-like state, in which they can survive for months. As soon as a combined nitrogen source becomes available again, chlorotic cells rapidly awake and resume metabolism (15, 18, 19). This is accompanied by a gradual decrease in the levels of Sll0944 (19).

This study aimed to clarify the role of the Sll0944 protein in *Synechocystis* and its involvement in P_{II} signaling. Our results indicate that Sll0944 regulates the glycolytic carbon flux in a P_{II}-dependent manner through interaction with the 2,3-phosphoglycerate–independent phosphoglycerate mutase (PGAM) in response to the nitrogen status sensed via 2-OG. Specifically, we found that Sll0944 swaps between P_{II} and PGAM in a 2-OG–dependent manner. This establishes PGAM as a key control point of cyanobacterial carbon flow, as predicted previously by kinetic modeling of the cyanobacterial low-carbon response (20, 21), and Sll0944 as the key regulator of cyanobacterial carbon metabolism. We therefore named the *sll0944* product PirC (P_{II}-interacting regulator of carbon metabolism).

Results

In Silico Analysis Reveals High Conservation of Sll0944 (PirC) among Cyanobacteria. According to the Uniprot database, the gene *sll0944* (from now on named PirC) of *Synechocystis* codes for a 164-amino-acid–long "uncharacterized protein" (https://www.uniprot.org/uniprot/P77971). A databank search for orthologues using the Basic Local Alignment Search Tool (BLAST) revealed that PirC is highly conserved among cyanobacteria. All the homologous proteins contain the Domain of Unknown Function 1830 (http://pfam.xfam.org/family/PF08865). A conserved NtcA-binding site 5′-GTN_{10}AC-3′, which is responsible for nitrogen-starvation–induced expression (22), is situated in front of the respective genes. These findings suggest that *pirC* and its orthologs might all be responsive to nitrogen starvation. Gene neighboring analysis in 53 cyanobacterial genomes revealed that in 67% of the cases, the *pirC* homologs are flanked by a gene encoding for a radical S-adenosyl methionine (SAM)-like protein, annotated as Elongator protein 3 (*SI Appendix*, Fig. S1), which was recently shown to be a non-canonical transfer RNA acetyltransferase (23). In *Synechocystis*, the *pirC* gene is upstream of *glgA1*, which encodes the major glycogen synthase that is required for acclimation to nitrogen deprivation (19).

Protein sequence alignments showed that the first 52 N-terminal amino acids of the annotated PirC sequence are not conserved in any of the other orthologs (*SI Appendix*, Fig. S2). Furthermore, the experimentally validated transcriptional start site from *Synechocystis* (24) suggests a shorter open reading frame (ORF) with Met-53 as putative translational start site for PirC. Our initial heterologous expression of the long and short *pirC* variant in *Escherichia coli* revealed that only the short variant can be expressed into a properly folded and soluble protein. This finding supports the notion that the 112-amino-acid–long version of PirC represents the physiologically relevant protein. Hence, this short variant was used in all subsequent work.

PirC Is a Strong P_{II}-Binding Partner. A first series of experiments were set out to verify the putative interaction between P_{II} and PirC (12). In vitro affinity purification experiments revealed that recombinant PirC coeluted with strep-tagged P_{II} in the presence of ATP or ADP, but not in the presence of ATP plus 2-OG (*SI Appendix*, Fig. S3*A*). As expected, in the control samples lacking strep-tagged P_{II}, the elution fractions did not contain any PirC. The observation that PirC is unable to interact with ATP- and 2-OG–bound P_{II} is common to many P_{II}-interacting partners and a sign of binding specificity (25). The influence of effector molecules on the interaction between PirC and P_{II} was further quantitatively analyzed by bio-layer interferometry (BLI). In this assay, binding of an analyte in solution to a ligand immobilized on a biosensor surface (or tip) produces a shift in wavelength, which serves as readout of analyte–ligand interaction. For our purposes, recombinant C-terminal His_8-tagged P_{II} was bound to the Ni-NTA biosensor surface, while strep-tagged PirC was added as analyte in solution. In the absence of effector molecules, we observed a weak interaction between P_{II} and PirC (Fig. 1 *A* and *B*). In the presence of ATP or ADP, PirC binding to P_{II} strongly increased. Quantitative measurements revealed apparent K_D values of 37.3 ± 2.5 nM and 14.1 ± 0.7 nM for P_{II}–PirC complex formation in the presence of 2 mM ATP and ADP, respectively. Similar results were obtained using surface plasmon resonance (SPR) spectrometry. The maximum response after injection of PirC in presence of ATP over the P_{II}-loaded sensor was 270 response units (RUs) when the SPR sensor chip was loaded with 1,000 RUs of His-tagged P_{II} (*SI Appendix*, Fig. S3*B*). Given that in SPR spectrometry, the response signal in RUs is proportional to the mass change on the sensor, the mass increase of 270 RUs by PirC on 1,000 RUs of P_{II}-loaded sensor is close to one PirC monomer per P_{II} trimer bound. The inhibitory effect of 2-OG on P_{II}–PirC interaction was further quantified by BLI through titration with increasing 2-OG concentrations at a constant concentration of 2 mM ATP (Fig. 1*C*). A half maximal inhibitory concentration (IC_{50}) of 123.4 ± 1.1 μM for 2-OG was determined, a value close to the K_D of the third (lowest affinity) 2-OG–binding site of P_{II} (26). Therefore, it seems that occupation of all three effector binding sites in P_{II} with 2-OG is required to prevent complex formation with PirC.

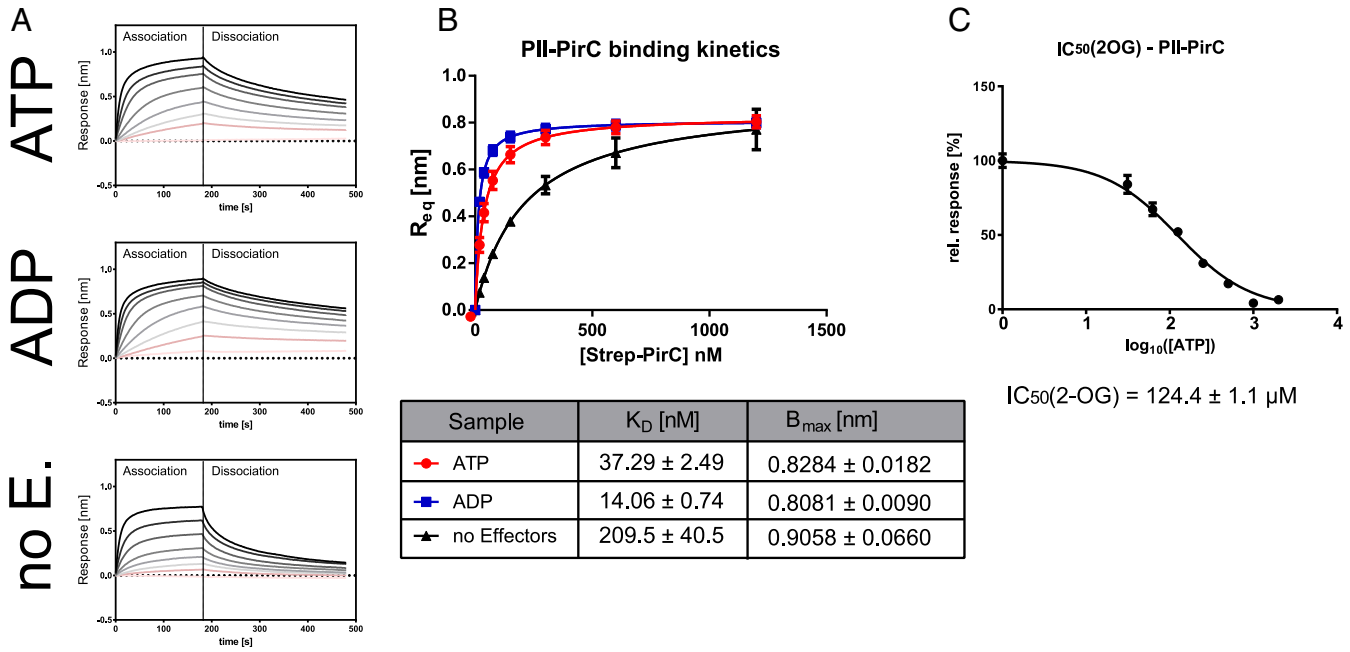

Sample	K_D [nM]	B_{max} [nm]
ATP	37.29 ± 2.49	0.8284 ± 0.0182
ADP	14.06 ± 0.74	0.8081 ± 0.0090
no Effectors	209.5 ± 40.5	0.9058 ± 0.0660

Fig. 1. Complex formation of P_{II} with PirC and modulation by effectors ADP, ATP, and 2-OG. (*A*) BLI binding assays. His-tagged P_{II} was immobilized on sensor tips and allowed to associate for 180 s with PirC in presence of either 2 mM ATP (*Top*), ADP (*Middle*), or without effectors (*Bottom*), followed by 300 s dissociation. The overlay of response curves with increasing concentrations of PirC (9.375 nM to 1,500 nM) is shown. (*B*) Plot of maximum binding responses from (*A*) for the calculation of binding constants (depicted below). (*C*) Plot of IC_{50} determination for inhibition of PirC–P_{II} binding by increasing 2-OG concentrations at a constant 2 mM of ATP. All experiments were performed in triplicates, and corresponding SDs are shown in *B* and *C*.

Physiological Role of PirC in *Synechocystis*. The high conservation of *pirC* in the cyanobacterial phylum, including conservation of the NtcA-binding site, indicated an important function for PirC during acclimation to nitrogen depletion, a feature common to all the members of this phylum. To identify such a function, we generated a *pirC*-deficient mutant (Δ*pirC*) as well as strains complemented either with the native *pirC* gene (ΔpirC::pirC) or with *pirC* variants encoding fluorescent proteins fused to PirC (*SI Appendix*, Fig. S4).

Acclimation of these strains to long-term nitrogen starvation was investigated under continuous light or in a day/night regime. Growth (as indicated by an increase in optical density) and degree of pigmentation as well as glycogen and PHB content were monitored over 1 mo. In the wild-type strain pigment degradation after removal of combined nitrogen required 21 d under day/night regimes but only 5 to 7 d in continuous light (*SI Appendix*, Fig. S5) (15). Pigment degradation was slightly retarded in the Δ*pirC* mutant compared to the wild-type and complemented strain. Moreover, the increase in optical density at 750 nm (OD_{750}) of the Δ*pirC* mutant was lower than that of the wild-type and complemented strains (Fig. 2*A*), which indicates that in the Δ*pirC* mutant, the final cell division upon nitrogen deprivation is delayed. In contrast to these rather modest effects, a striking phenotype for the Δ*pirC* strain was observed with respect to glycogen accumulation. After the removal of combined nitrogen sources, both the wild-type and complemented strain showed the typical rapid and steep increase in cellular glycogen levels, which were maintained throughout the entire period of nitrogen-starvation–induced chlorosis. By contrast, glycogen content in the Δ*pirC* mutant reached only 28% of the wild-type level and subsequently declined again. As opposed to glycogen, the Δ*pirC* mutant accumulated significantly more PHB (up to 49% of the cell dry mass) than the wild-type and the complemented strain (30% and 29% PHB per cell dry mass, respectively) (Fig. 2*B*). To confirm this result, PHB granules were visualized by fluorescence microscopy after staining the cells with Nile Red or by transmission electron microscopy (TEM) (Fig. 2*C*). After 35 d of nitrogen depletion, a much higher PHB content was observed in the Δ*pirC* mutant than in the wild-type or complemented strain in both fluorescent and TEM micrographs, confirming the results of the chemical PHB quantification.

Identification of PirC-Controlled Processes. The altered glycogen and PHB accumulation patterns in nitrogen-deprived Δ*pirC* cells suggested a crucial role for PirC in carbon storage metabolism during nitrogen starvation. To elucidate the corresponding molecular mechanism, we aimed to identify additional molecular targets of PirC. To this end, coimmunoprecipitation (CoIP) experiments were conducted using crude extract of nitrogen-starved Δ*pirC* cells expressing a PirC–mCitrine fusion protein (Δ*pirC*::*pirC–mCitrine*). PirC–mCitrine in the crude extract of Δ*pirC*::*pirC–mCitrine* was precipitated using a GFP-trap consisting of an anti-GFP Nanobody/V_HH coupled to magnetic agarose beads (http://www.chromotek.com). Note that the anti-GFP nanobodies bind different variants of GFP, including mCitrine. Chromotek binding control magnetic agarose was used to determine the unspecific background binding. IPs were performed in the presence of Mg^{2+}, ATP, and 2-OG or in the absence of additionally supplemented effectors. The eluates from independent experiments were analyzed after tryptic digestion by quantitative mass spectrometry to identify coimmunoprecipitating proteins. In the absence of 2-OG, immunoprecipitation of PirC–mCitrine only enriched for P_{II}, confirming that P_{II} is the major PirC-interaction partner in these conditions (*SI Appendix*, Fig. S6). The addition of 2-OG/ATP to the extract completely changed the pattern of coimmunoprecipated proteins: instead of P_{II}, the enzyme 2,3-bisphosphoglycerate–independent PGAM, encoded by the gene *slr1945*, appeared as dominant PirC interactor (*SI Appendix*, Fig. S7). PGAM converts 3-phosphoglycerate (3-PGA) into 2-phosphoglycerate (2-PGA) at the beginning of

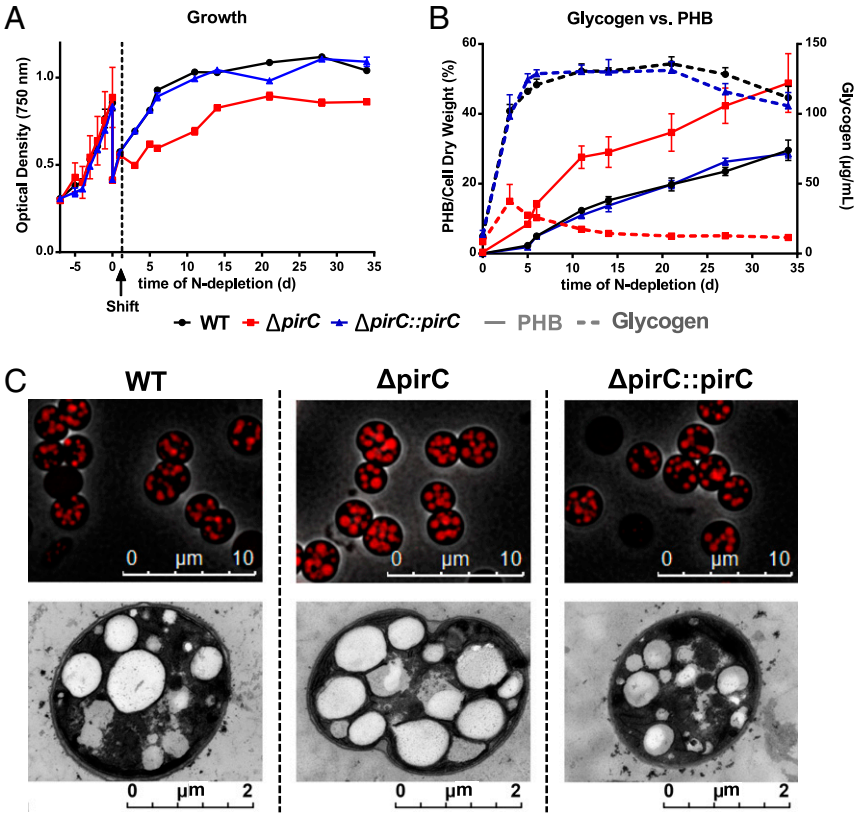

Fig. 2. Effect of PirC deletion on growth, carbon storage, and carbon polymer accumulation during chlorosis. The graphs represent the mean and SD from three biological replicates. (*A*) Growth curves of the wild-type (WT), the *pirC* null mutant (*ΔpirC*), and the complemented (*ΔpirC::pirC*) strain as measured by OD_{750} starting 7 d before nitrogen depletion and during the 35 d of acclimation to nitrogen starvation, also known as chlorosis. (*B*) Glycogen and carbon polymer (PHB) content during chlorosis. PHB: plane lines; Glycogen: dashed lines. (*C*) Fluorescent and TEM micrographs of cells stained with Nile Red after 35 d of chlorosis. Top rows: three-dimensional (3D)–deconvoluted overlay pictures of phase contrast- and fluorescence microscopy images (1,000× magnification). Note that Nile Red stains the PHB granules within each cell. Bottom rows: TEM Pictures (5,000× magnification).

lower glycolysis. In addition to PGAM, an ortholog of the CcmP protein, encoded by the gene *slr0169*, was also found as a PirC-interacting protein, but with a lower enrichment factor compared to PGAM. CcmP has been identified as a minor shell protein in carboxysomes of *Synechococcus elongatus* PCC 7249. The trimeric shell protein has a central pore that can be opened and closed, most likely for the movement of metabolites such as the PGAM substrate 3-PGA (27, 28).

PirC Swaps from P_{II}- to PGAM-Binding in a 2-OG–Dependent Manner, Thus Inhibiting PGAM Activity during Chlorosis. The observed interaction of PirC with PGAM suggested that PirC negatively regulates PGAM activity. This assumption is consistent with the decreased glycogen and increased PHB levels in the Δ*pirC* mutant because PGAM diverts newly fixed carbon from the Calvin cycle toward lower glycolysis, through which acetyl-CoA, the precursor metabolite of PHB, is produced. To validate the putative role of PirC in the regulation of PGAM, recombinant PGAM was purified via an N-terminal His_6-tag for biochemical characterization.

First, we tested the influence of PirC on PGAM catalytic activity using an enzymatic assay, in which the PGAM-catalyzed conversion of 3-PGA to 2-PGA is coupled with enolase, pyruvate kinase, and lactate dehydrogenase to the final oxidation of reduced nicotinamide adenine dinucleotide (NADH). The His-tag was removed from recombinant PGAM by thrombin cleavage to prevent interference with catalysis. Furthermore, we verified that PirC had no effect on the activities of the coupling enzymes (*SI Appendix*, Fig. S8). A clear PirC-dependent inhibition of PGAM activity was observed when PirC was added at increasing concentrations to the reaction mix of the enzymatic assay. PirC inhibited PGAM in a competitive manner by increasing the K_M for the substrate 3-PGA rather than lowering the V_{max}. At nearly equimolar concentrations of PirC (200 nM) and PGAM (166 nM), the catalytic efficiency was reduced to one third. In the presence of an excess of PirC, the catalytic activity of PGAM could be reduced more than 10-fold as compared to the absence of PirC (Fig. 3*A* and Table 1).

Second, the interplay of P_{II} and PirC on PGAM activity was analyzed because we assumed that P_{II} might regulate the inhibitory interaction of PirC with PGAM, in analogy to the effect of P_{II} on PipX–NtcA interaction (14). To this end, we performed PGAM assays in the presence of PirC and P_{II} and supplemented the assays with ATP and different 2-OG concentrations, respectively (Fig. 3*B*). Addition of P_{II} in the absence of 2-OG abolished the inhibitory effect of PirC on PGAM activity. The K_M for 3-PGA returned to the value of noninhibited PGAM (Table 1). However, in the presence of 1 mM of 2-OG, a concentration corresponding to high C/N conditions in *Synechocystis* cells, PirC was again able to inhibit PGAM as in the absence of P_{II}. When 2-OG was added at a concentration of 0.123 mM (corresponding to the $IC50_{2\text{-}OG}$ value of P_{II}–PirC complex formation), the inhibition of PGAM was ∼50% of the maximal inhibition with PirC in the absence of 2-OG. These results unambiguously indicate that in vitro, in presence of high 2-OG levels, binding of 2-OG to P_{II} disrupts P_{II}–PirC interaction and promotes binding of PirC to PGAM, thus inhibiting its activity.

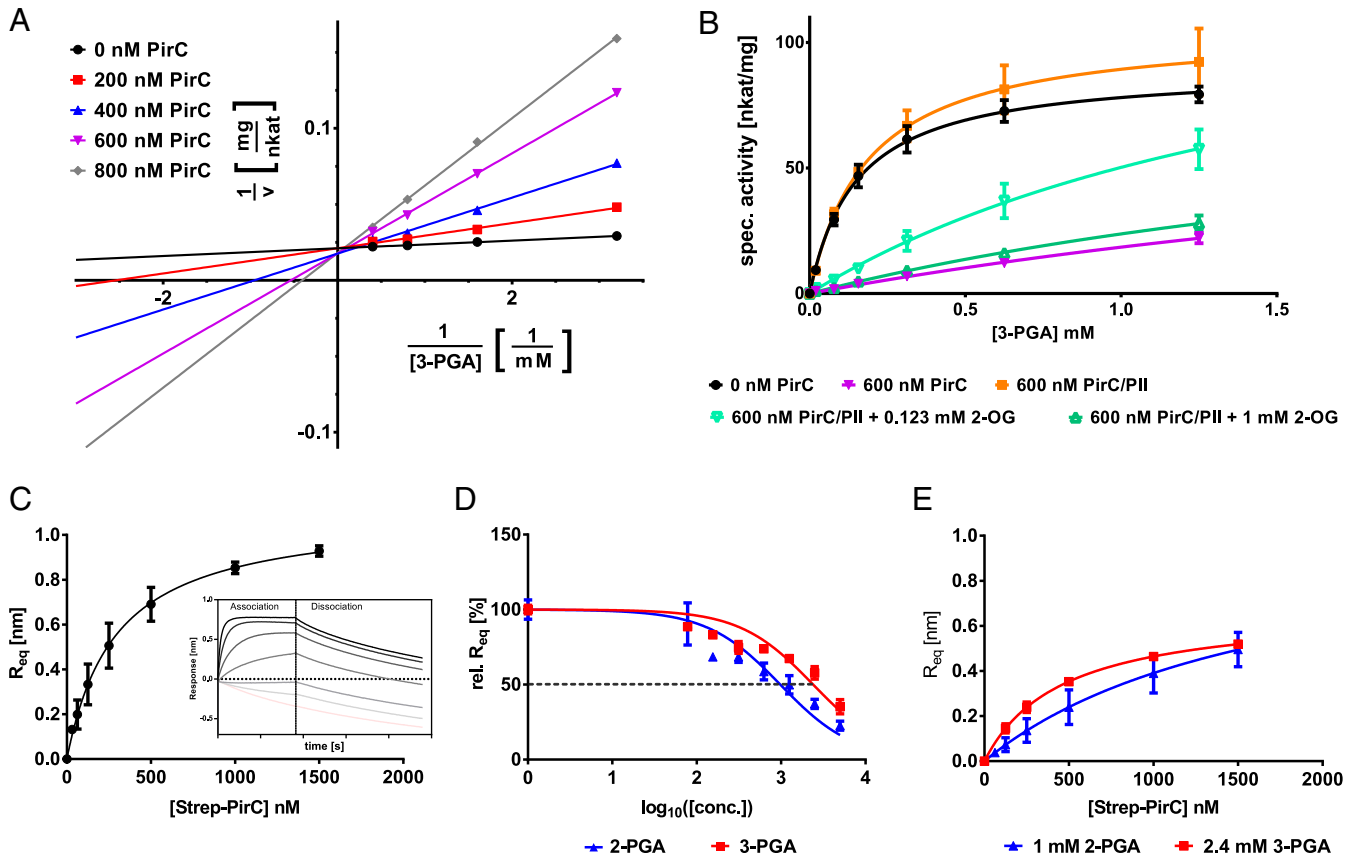

Fig. 3. Effect of PirC on PGAM enzyme activity and PGAM–PirC complex formation. (*A*) Inhibition of PGAM activity by increasing PirC concentrations represented as Lineweaver–Burk plot. The corresponding kinetic constants are shown in Table 1. PirC has no effect on coupling enzymes as shown in supplements (*SI Appendix*, Fig. S8). (*B*) Modulation of PGAM activity by PirC (600 nM) in presence or absence of P_{II} (600 nM trimer) and 0.4 mM ATP without or with 0.123 mM or 1 mM 2-OG. Each point represents the mean of triplicates. (*C*) Steady-state graph of PirC–PGAM binding assays using BLI. The mean of the R_{eq} value (three independent replicates) was plotted against the molar concentration of Strep–PirC. The inset shows the raw binding curves at different PirC concentrations. (*D*) Competitive inhibition of PirC–PGAM interaction by 2-PGA and 3-PGA. Plot shows determination of IC_{50}. (*E*) Steady-state graph of PirC–PGAM binding in presence of 2-PGA or 3-PGA at their IC_{50} concentrations.

The inhibitory effect of PirC binding on PGAM activity was further investigated using BLI assays. To this end, His_6-tagged PGAM was bound to the biosensor tip, and strep-tagged PirC protein was added in solution as analyte at varying concentrations (Fig. 3*C*). A stable PGAM–PirC complex formed in the absence of any effector molecules. The competitive inhibition mode (Fig. 3*A*) suggested that the substrates of PGAM could compete with PGAM–PirC interaction. Indeed, the addition of the PGAM substrates 3-PGA or 2-PGA (for the forward and backward reaction, respectively) had inhibitory effects on complex formation. Addition of 2-PGA inhibited complex formation 2.4 times stronger (IC_{50} = 0.97 mM) than 3-PGA (IC_{50} = 2.4 mM) (Fig. 3*D*). When the metabolites were added at their IC_{50} concentration, 2-PGA (1 mM) increased the K_D of PirC–PGAM interaction to 1,702 nM and 3-PGA (2.4 mM) to 459 nM, respectively (Fig. 3*E* and Table 1).

PirC Deletion Leads to Accumulation of the Metabolites of Lower Glycolysis. The above-described analysis of the PGAM–PirC–P_{II} triad demonstrated inhibition of PGAM activity by PirC, in response to the binding of the C/N-status reporter metabolite 2-OG to P_{II}. This suggests that in wild-type cells, during nitrogen starvation (i.e., when high 2-OG levels accumulate), the inhibition of PGAM by PirC supports the formation of high glycogen levels by diminishing carbon catabolism via lower glycolysis. In the absence of this inhibition (i.e., in the Δ*pirC* mutant), glycogen catabolism via glycolysis increases. To further verify this hypothesis, we monitored over time the levels of metabolites in wild-type and Δ*pirC* mutant cells during the shift from nitrate-replete (NO_3) to nitrogen-depleted (−N) medium. Samples for metabolome analysis were withdrawn after 0, 6, 24, and 48 h from the shift. Nitrogen depletion had the expected effect on the total cellular steady-state metabolite pools (i.e., soluble amino acids were depleted to large extent, while organic acids accumulated), resulting in lowered N/C ratios under −N conditions (*SI Appendix*, Fig. S9). Most organic acids participating in the TCA cycle such as citrate, malate, and succinate accumulated in both strains in a similar manner when shifted to –N conditions (Fig. 4). Also, the products of ammonium assimilation via GS/GOGAT, glutamine (Gln), and glutamate (Glu) showed similar changes in the wild-type and Δ*pirC* strain with rapid decrease in Glu and slower decrease in Gln. Besides these general metabolic responses, in which the Δ*pirC* mutant showed no discernable differences, a few very specific and intriguing differences were recorded at decisive steps: the C/N-status reporter molecule 2-OG accumulated immediately after −N shift in both strains. In the wild-type, the 2-OG levels decreased gradually over the following 48 h, whereas they remained constantly elevated in Δ*pirC* cells, and they even slightly increased (Fig. 4). Moreover, the 3-PGA concentration increased in the wild-type over the course of nitrogen starvation, whereas it gradually declined in the Δ*pirC* mutant. The increasing 3-PGA levels, substrate of the PGAM, in the wild-type cells indicate in vivo inhibition of the PGAM reaction, whereas lack of PGAM inhibition by PirC

Table 1. Kinetic constants of PGAM under varying concentrations of PirC and changes of constants by addition of PirC-interacting molecules

Inhibition of PGAM by PirC at varying concentrations

PirC, nM	K_M, mM	v_{max}, nkat · mg^{-1}	k_{cat}, s^{-1}	$k_{cat} \cdot K_M^{-1}$, $s^{-1} \cdot M^{-1}$
0	0.1266 ± 0.0064	47.54 ± 0.52	2.776 ± 0.030	21959.0 ± 1104.7
200	0.3584 ± 0.0216	44.92 ± 0.75	2.623 ± 0.044	7329.8 ± 441.1
400	0.7056 ± 0.0499	46.56 ± 1.09	2.719 ± 0.063	3859.1 ± 273.0
600	1.376 ± 0.102	47.11 ± 1.39	2.751 ± 0.081	2002.2 ± 148.4
800	1.715 ± 0.145	43.27 ± 4.10	2.526 ± 0.239	1618.7 ± 369.4
Antagonistic effect of P_{II} and its modulation by 2-OG (0.4 mM ATP, 600 nM PirC, and 600 nM P_{II3})				
Modulators of PGAM	K_M, mM	v_{max}, nkat · mg^{-1}	k_{cat}, s^{-1}	$k_{cat} \cdot K_M^{-1}$, $s^{-1} \cdot M^{-1}$
None	0.1499 ± 0.0121	89.76 ± 2.17	5.41 ± 0.13	36097.4 ± 2921.0
PirC	4.0220 ± 1.338	92.80 ± 24.78	5.59 ± 1.49	1390.9 ± 462.7
PirC/P_{II}	0.1855 ± 0.0247	105.90 ± 4.51	6.38 ± 0.27	34409.7 ± 4572.5
PirC/P_{II} + 0.123 mM 2-OG	1.8410 ± 0.5461	142.70 ± 28.47	5.56 ± 1.24	3021.7 ± 896.3
PirC/P_{II} + 1 mM 2-OG	2.887 ± 0.8542	92.28 ± 20.51	8.60 ± 1.72	2980.3 ± 881.8
Binding constants for PGAM–PirC binding and modulation by substrates				
Sample	K_D, nM	IC_{50}, mM		
No Effectors	2.89± 34.49	—		
2-PGA	1702 ± 744 (at IC_{50})	0.97 ± 0.001		
3-PGA	459.1 ± 32.0 (at IC_{50})	2.4 ± 0.001		

Binding constants of PGAM/PirC complex with or without the presence of the substrates.

explains the low 3-PGA levels in the Δ*pirC* mutant. 3-PGA is known as an allosteric activator of the glucose 1-phosphate–adenylyltransferase (GlgC) in bacteria, which catalyzes the initial step of glycogen synthesis (29). Downstream of the PGAM reaction, the levels of pyruvate responded inversely to 3-PGA, with decreasing levels in the wild-type but a strong increase in the Δ*pirC* mutant. The pyruvate level in the mutant was 14-fold higher than in the wild-type after 48 h of N starvation. Again, this observation is consistent with an increased flux through the PGAM reaction due to the missing inhibition by PirC, since the produced 2-PGA is further converted into pyruvate. The increased carbon flux toward pyruvate in the Δ*pirC* mutant lowers the carbon flux toward glycogen and increases the levels of PHB, which is derived from acetyl-CoA (i.e., the immediate reaction product from pyruvate).

Subcellular Localization of PirC. To determine the subcellular localization of PirC during different growth stages, when PirC presumably interacts preferentially with either P_{II} or PGAM, we analyzed cells expressing a PirC–GFP fusion protein (Δ*pirC*::*pirC*–eGFP) by fluorescence microscopy. The eGFP signal was centrally localized in the cytoplasm (*SI Appendix*, Fig. S10) in cells during exponential growth in nitrate-containing BG_{11} medium, conditions that promote binding of PirC to P_{II}. Shifting the cells to nitrogen-depleted medium increased the 2-OG levels (see Fig. 4), which should promote dissociation of the P_{II}–PirC complexes and allow interaction of PirC with PGAM. Accordingly, the localization of PirC–eGFP changed after nitrogen downshift. The centrally localized eGFP signal slowly expanded to the peripheral region of the cytoplasm during the first 24 h after nitrogen starvation, where it then remained throughout chlorosis. This result corroborated the dynamics of PirC interactions and its response to nitrogen limitation.

Discussion

In this study, we identified a key control point of cyanobacterial carbon metabolism, the glycolytic PGAM reaction, converting 3-PGA into 2-PGA. In animal systems, where glycolysis supplies energy, it has been shown that glycolytic breakdown of glucose 6-phosphate is mainly regulated at the phosphofructokinase level according to the energy demand of the cells (30). By contrast, in photoautotrophic organisms, glycolytic steps are used in two directions, in the gluconeogenic direction toward glycogen or starch synthesis and in the glucose catabolic direction, respectively, to produce precursors for multiple biosynthetic routes required for cell growth. The PGAM reaction is at the branch point of newly fixed CO_2. 3-PGA, the first stable reaction product from RubisCO-catalyzed CO_2 fixation, can be metabolized in two directions. Most of it is converted into 2,3-bisphosphoglycerate and further to glyceraldehyde-3-phosphate (GAP), from which the acceptor of RubisCO, ribulose 1,5-bisphosphate, is regenerated via the Calvin cycle reactions. Excess GAP is used via gluconeogenic reactions to synthesize glycogen (in plant starch). Alternatively, 3-PGA can be diverted from the Calvin cycle through its direct conversion to 2-PGA by PGAM. 2-PGA is further metabolized in lower glycolytic reactions, from where the majority of cellular amino acids and lipids are derived in photoautotrophs, with pyruvate, acetyl-CoA, and 2-OG representing key precursors.

The PGAM reaction was previously predicted as a key control point of carbon metabolism by kinetic modeling of the cyanobacterial low-carbon response (20, 21). It was shown that 2-PGA accumulates to high amounts (5 to 7 times) in cells shifted from high CO_2 (5%) to ambient air (0.04% CO_2) in *Synechocystis* (31) as well as in *Synechococcus elongatus* PCC 7942 (32). The high 2-PGA accumulation was taken as an indication that under carbon-limiting conditions, newly fixed organic carbon is directly deviated from the Calvin cycle into lower glycolysis by the PGAM reaction to sustain biosynthesis of amino acids and other cellular compounds. Here, we provide in vitro and in vivo evidence that the reaction catalyzed by the product of the *slr1945* gene, PGAM, represents a key control point for acclimation to nitrogen starvation. This control operates through a regulatory mechanism, in which the small regulatory protein PirC acts as a mediator of the signal from the pervasive P_{II} regulatory protein to tune the activity of PGAM, a control mechanism so far never described for enzymatic reactions. To further understand the competitive inhibition of PGAM by PirC, as demonstrated here through kinetic and binding studies, structural analysis of the enzyme complexes will be required.

According to our model depicted in Fig. 5, P_{II} binds to PirC under nitrogen-sufficient conditions, when 2-OG levels are low, thereby preventing the interaction with PGAM. Efficient conversion of 3-PGA to 2-PGA by highly active PGAM directs newly fixed carbon toward lower glycolysis to support the synthesis of amino acids and fatty acids. Only a minor fraction is converted into glycogen. When the cells experience nitrogen

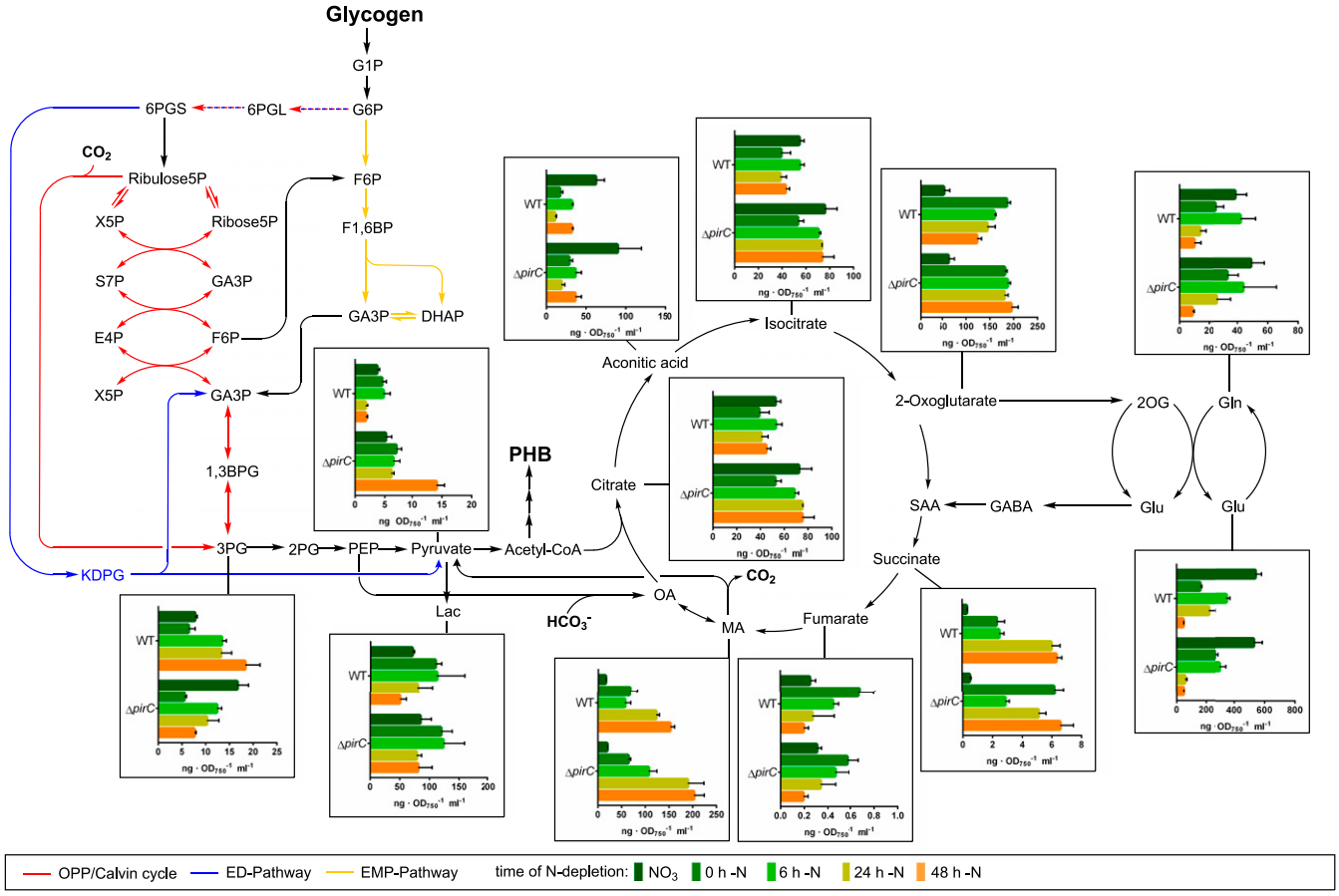

Fig. 4. Time course LC-MS analysis of steady-state levels of relevant metabolites during the short-term shift of wild-type (WT) and Δ*pirC* cells from NO_3 to –N conditions depicted in a metabolic background. Totals of 0 h, 6 h, 24 h, and 48 h indicate the time from nitrogen depletion at which samples were withdrawn from the cultures for analysis. Each bar represents the metabolite level at a certain time point determined from two independent biological replicates each in technical duplicates. The error bars represent the SD of the combined data. The values are in ng per optical density at 750 nm per ml (ng · OD_{750}^{-1} · ml^{-1}). The result of the entire metabolite analysis is shown in *SI Appendix*, Fig. S9.

limitation, they accumulate the intracellular 2-OG levels. As a result of 2-OG binding to P_{II}, the P_{II}–PirC complex dissociates, and PirC interacts with PGAM, thereby inhibiting its enzymatic activity. This is accompanied by a relocalization of the PirC–eGFP signal from the central region of the cell to the periphery. The central localization of PirC–eGFP is indicative of the presence of PirC–P_{II} complexes as P_{II} was previously shown to localize in the central cytoplasm of cells grown in the presence of nitrate (11). As a consequence of the PirC–PGAM interaction, conversion of 3-PGA to 2-PGA is blocked in nitrogen-starved cells, leading to increased 3-PGA levels, which are now redirected toward glycogen. Due to this metabolic switch, the flux toward amino acid synthesis is slowed down, thus adjusting cellular metabolism to the limited supply of nitrogen. Furthermore, 3-PGA is an allosteric activator of GlgC, which catalyzes the initial and regulated step of the glycogen synthesis (29). Hence,

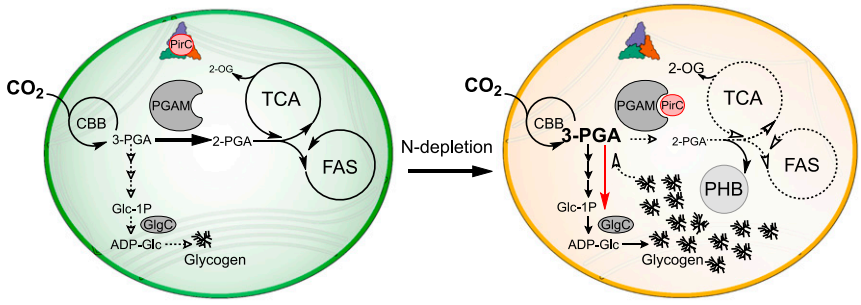

Fig. 5. Model of regulation of central carbon metabolism by PirC, P_{II}, and PGAM interactions. In vegetative cells, when 2-OG levels are low, P_{II} (depicted as trimer in blue, green, and red) binds to PirC and prevents the inhibition of PGAM. PGAM directs 3-PGA downstream to the biosynthesis of fatty acids (FAS) and amino acids mainly via the TCA cycle. When the cells are N depleted, 2-OG levels increase and promote release of PirC from P_{II}. PirC binds to and inhibits PGAM. This results in an elevation of the 3-PGA concentration. 3-PGA enhances the activity of GlgC and directs the carbon flux toward glycogen, resulting in enhanced glycogen accumulation. CBB: Calvin-Benson-Bassham cycle.

the PirC-mediated PGAM inhibition not only slows down lower glycolysis but also stimulates glycogen accumulation via the GlgC activation. The glycogen levels increase until the cells are densely packed with glycogen, which can amount up to 50% of the dry weight in chlorotic cells (15). Already after 24 h of nitrogen starvation, accumulation of glycogen reaches a maximum, and the levels remain high throughout chlorosis. Recent data indicate a constant turnover of glycogen until the cells enter complete dormancy (17). In *Synechocystis*, which expresses the PHB synthesis machinery, acetyl-CoA molecules arising from the residual glycolytic flux during chlorosis are directed toward PHB synthesis. Hence, the amount of PHB steadily increases during prolonged nitrogen starvation. In the Δ*pirC* mutant, PGAM cannot be appropriately inhibited. Therefore, increased flux toward 2-PGA and lower glycolysis leads to a massive accumulation of PHB. In agreement with this model, P_{II}-deficient *Synechocystis* mutants are unable to accumulate PHB during nitrogen-starvation–induced chlorosis (33). In the absence of P_{II}, PirC will constantly inhibit PGAM activity, resulting in decreased levels of metabolites downstream of 2-PGA (10) due to the limited supply of acetyl-CoA for PHB synthesis.

This glycolytic switch at the enzymatic level of PGAM via the small P_{II}-interacting regulatory protein PirC is reminiscent of the control of NtcA-dependent transcription by the small P_{II}-interacting protein PipX. The latter is either complexed to P_{II} under low 2-OG levels or bound to NtcA at elevated 2-OG levels (6). Hence, the two small P_{II}-mediator proteins, PirC as well as PipX, functionally interact to coherently reprogram metabolism and gene expression under low-nitrogen conditions. Through release of the P_{II}–PirC complex in response to increasing 2-OG levels, PirC tunes down PGAM activity. This response is further amplified by the concomitant dissociation of the P_{II}–PipX complex and association of PipX to NtcA, accompanied by NtcA-dependent expression of many low-nitrogen–induced genes, among which is the *pirC* gene. In chlorotic cells, *pirC* (*sll0944*) is among the most strongly up-regulated genes within the entire transcriptome (15), and, accordingly, PirC is one of the most highly enriched proteins during chlorosis (16). In an advanced stage of chlorosis, this strong accumulation of PirC ensures tight inhibition of glycolysis to maintain high glycogen levels, which are required for efficient exit from the dormant state of chlorosis (19).

Through engagement of such mediator proteins, P_{II} can largely expand its regulatory space. In principle, any cellular activity, which can be modulated through interaction with a peptide, could be tuned by P_{II} by engineering the peptide to bind P_{II}, thus providing a new toolbox for synthetic biology. It is also reasonable to speculate that disabling the regulation of PirC can be used for metabolic engineering in cyanobacteria, in particular, for the bioproduction of metabolites derived from lower glycolysis, such as succinate, malate, or lipids as well as fatty acids. Furthermore, cyanobacteria have the potential to synthesize isoprenoids or terpenes via the methylerythritol phosphate pathway whose precursors are pyruvate and GAP (34). In addition, genetically engineered cyanobacteria can be used for the synthesis of heterologous compounds such as l-butanol from acetyl-CoA (35). However, it should be kept in mind that the utility of the PirC mutation is especially beneficial for processes that are performed under nitrogen-limited conditions. As a proof of principle, we took advantage of the redirection of the carbon metabolism toward PHB synthesis in the PirC-deficient mutant to further increase the levels of PHB in the cell: we engineered the PirC-deficient mutant to express the high processive PHB biosynthetic enzymes from *Cupriavidus necator*, resulting in a strain that accumulates more than 80% PHB of cell dry mass under nitrogen-depleted conditions. This is by far the highest accumulation of PHB ever reported in a cyanobacterium (36). This result impressively demonstrates the impact and biotechnological potential of decoupling the regulation by PirC.

Materials and Methods

Full protocols are available in *SI Appendix, SI Materials and Methods*.

Strains and Cultivation. A list of all used strains for this study is provided in *SI Appendix*, Table S1. *Synechocystis* sp. PCC 6803 strains were cultivated in BG_{11} medium according to Rippka (37) either at continuous illumination (~50 $\mu E\ m^{-2} \cdot s^{-1}$) or light–dark conditions (12 h light and 12 h darkness) and 28 °C. For nitrogen depletion, cultures were cultivated in BG-11 media without 17.65 mM $NaNO_3$. Whenever necessary, appropriate antibiotics were added to the different strains to ensure the continuity of the mutation. Cultivation of *E. coli* cultures was performed with lysogeny broth (LB) medium and LB-agar.

Plasmids and Cloning. A list of all used primers, plasmids, and the cloning procedures is in *SI Appendix*, Table S2 as well as in *SI Appendix*, Fig. S4.

Overexpression and Purification of Proteins. Recombinant proteins were overexpressed in *E. coli* Lemo21. His-tag proteins were purified on 1 mL Ni-NTA HisTrap columns (GE Healthcare) as described previously (10). For purification of strep-tagged proteins, 5 mL strep-tactin superflow columns were used as described previously (10). The His-tag of PGAM was removed by Thrombin cleavage using bovine thrombin of Sigma-Aldrich according to protocol (38).

CoIP and Liquid Chromatography–Mass Spectrometry. For CoIP experiments in presence of the P_{II} effector molecules, cells of *Synechocystis* ΔPirC::PirC–mCitrine cultures were harvested after 24 h N depletion and resuspended in 2 mL binding buffer (100 mM Tris [pH 7.5], 100 mM KCl, 1 mM MgCl2, 1 mM DTT, 0.5 mM EDTA, 2 mM ATP, and 2-OG). After lysing the cells, the lysate was centrifuged, and from the supernatant, a volume containing 3 mg of protein was used for the immunoprecipitation using GFP-Trap Magnetic Agarose beads or control beads without antibodies according to the manufacturer's protocol (Chromotek, Planegg-Martinsried, Germany). Bound proteins were eluted by heating in sodium dodecyl sulfate (SDS) loading buffer, and the solution was subjected to short SDS-polyacrylamide gel electrophoresis (PAGE) runs on 12% Bis-Tris Gels (Invitrogen). After staining with Coomassie blue, protein regions were isolated and InGel digested with trypsin as described (39). After cleaning peptides with StageTips (40), liquid chromotography–mass spectometry (LC-MS/MS) analysis was performed on a Q Exactive HF mass spectrometer (Thermo Fisher Scientific, Germany), using linear, segmented 60-min nano liquid chromatography (nanoLC) reversed phase (RP) gradients as described (16). From triplicate experiments, all raw data were processed using MaxQuant software suite (version 1.6.5.0) at default settings. Tandem mass spectrometry peak lists were searched against a target-decoy database of the *Synechocystis* proteome, including the sequence of PirC (Sll0944)–mCitrine. Label-free quantification (LFQ) was used to calculate LFQ intensities for each CoIP sample as described in extended protocol in the supplement.

BLI Using the Octet K2 System. In vitro binding studies were done by BLI using Octet K2 system (FortéBio) as described previously (10). In the first step, P_{II}-His_8 (400 nM, trimeric) or PGAM-His_6 (500 nM) was immobilized on Ni-NTA sensors (FortéBio), followed by a 60-s baseline measurement. For the binding of PirC, the biosensors were dipped into the PirC solution for 180 s (association), with concentrations ranging between 9.375 nM to 1,500 nM. In P_{II}-binding studies, effector molecules ADP, ATP, or 2-OG were added to the binding buffer as indicated and in PGAM binding assays, 2PG or 3 PGA. Finally, the complexes were allowed to dissociate for 300 s. For each binding experiment, a negative control without an interaction partner was performed in parallel. The response in equilibrium (R_{eq}) was calculated using the data analysis software of the Octet System. To calculate the dissociation constant K_D, the concentration versus R_{eq} plots were made for each set of experiments.

Glycogen Measurement and PHB Quantification. Glycogen was quantified according to ref. 19. PHB was detected by high-performance LC as described previously (41).

PGAM Enzymatic Assay. The PGAM activity and the effect of PirC was determined by a coupled enzyme assay as described previous (42, 43) with 10 μg of purified PGAM used in a 1 mL reaction. The reaction mixture containing 20 mM Hepes-KOH (pH 8.0), 100 mM KCl, 5 mM $MgSO_4$, 0.4 mM $MnCl_2$, 50 $\mu g \cdot ml^{-1}$ BSA, 1 mM DTT, 0.4 mM ADP, 0.2 mM NADH, 0.5 U enolase (Sigma Aldrich), 2 U Pyruvate kinase (Sigma Aldrich), 2 U Lactate dehydrogenase

(Roche), and 10 μg PGAM was prewarmed to 30 °C. The assay was started by adding the 3-PGA solutions. The resulted decrease of NADH over time was recorded with Specord50 (Jena Analytics) at 340 nm. As blank, an assay without 3-PGA was performed.

Fluorescence Microscopy and TEM. The visualization of PHB granules was done by phase contrast fluorescence microscopy using the Leica DM5500 B with the Leica CTR 5500 illuminator as described previously. Electron microscopic pictures of lead-citrate– and uranyl-acetate–stained microtome sections of glutaraldehyde and potassium-permanganate–fixed *Synechocystis* cells were prepared as described (44). The samples were then examined using a Philips Tecnai 10 electron microscope at 80 kHz.

Metabolome Analysis. For metabolome analysis by LC-MS, *Synechocystis* was cultivated in 200 mL under N depletion as described previously for 48 h under continuous lightning. The sampling was carried out 0, 6, 24, and 48 h after the shift. Samples of 5 mL liquid culture were quickly harvested onto nitrocellulose membrane filters and subjected to metabolome analytics as detailed in *SI Appendix*.

Data Availability. Proteome raw data files acquired by mass spectrometry were deposited at the ProteomeXchange Consortium via the Proteomics Identifications Database partner repository (45) under the identifier PXD021415.

ACKNOWLEDGMENTS. The project was funded by grants from the German Research Foundation (DFG) Fo195/9-2 and as part of the research group (FOR2816) SCyCode "The Autotrophy-Heterotrophy Switch in Cyanobacteria: Coherent Decision-Making at Multiple Regulatory Layers" to M.H. (HA 2002/23-1) and B.M. (MA 4918/4-1). LC-MS/MS systems at the Department of Quantitative Proteomics were supported through the DFG grants INST 37/935-1 and INST 37/741-1 FUGG. The LC-MS/MS equipment at University of Rostock was financed through the HBFG program (GZ: INST 264/125-1 FUGG). The work was further supported by infrastructural funding from the DFG Cluster of Excellence EXC 2124 Controlling Microbes to Fight Infections. We thank Libera Lo Presti for proofreading the manuscript, Karl-Heinz Grenzendorf for technical assistance in protein purification, and Claudia Menzel for TEM preparations. We want to acknowledge Alexander Klotz for initial contributions on Sll0944 research.

1. M. Y. Galperin, A census of membrane-bound and intracellular signal transduction proteins in bacteria: Bacterial IQ, extroverts and introverts. *BMC Microbiol.* **5**, 35 (2005).
2. K. A. Selim, E. Ermilova, K. Forchhammer, From cyanobacteria to archaeplastida: New evolutionary insights into P_{II} signalling in the plant kingdom. *New Phytol.* **227**, 722–731 (2020).
3. K. Forchhammer, K. A. Selim, Carbon/nitrogen homeostasis control in cyanobacteria. *FEMS Microbiol. Rev.* **44**, 33–53 (2020).
4. L. F. Huergo, R. Dixon, The emergence of 2-oxoglutarate as a master regulator metabolite. *Microbiol. Mol. Biol. Rev.* **79**, 419–435 (2015).
5. K. Forchhammer, J. Lüddecke, Sensory properties of the P_{II} signalling protein family. *FEBS J.* **283**, 425–437 (2016).
6. A. Forcada-Nadal, J. L. Llácer, A. Contreras, C. Marco-Marín, V. Rubio, The P_{II}-NAGK-PipX-NtcA regulatory axis of cyanobacteria: A tale of changing partners, allosteric effectors and non-covalent interactions. *Front. Mol. Biosci.* **5**, 91 (2018).
7. S. Burillo, I. Luque, I. Fuentes, A. Contreras, Interactions between the nitrogen signal transduction protein P_{II} and N-acetyl glutamate kinase in organisms that perform oxygenic photosynthesis. *J. Bacteriol.* **186**, 3346–3354 (2004).
8. A. Heinrich, M. Maheswaran, U. Ruppert, K. Forchhammer, The Synechococcus elongatus P signal transduction protein controls arginine synthesis by complex formation with N-acetyl-L-glutamate kinase. *Mol. Microbiol.* **52**, 1303–1314 (2004).
9. Y.-M. Zhang, S. W. White, C. O. Rock, Inhibiting bacterial fatty acid synthesis. *J. Biol. Chem.* **281**, 17541–17544 (2006).
10. J. Scholl, L. Dengler, L. Bader, K. Forchhammer, Phosphoenolpyruvate carboxylase from the cyanobacterium Synechocystis sp. PCC 6803 is under global metabolic control by P_{II} signaling. *Mol. Microbiol.* **114**, 292–307 (2020).
11. A. R. S. Santos *et al*., NAD^+ biosynthesis in bacteria is controlled by global carbon/nitrogen levels via PII signaling. *J. Biol. Chem.* **295**, 6165–6176 (2020).
12. B. Watzer *et al*., The signal transduction protein P_{II} controls ammonium, nitrate and urea uptake in cyanobacteria. *Front. Microbiol.* **10**, 1428 (2019).
13. J. Giner-Lamia *et al*., Identification of the direct regulon of NtcA during early acclimation to nitrogen starvation in the cyanobacterium Synechocystis sp. PCC 6803. *Nucleic Acids Res.* **45**, 11800–11820 (2017).
14. J. Espinosa, K. Forchhammer, S. Burillo, A. Contreras, Interaction network in cyanobacterial nitrogen regulation: PipX, a protein that interacts in a 2-oxoglutarate dependent manner with P_{II} and NtcA. *Mol. Microbiol.* **61**, 457–469 (2006).
15. A. Klotz *et al*., Awakening of a dormant cyanobacterium from nitrogen chlorosis reveals a genetically determined program. *Curr. Biol.* **26**, 2862–2872 (2016).
16. P. Spät, A. Klotz, S. Rexroth, B. Maček, K. Forchhammer, Chlorosis as a developmental program in cyanobacteria: The proteomic fundament for survival and awakening. *Mol. Cell. Proteomics* **17**, 1650–1669 (2018).
17. M. Koch, S. Doello, K. Gutekunst, K. Forchhammer, PHB is produced from glycogen turn-over during nitrogen starvation in *Synechocystis* sp. PCC 6803. *Int. J. Mol. Sci.* **20**, 20 (2019).
18. M. Koch, K. W. Berendzen, A. K. Forchhammer, On the role and production of polyhydroxybutyrate (PHB) in the cyanobacterium *Synechocystis* sp. PCC 6803. *Life (Basel)* **10**, 10 (2020).
19. S. Doello, A. Klotz, A. Makowka, K. Gutekunst, K. Forchhammer, A specific glycogen mobilization strategy enables rapid awakening of dormant cyanobacteria from chlorosis. *Plant Physiol.* **177**, 594–603 (2018).
20. J. Jablonsky, M. Hagemann, D. Schwarz, O. Wolkenhauer, Phosphoglycerate mutases function as reverse regulated isoenzymes in Synechococcus elongatus PCC 7942. *PLoS One* **8**, e58281 (2013).
21. J. Jablonsky, D. Schwarz, M. Hagemann, Multi-level kinetic model explaining diverse roles of isozymes in prokaryotes. *PLoS One* **9**, e105292 (2014).
22. M. F. Vázquez-Bermúdez, E. Flores, A. Herrero, Analysis of binding sites for the nitrogen-control transcription factor NtcA in the promoters of Synechococcus nitrogen-regulated genes. *Biochim. Biophys. Acta* **1578**, 95–98 (2002).
23. T.-Y. Lin *et al*., The Elongator subunit Elp3 is a non-canonical tRNA acetyltransferase. *Nat. Commun.* **10**, 625 (2019).
24. J. Mitschke *et al*., An experimentally anchored map of transcriptional start sites in the model cyanobacterium Synechocystis sp. PCC6803. *Proc. Natl. Acad. Sci. U.S.A.* **108**, 2124–2129 (2011).
25. K. Zeth, O. Fokina, K. Forchhammer, Structural basis and target-specific modulation of ADP sensing by the Synechococcus elongatus P_{II} signaling protein. *J. Biol. Chem.* **289**, 8960–8972 (2014).
26. O. Fokina, V.-R. Chellamuthu, K. Forchhammer, K. Zeth, Mechanism of 2-oxoglutarate signaling by the Synechococcus elongatus P_{II} signal transduction protein. *Proc. Natl. Acad. Sci. U.S.A.* **107**, 19760–19765 (2010).
27. F. Cai *et al*., The structure of CcmP, a tandem bacterial microcompartment domain protein from the β-carboxysome, forms a subcompartment within a microcompartment. *J. Biol. Chem.* **288**, 16055–16063 (2013).
28. A. M. Larsson, D. Hasse, K. Valegård, I. Andersson, Crystal structures of β-carboxysome shell protein CcmP: Ligand binding correlates with the closed or open central pore. *J. Exp. Bot.* **68**, 3857–3867 (2017).
29. J. Preiss, Bacterial glycogen synthesis and its regulation. *Annu. Rev. Microbiol.* **38**, 419–458 (1984).
30. L. B. Tanner *et al*., Four key steps control glycolytic flux in mammalian cells. *Cell Syst.* **7**, 49–62.e8 (2018).
31. M. Eisenhut *et al*., Metabolome phenotyping of inorganic carbon limitation in cells of the wild type and photorespiratory mutants of the cyanobacterium Synechocystis sp. strain PCC 6803. *Plant Physiol.* **148**, 2109–2120 (2008).
32. D. Schwarz *et al*., Metabolic and transcriptomic phenotyping of inorganic carbon acclimation in the Cyanobacterium Synechococcus elongatus PCC 7942. *Plant Physiol.* **155**, 1640–1655 (2011).
33. W. Hauf, "Regulation of carbon polymer accumulation in Synechocystis sp. PCC 6803," PhD thesis, University of Tübingen, Tübingen, Germany (2016).
34. B. Pattanaik, P. Lindberg, Terpenoids and their biosynthesis in cyanobacteria. *Life (Basel)* **5**, 269–293 (2015).
35. J. Anfelt *et al*., Genetic and nutrient modulation of acetyl-CoA levels in Synechocystis for n-butanol production. *Microb. Cell Fact.* **14**, 167 (2015).
36. M. Koch *et al*., Maximizing PHB content in Synechocystis sp. PCC 6803: Development of a new photosynthetic overproduction strain. *Microb. Cell Fact.* **19**, 231, https://doi.org/10.1101/2020.10.22.350660 (2020).
37. R. Y. Stanier, J. Deruelles, R. Rippka, M. Herdman, J. B. Waterbury, Generic assignments, strain histories and properties of pure cultures of cyanobacteria. *Microbiology* **111**, 1–61 (1979).
38. K. L. Guan, J. E. Dixon, Eukaryotic proteins expressed in Escherichia coli: An improved thrombin cleavage and purification procedure of fusion proteins with glutathione S-transferase. *Anal. Biochem.* **192**, 262–267 (1991).
39. A. Shevchenko, H. Tomas, J. Havlis, J. V. Olsen, M. Mann, In-gel digestion for mass spectrometric characterization of proteins and proteomes. *Nat. Protoc.* **1**, 2856–2860 (2006).
40. J. Rappsilber, M. Mann, Y. Ishihama, Protocol for micro-purification, enrichment, pre-fractionation and storage of peptides for proteomics using StageTips. *Nat. Protoc.* **2**, 1896–1906 (2007).
41. M. Koch, T. Orthwein, J. T. Alford, K. Forchhammer, The Slr0058 protein from *Synechocystis* sp. PCC 6803 is a novel regulatory protein involved in PHB granule formation. *Front. Microbiol.* **11**, 809 (2020).
42. M. Chander, B. Setlow, P. Setlow, The enzymatic activity of phosphoglycerate mutase from gram-positive endospore-forming bacteria requires Mn2+ and is pH sensitive. *Can. J. Microbiol.* **44**, 759–767 (1998).
43. N. J. Kuhn, B. Setlow, P. Setlow, Manganese(II) activation of 3-phosphoglycerate mutase of Bacillus megaterium: pH-sensitive interconversion of active and inactive forms. *Arch. Biochem. Biophys.* **306**, 342–349 (1993).
44. G. Fiedler, M. Arnold, S. Hannus, I. Maldener, The DevBCA exporter is essential for envelope formation in heterocysts of the cyanobacterium Anabaena sp. strain PCC 7120. *Mol. Microbiol.* **27**, 1193–1202 (1998).
45. Y. Perez-Riverol *et al*., The PRIDE database and related tools and resources in 2019: Improving support for quantification data. *Nucleic Acids Res.* **47**, D442–D450 (2019).

Publication 2

Kinetic Analysis of a Protein-protein Complex to Determine its Dissociation Constant (KD) and the Effective Concentration (EC50) of an Interplaying Effector Molecule Using Bio-layer Interferometry

Tim Orthwein, Luciano F. Huergo, Karl Forchhammer and Khaled A. Selim

Available at: DOI: 10.21769/BioProtoc.4152

Please cite this article as: Orthwein, T. *et al.* (2021). Kinetic Analysis of a Protein-protein Complex to Determine its Dissociation Constant (K_D) and the Effective Concentration (EC_{50}) of an Interplaying Effector Molecule Using Bio-layer Interferometry. *Bio-protocol* 11(17): e4152. DOI: 10.21769/BioProtoc.4152.

bio-protocol www.bio-protocol.org/4152 Bio-protocol 11(17): e4152. DOI:10.21769/BioProtoc.4152

Kinetic Analysis of a Protein-protein Complex to Determine its Dissociation Constant (K_D) and the Effective Concentration (EC_{50}) of an Interplaying Effector Molecule Using Bio-layer Interferometry

Tim Orthwein[1, *], Luciano F. Huergo[2], Karl Forchhammer[1] and Khaled A. Selim[1, 3, 4, *]

[1]Organismic Interactions Department, Interfaculty Institute for Microbiology and Infection Medicine, Cluster of Excellence 'Controlling Microbes to Fight Infections', Tübingen University, Auf der Morgenstelle 28, 72076 Tübingen, Germany; [2]Setor Litoral, Federal University of Paraná (UFPR), Matinhos, Brazil; [3]Department of Protein Evolution, Max Planck Institute for Developmental Biology, Tübingen, Germany; [4]Pharmaceutical and Drug Industries Research Division, National Research Center, Giza, Egypt

*For correspondence: tim.orthwein@uni-tuebingen.de; khaled.selim@uni-tuebingen.de

[Abstract] Biolayer interferometry (BLI) is an emerging analytical tool that allows the study of protein complexes in real time to determine protein complex kinetic parameters. This article describes a protocol to determine the K_D of a protein complex using a 6×His tagged fusion protein as bait immobilized on the NTA sensor chip of the FortéBio® Octet K2 System (Sartorius). We also describe how to determine the half maximal effective concentration (EC_{50}, also known as IC_{50} for inhibiting effectors) of a metabolite. The complete protocol allows the determination of protein complex K_D and small molecular effector EC_{50} within 8 h, measured in triplicates.

Graphic abstract:

Please cite this article as: Orthwein, T. *et al.* (2021). Kinetic Analysis of a Protein-protein Complex to Determine its Dissociation Constant (K_D) and the Effective Concentration (EC_{50}) of an Interplaying Effector Molecule Using Bio-layer Interferometry. *Bio-protocol* 11(17): e4152. DOI: 10.21769/BioProtoc.4152.

bio-protocol www.bio-protocol.org/4152 Bio-protocol 11(17): e4152. DOI:10.21769/BioProtoc.4152

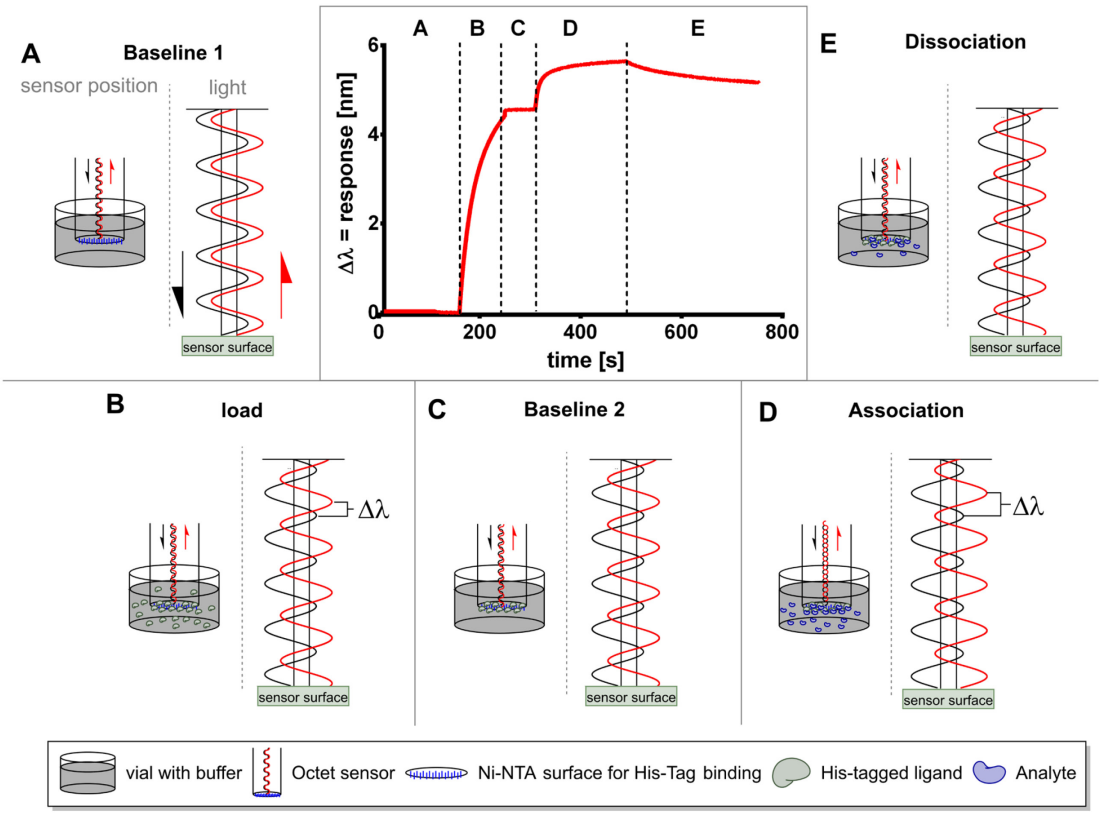

Principle of the Biolayer interferometry measurement. (Middle, top) Exemplary result of the BLI measurement using Octet® (Raw Data). Wavelength shift (Δλ) against time. (A) Baseline 1. Baseline measurement. When the sensor is equilibrated in the kinetics buffer. The light is reflected with no difference. (B) Load. The his-tagged proteins (ligand) are loaded onto the sensor surface. The light is reflected with a shift of the wavelength. (C) Baseline 2. The loaded sensor is equilibrated in the kinetics buffer. No further wavelength shift appears. (D) Association. The loaded sensor is dipped into the analyte solution. The analyte binds to the immobilized ligand along with an increased wavelength shift. (E) Dissociation. Afterward, the sensor is dipped again into the kinetics buffer without the analyte. Some analyte molecules dissociate. The wavelength shift decreases. (Subfigures A-E) The left side shows the position of the sensor during the measurement seen in the representative BLI measurement, marked with the figure label. The right side shows the light path in the sensor. Black waves represent the light emitted to the sensor surface. The red waves show the light reflected from the sensor surface back to the detector.

Keywords: Protein-protein interaction, Biolayer interferometry, Binding kinetics, K_D, IC_{50}, EC_{50}, PII signaling protein

[Background] The Investigation of protein-protein interactions is an important field in life sciences since protein interactions play crucial roles in living organisms. Many biochemical and physiological reactions are under the control of proteins that require physical communication to other proteins within the cell. For example, human cell invasion by SARS-CoV-2 starts with interactions between the viral Spike

Please cite this article as: Orthwein, T. *et al.* (2021). Kinetic Analysis of a Protein-protein Complex to Determine its Dissociation Constant (K_D) and the Effective Concentration (EC_{50}) of an Interplaying Effector Molecule Using Bio-layer Interferometry. *Bio-protocol* 11(17): e4152. DOI: 10.21769/BioProtoc.4152.

protein and the human ACE2 receptor (Shang *et al.*, 2020). Determination of the kinetic and affinity parameters of specific protein complexes provides important information about their properties and helps to discover their function and regulatory properties. Furthermore, the determination of the half maximal effective concentration (EC_{50}) of a metabolite, which inhibits or enhances protein complex formation, is crucial for the understanding of regulatory mechanisms and/or the development of drugs to combat infectious diseases.

Several methods are available to study protein interactions in real time, such as biolayer interferometry (BLI), surface plasmon resonance (SPR), or isothermal titration calorimetry (ITC). BLI is an emergent optical analytic technique that provides a good trade-off between sensitivity, cost intensity, reproducibility, and the ability for high-throughput measurements. The physics of BLI is based on the principle of a wavelength shift when white light is reflected from two layers, first from an internal reference layer and second from a protein coated layer (FortéBio, 2005-2006). The wavelength shift is detected by the machine and is recorded over time. The length of the shift is proportional to the bound proteins on the layer and can be used to calculate the binding affinities and kinetics. Compared to ITC, BLI measurement requires lower amounts of the target proteins, which is especially important for proteins that are difficult to express and purify, *e.g.*, membrane proteins. BLI has lower sensitivity compared to SPR methods; however, in terms of equipment maintenance, BLI is advantageous compared to the micro-fluidic SPR systems, which are prone to clogging and require high sample purity, buffer degassing, and constant maintenance of the sensor chips and micro-fluidic devices. In addition, BLI is tolerant to the use of analytes in complex matrices (Shah and Duncan, 2014), enabling high-throughput measurements of crude analyte preparations.

Recently, we employed BLI to characterize the interaction between the P_{II} signaling proteins and different binding target proteins, including NAD synthetase (NadE), phosphoenolpyruvate carboxylase (PEPC), P_{II}-**i**nteracting regulator of arginine synthesis (PirA), and P_{II}-**i**nteracting regulator of carbon metabolism (PirC) (Santos *et al.*, 2020; Scholl *et al.*, 2020; Bolay *et al.*, 2021; Orthwein *et al.*, 2021). P_{II} proteins sense the cellular energy state through the competitive binding of ATP and ADP, and sense carbon/nitrogen balance through binding of the citric acid cycle metabolite 2-oxoglutarate (2-OG) (Forchhammer and Selim, 2020; Selim *et al.*, 2020). Here, we describe a robust, simple, and quick protocol for the detection of protein interactions using a His-tagged bait protein (ligand) and a non-His-tagged prey protein (analyte). The BLI measurements were performed using a FortéBio® Octet K2 system (Sartorius). The protocol describes the procedure to determine the dissociation constant (K_D) of the protein complex and also the EC_{50} of small effector molecules (2-OG here), which can promote or disrupt the protein complex. The protocol is exemplified using the P_{II} protein from the unicellular cyanobacterium *Synechocystis* sp PCC 6803 for studying P_{II}-PirC interactions. In cyanobacteria, the interaction between P_{II}-PirC regulates the central carbon metabolism in response to the intracellular concentrations of the carbon/nitrogen indicator 2-OG (Orthwein *et al.*, 2021).

Please cite this article as: Orthwein, T. *et al.* (2021). Kinetic Analysis of a Protein-protein Complex to Determine its Dissociation Constant (K_D) and the Effective Concentration (EC_{50}) of an Interplaying Effector Molecule Using Bio-layer Interferometry. *Bio-protocol* 11(17): e4152. DOI: 10.21769/BioProtoc.4152.

Materials and Reagents

1. Microplate, 96-well plate, PS, F-Bottom (Chimney well) Black, Non-Binding (Greiner Bio-One, catalog number: 655900)
2. HEPES (Thermo Scientific, Fischer Bioreagents, catalog number: BP-310)
3. KOH (Merck, Millipore, catalog number: 1.05033)
4. Nonident-P40 (Thermo Fischer Scientific, Fluka, catalog number: 74358)
5. KCl (Carl Roth, catalog number: 6781.1)
6. $MgCl_2 \cdot 6H_2O$ (Merck, Millipore, catalog number: 7791-18-6)
7. ATP (store at -20°C) (Carl Roth, catalog number: K054.3)
8. α-ketoglutaric acid disodium salt hydrate (store at 4°C) (Thermo Fischer Scientific, Fluka, catalog number: K3752) – another name for 2-oxoglutarate (2-OG)
9. Glycine (Merck, Sigma-Aldrich, catalog number: 33226)
10. $NiCl_2 \cdot 6H_2O$ (Carl Roth, catalog number: 4489.1)
11. Kinetics buffer (see Recipes)

Equipment

1. Ni-NTA (NTA) Dip and Read™ Biosensors (tray) (Sartorius, FortéBio®, catalog number: 18-5103)
2. FortéBio® Octet K2 System (Sartorius)

Software

1. Data Acquisition 11.0.0.64 (FortéBio®, https://www.sartorius.com/en/products/protein-analysis/octet-systems-software)
2. Data Analysis HT 11.0.0.50 (FortéBio®, https://www.sartorius.com/en/products/protein-analysis/octet-systems-software)
3. Prism, Version 6.01 or higher (GraphPad Software Inc.)

Procedure

For this protocol, we used purified 6×His-tagged P_{II} protein as the bait protein (ligand) and a Strep-tagged PirC protein (analyte), as described previously (Orthwein *et al.*, 2021). It is recommended to use 5-25 µg/ml of ligand per well of a 96-well plate when loading the proteins onto the Ni-NTA biosensors. A purified ligand concentration of 0.5 mg/ml in 500 µl at a minimum is needed to perform 50 measurements if 25 µg/ml is used in the assay. This provides an acceptable dilution of the kinetics buffer with a sufficient amount of protein. A minimum analyte molar concentration that is 5-times higher is needed.

Note: It is possible to store your proteins in a buffer containing glycerol.

An overview of the method: The ligand is loaded specifically onto the Ni-NTA sensor tips via the 6× His-

Please cite this article as: Orthwein, T. *et al.* (2021). Kinetic Analysis of a Protein-protein Complex to Determine its Dissociation Constant (K_D) and the Effective Concentration (EC_{50}) of an Interplaying Effector Molecule Using Bio-layer Interferometry. *Bio-protocol* 11(17): e4152. DOI: 10.21769/BioProtoc.4152.

tag tail (loading) followed by a washing step in kinetics buffer. The loaded tips are then dipped into the analyte solution to measure the complex formation (association), indicated by an increasing signal. Afterward, the sensors with the complex are dipped back into the kinetic buffer (decreased signal dissociation). Before and after the procedure, the sensors are washed and regenerated with an acidic 10 mM glycine solution (pH 1.7) and a 10 mM $NiCl_2$ solution. The software calculates the response in equilibrium (R_{eq}) using the association and dissociation signal. The values of R_{eq} for each analyte concentration are plotted in a graph (R_{eq} against the analyte concentration), which is used for the determination of the kinetics parameters. For this purpose, the measurement is performed with different concentrations of the analyte to determine the K_D and with different concentrations of the effector to determine the EC_{50}. The R_{eq} values are then plotted against the related analyte concentrations. For EC_{50} determination, the values are transformed and the relative response is plotted against the $\log_{10}$ of the analyte. Afterward, kinetic analysis with a statistical software (*e.g.*, GraphPad Prism) is performed for the calculation of the kinetic parameters.

A. Bio-layer interferometry kinetic binding assay

The assay was performed using the FortéBio® Octet K2 System (Sartorius).

Note: Make sure that other tags used for the analyte do not interact with poly histidine (possibly metalloproteins) or bind non-specifically to Ni-NTA. It is possible to use a His-tagged protein as an analyte after the cleavage removal of the tag; however, it is not recommended. Test this via trial loading experiments of the analyte onto the biosensor. If there is a signal, there is unspecific binding of the analyte. If there is non-specific binding of the analyte, it is recommended to load the remaining loading positions with a His-tagged protein that does not interact with the analyte. For triplicates, measure three times with newly prepared 96-well plates.

1. Switch on the machine and prewarm the sample holder for a minimum of 30 min. Adjust the working temperature of choice.

   Note: We used 30 °C because of the growth temperature of cyanobacteria.

2. Prepare the kinetics buffer, the sensor washing solution, *i.e.*, 10 mM glycine pH 1.7 (adjust pH with HCl), and the regeneration solution, *i.e.*, 10 mM $NiCl_2$.

   Note: The optimal conditions for interaction depend on the proteins under study. A preliminary buffer screening test (e.g., different pH and salts) may be required to determine the optimal conditions for protein-protein interaction. We used the kinetics buffer described in the recipes section.

3. Dilute the ligand in the kinetics buffer for the Ni-NTA sensor tip loading.

   Note: The optimal concentration of the ligand should be tested before the start of the kinetic protein-protein interaction assay. For this, perform a trial loading experiment with different ligand concentrations. The manufacturer protocol recommends a ligand concentration between 5-25 µg/ml. We used concentrations that did not exceed a binding signal of $\Delta\lambda$ = 5 nm.

4. Prepare a dilution series of 7 different concentrations of the analyte.

   Note: We recommend starting the dilution with ~10x the expected K_D, as described in the

Please cite this article as: Orthwein, T. *et al.* (2021). Kinetic Analysis of a Protein-protein Complex to Determine its Dissociation Constant (K_D) and the Effective Concentration (EC_{50}) of an Interplaying Effector Molecule Using Bio-layer Interferometry. *Bio-protocol* 11(17): e4152. DOI: 10.21769/BioProtoc.4152.

manufacturer protocol.

5. Fill the vials of the 96-well plate with 200 µl of solutions as shown in Figure 1.

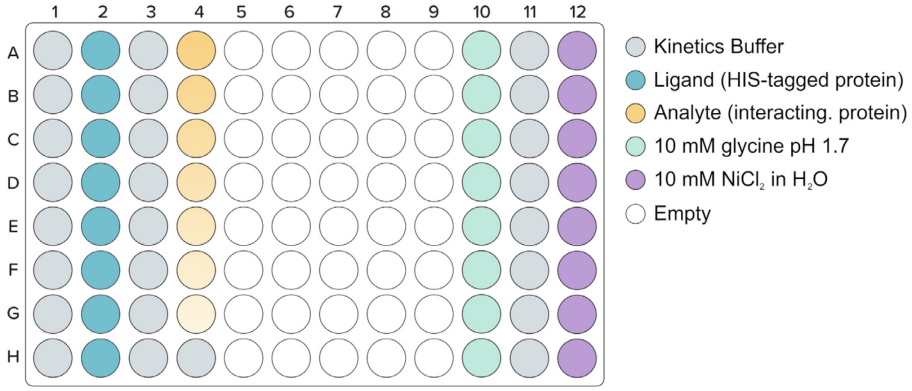

Figure 1. Pipetting scheme of the 96-well plate for a kinetic assay. Column 4 contains the dilution series from the highest (A) to the lowest concentration (G) of the analyte. Vial 4H contains the control without analyte. Adapted from the manufacturer protocol - technical note Ni-NTA biosensor kinetic assays (FortéBio, 2019).

6. Place your plate in the machine for prewarming.
7. Define the experiment in Data Acquisition 11.0.0.64 (Sartorius, FortéBio®) by following the top menu and start the measurement.
   a. Plate definition: Define the plate position and enter additional information in the table, as shown in Figure 2.

Please cite this article as: Orthwein, T. *et al.* (2021). Kinetic Analysis of a Protein-protein Complex to Determine its Dissociation Constant (K_D) and the Effective Concentration (EC_{50}) of an Interplaying Effector Molecule Using Bio-layer Interferometry. *Bio-protocol* 11(17): e4152. DOI: 10.21769/BioProtoc.4152.

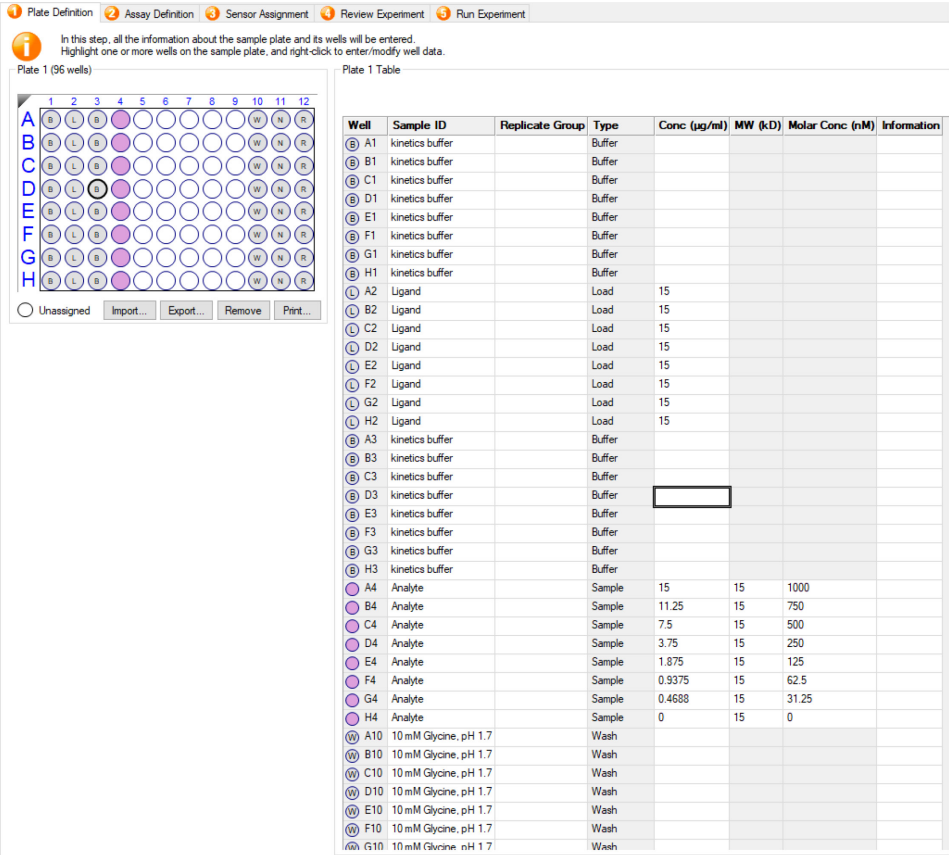

Well	Sample ID	Replicate Group	Type	Conc (µg/ml)	MW (kD)	Molar Conc (nM)	Information
B A1	kinetics buffer		Buffer				
B B1	kinetics buffer		Buffer				
B C1	kinetics buffer		Buffer				
B D1	kinetics buffer		Buffer				
B E1	kinetics buffer		Buffer				
B F1	kinetics buffer		Buffer				
B G1	kinetics buffer		Buffer				
B H1	kinetics buffer		Buffer				
L A2	Ligand		Load	15			
L B2	Ligand		Load	15			
L C2	Ligand		Load	15			
L D2	Ligand		Load	15			
L E2	Ligand		Load	15			
L F2	Ligand		Load	15			
L G2	Ligand		Load	15			
L H2	Ligand		Load	15			
B A3	kinetics buffer		Buffer				
B B3	kinetics buffer		Buffer				
B C3	kinetics buffer		Buffer				
B D3	kinetics buffer		Buffer				
B E3	kinetics buffer		Buffer				
B F3	kinetics buffer		Buffer				
B G3	kinetics buffer		Buffer				
B H3	kinetics buffer		Buffer				
A4	Analyte		Sample	15	15	1000	
B4	Analyte		Sample	11.25	15	750	
C4	Analyte		Sample	7.5	15	500	
D4	Analyte		Sample	3.75	15	250	
E4	Analyte		Sample	1.875	15	125	
F4	Analyte		Sample	0.9375	15	62.5	
G4	Analyte		Sample	0.4688	15	31.25	
H4	Analyte		Sample	0	15	0	
W A10	10 mM Glycine, pH 1.7		Wash				
W B10	10 mM Glycine, pH 1.7		Wash				
W C10	10 mM Glycine, pH 1.7		Wash				
W D10	10 mM Glycine, pH 1.7		Wash				
W E10	10 mM Glycine, pH 1.7		Wash				
W F10	10 mM Glycine, pH 1.7		Wash				
W G10	10 mM Glycine, pH 1.7		Wash				

Figure 2. Plate definition and sample information table. Definitions: (1A-H) Buffer, (2A-H) Loading, (3A-H) Buffer, (4A-H) Sample, (10A-H) Wash, (11A H) Neutralization, and (12A-H) Regeneration. Concentrations are example values.

Note: Use the concentrations and MW of your analyte.

b. Assay Definition. Define the assay as shown in Figure 3.

Note: The time of the association and dissociation steps depends on the proteins under study. For kinetic investigation, we suggest determining the optimal association and dissociation times by performing preliminary assays using different association/dissociation times ranging between 2-10 min and using saturating concentrations of the analyte (~10× the expected K_D). Define the assay steps method for row A and B. Mark the assay step list and click "Replicate" to clone the steps for the other rows (> Replicate> Replication type: add a new assay > Offset step > vertically > OK).

Please cite this article as: Orthwein, T. *et al.* (2021). Kinetic Analysis of a Protein-protein Complex to Determine its Dissociation Constant (K_D) and the Effective Concentration (EC_{50}) of an Interplaying Effector Molecule Using Bio-layer Interferometry. *Bio-protocol* 11(17): e4152. DOI: 10.21769/BioProtoc.4152.

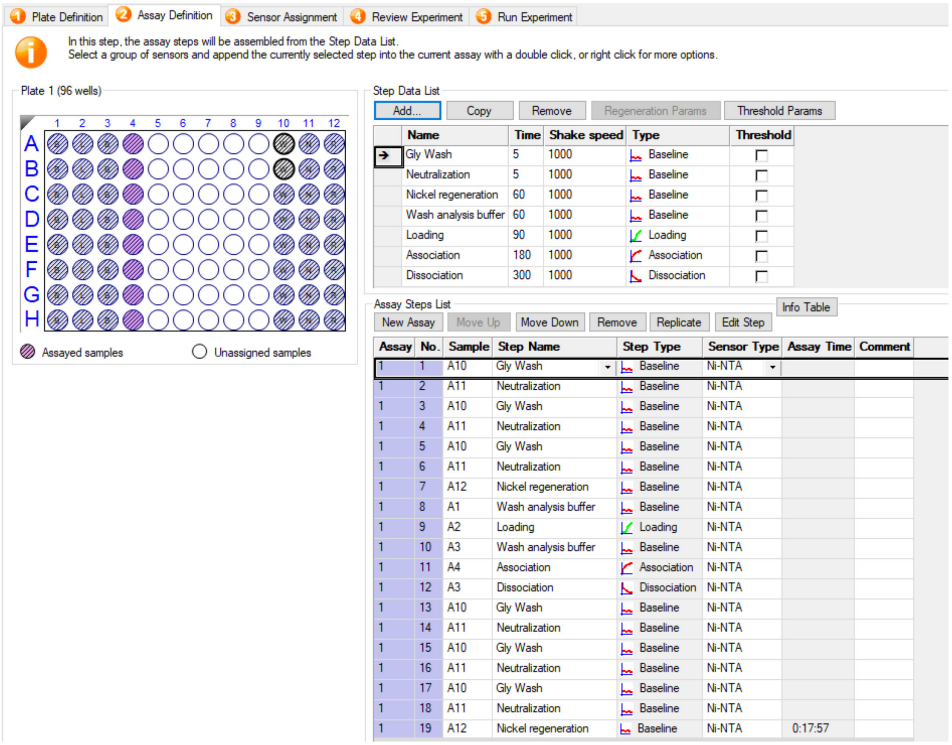

Figure 3. Assay definition for the kinetic binding assay

c. Sensor Assignment. Assign the Sensors in the correct line.

d. Review Experiment. Review your experiment.

e. Run Experiment. Define the localization, name the results and start the experiment.
Note: If you wet your biosensors immediately before, use click on "delayed experiment starts: 600 s". Do this also if you did not prewarm your plates previous to the experiment.

B. Determination of the EC_{50} of a small effector molecule (effector) that interferes in the protein-protein complex

1. Prepare a dilution series of the investigated effector.
Note: In the example, we used the 2-OG metabolite as it inhibits the P_{II}-PirC complex. Prepare a dilution series of the effector without the analyte for the pre-washing step (to be used to fill the wells in column 3) and a dilution series that contains the analyte (constant amount of analyte in each dilution of the effector) for analyte binding (to be used to fill the wells in column 4). The analyte should be used in amounts enabling saturation of the ligand as determined from the previous kinetic data.
2. Fill the vials of the 96-well plate with 200 µl of solutions as shown in Figure 4.

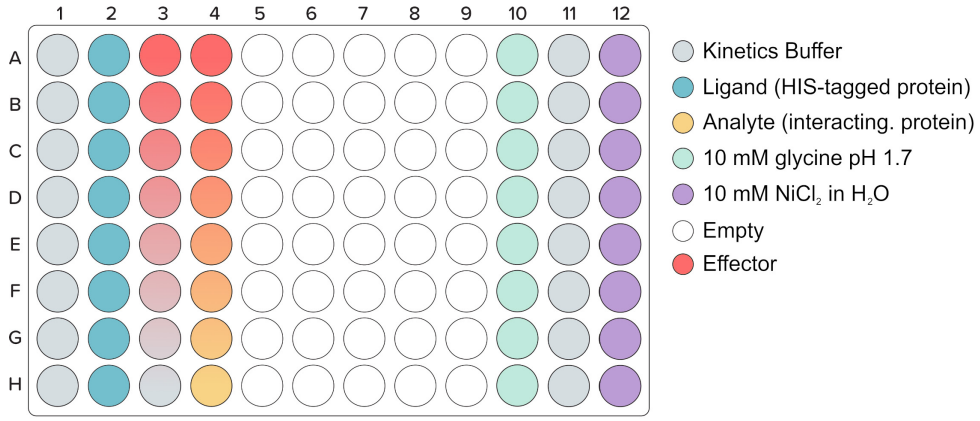

Figure 4. Pipetting scheme of the 96-well plate for a determination of the EC_{50} for an effector that affects the stability of the protein complex. Columns 3 and 4 contain dilution series of the effector from highest (A) to lowest concentrations (G), without and with constant amount of analyte, respectively. Vial 4H contains the control without the effector [adapted from the manufacturer protocol – technical note Ni-NTA biosensor kinetic assays (FortéBio, 2019)].

3. Repeat Steps A6 and A7.

Data analysis

A. Kinetic binding assay
   1. Start the Data Analysis HT 11.0.0.50 (Sartorius, FortéBio®) software and open the results of the measurement.
   2. Go to preprocessed Data > Data Correction and adjust the settings as follows:
      a. Align Axis: Align Data to: Average of Baseline.
      b. Inter-step Correction: Align Data to: Association Step.
      c. Activate Savitky-Golay Filtering.
   3. Go to kinetics analysis and adjust the settings as follows:
      a. Step to Analyze: Association and Dissociation.
      b. Binding Model: depending on protein.

         The 1:1 model is recommended for protein complexes where the analyte binds to one specific binding site of the ligand. If the analyte binds at two independent ligand sites, use the 2:1 (heterogeneous ligand) model. The Mass Transport model is recommended for bindings that are limited by diffusion. The bivalent model fits the binding of one analyte that interacts with two sites of the immobilized ligand. Detailed information is provided in the manufacturer's user manual (Page 114, Pall FortéBio LLC, Octet System Data Analysis User Guide).
      c. Fitting.

         Type: Global (Group)

Please cite this article as: Orthwein, T. *et al.* (2021). Kinetic Analysis of a Protein-protein Complex to Determine its Dissociation Constant (K_D) and the Effective Concentration (EC_{50}) of an Interplaying Effector Molecule Using Bio-layer Interferometry. *Bio-protocol* 11(17): e4152. DOI: 10.21769/BioProtoc.4152.

Group by: Sensor Type

R_{max} Values: Linked

d. Steady State Analysis: R equilibrium.

The software calculates the response values in the equilibrium and creates a steady-state graph of your measurement, as shown in Figure 5.

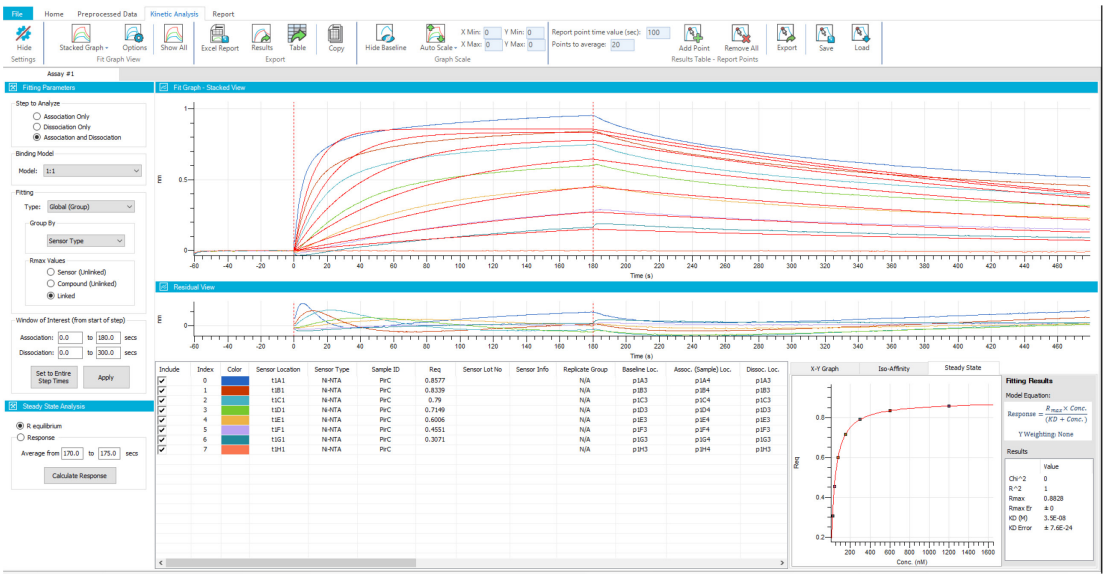

Figure 5. Kinetic Analysis page in the data analysis software. Graphs (fit graph) below the function tab show how the preprocessed data is fitted with the settings in step 3. The list below shows the calculated R_{eq} values and additional information about the sensors. On the right edge, the Steady-State calculation of one measurement row is shown. The calculated K_D is also reported.

Note: You can use this calculation to determine the K_D, but the combination of several measurements is not possible.

4. Export the data by clicking on “Excel Report.”
5. Open Prism and create a new Table and Graph Project.

   Enter and import data:

   a. Click on XY.

   b. Enter three replicate values in side-by-side sub columns.

      Note: It is also possible to use a different software for the calculation and fitting of the binding kinetics. Make sure that the software contains the correct binding kinetic equations.
6. Transfer the R_{eq} values into the GraphPad table as Y-values.
7. Add the interactor concentrations as X Values.
8. Click on the automatically created graph and perform the “Analyze” function.

   a. Nonlinear regression (curve fit).

   b. Binding – Saturation.

   c. One site – Specific binding.

Please cite this article as: Orthwein, T. *et al.* (2021). Kinetic Analysis of a Protein-protein Complex to Determine its Dissociation Constant (K_D) and the Effective Concentration (EC_{50}) of an Interplaying Effector Molecule Using Bio-layer Interferometry. *Bio-protocol* 11(17): e4152. DOI: 10.21769/BioProtoc.4152.

The software fits the graph and creates a results file with the calculated B_{max} (= R_{max}) and K_D, as shown in Figure 6.

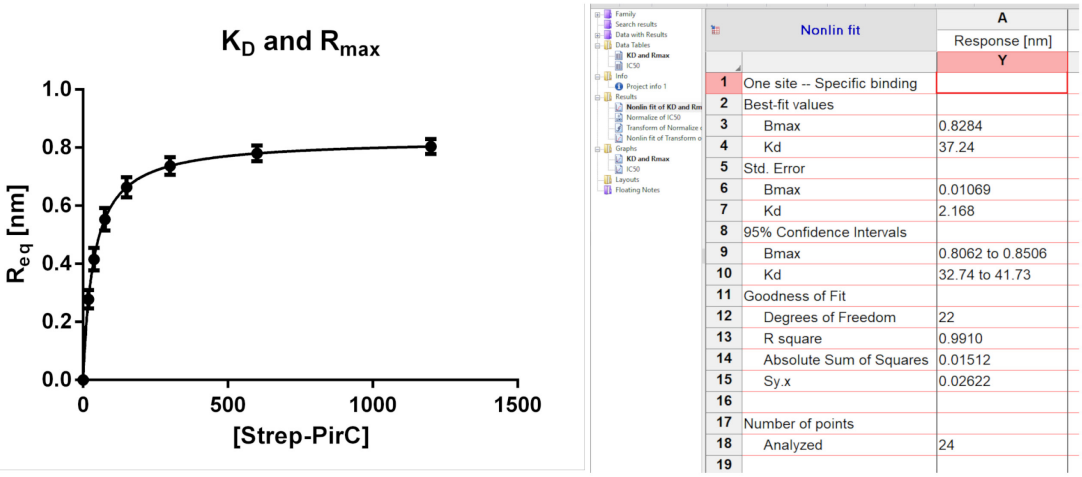

	Nonlin fit	A
		Response [nm]
		Y
1	One site -- Specific binding	
2	Best-fit values	
3	Bmax	0.8284
4	Kd	37.24
5	Std. Error	
6	Bmax	0.01069
7	Kd	2.168
8	95% Confidence Intervals	
9	Bmax	0.8062 to 0.8506
10	Kd	32.74 to 41.73
11	Goodness of Fit	
12	Degrees of Freedom	22
13	R square	0.9910
14	Absolute Sum of Squares	0.01512
15	Sy.x	0.02622
16		
17	Number of points	
18	Analyzed	24
19		

Figure 6. Representative Data of Analysis for kinetic analysis of protein interactions for the P_{II}-PirC example. (A) Fit of the binding (R_{eq}) against the concentration of the analyte (Strep-PirC). (B) Prism document (results file) of calculated kinetics in the results folder. The window shows the maximal binding (B_{max}), the calculated K_D, and the standard error of both. Confidence intervals and the quality of the fit are also calculated.

B. EC_{50} determination

1. Repeat the steps of Data analysis A1-A4.
2. Add the effector concentrations as X Values.
3. Export the data by clicking on “Excel Report” and transfer the R_{eq} values into a GraphPad table as Y-values.

   Note: For triplicates, measure three times with newly prepared 96-well plates.
4. Perform the “Analyze” function “Normalize” with y = 0.0 as 0% and the largest value in each data set as 100%.
5. Perform the “Analyze” function “Transform” and transform X values using X = Log[X]. In the original data table, change the concentration from 0 to 1.
6. Perform the “Analyze” function “Nonlinear Regression (curve fit)”
   a. Dose-response – inhibition (negative effector; IC_{50})/Dose-response – Stimulation (positive effector).
   b. Log(inhibitor) vs. normalized response/Log(agonist) vs. normalized response.

   The software fits the graph and creates a results file with the calculated EC_{50}. The example IC_{50} is shown in Figure 7.

Please cite this article as: Orthwein, T. *et al.* (2021). Kinetic Analysis of a Protein-protein Complex to Determine its Dissociation Constant (K_D) and the Effective Concentration (EC_{50}) of an Interplaying Effector Molecule Using Bio-layer Interferometry. *Bio-protocol* 11(17): e4152. DOI: 10.21769/BioProtoc.4152.

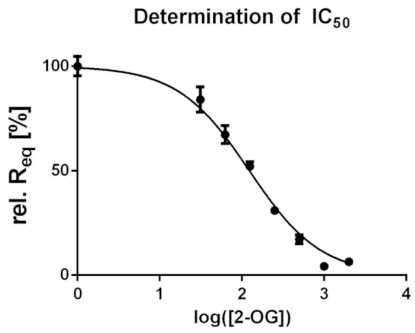

	Nonlin fit	A
		Req
		Y
1	log(inhibitor) vs. normalized response	
2	Best-fit values	
3	LogIC50	2.091
4	IC50	123.4
5	Std. Error	
6	LogIC50	0.02651
7	95% Confidence Intervals	
8	LogIC50	2.035 to 2.148
9	IC50	108.4 to 140.6
10	Goodness of Fit	
11	Degrees of Freedom	15
12	R square	0.9864
13	Absolute Sum of Squares	251.5
14	Sy.x	4.095
15		
16	Number of points	
17	Analyzed	16
18		

Figure 7. Representative Data Analysis for determination of the IC_{50} of 2-OG in the P_{II}-PirC interaction. (A) Fitted data of a triplicate measurement of P_{II}-PirC binding for determination of the IC_{50} of 2-OG. X-Axis logarithm of 2-OG concentration (dilution series of 2 mM, 1 mM, 0.5 mM, 0.25 mM, 0.125 mM, 0.0625 mM, and 0.03125 mM), and Y-Axis: relative response in equilibrium. (B) Prism document (results file) of calculated IC_{50} in the results folder. The window shows the logarithmic IC_{50}, the calculated IC_{50} and the logarithmic standard error of both. Confidence intervals and the quality of the fit are also calculated.

Recipes

1. Kinetics buffer
   20 mM HEPES pH 8
   150 mM KCl
   5 mM $MgCl_2$
   1 mM ATP
   0.005% Nonident P40
   KOH for pH adjustment

Acknowledgments

This work was funded by grants from DFG to K.F. (Fo195/9-2, Fo195/21-1) and from Cluster of Excellence 'Controlling Microbes to Fight Infections' (EXC 2124 – 1-06.010_0) to K.A.S. Furthermore, we would like to acknowledge Janette Alford for her assistance in writing the first draft and Libera Lo Presti for critical scientific and linguistic editing of the manuscript, and the infrastructural support by the Cluster of Excellence 'Controlling Microbes to Fight Infections' (EXC 2124) of the German research foundation (DFG).

This protocol was based on our original research article published in the Journal of Biological Chemistry: Santos, A. R. S., Gerhardt, E. C. M., Parize, E., Pedrosa, F. O., Steffens, M. B. R., Chubatsu, L. S., Souza, E. M., Passaglia, L. M. P., Sant'Anna, F. H., de Souza, G. A., Huergo, L. F.

and Forchhammer, K. (2020). NAD+ biosynthesis in bacteria is controlled by global carbon/nitrogen levels via PII signaling. *J Biol Chem* 295(18): 6165-6176.

Competing interests

The authors declare no competing interest.

Ethics

K.A.S. conceived and initiated the project. T.O. performed the experiments, wrote the first draft and edited the manuscript. L.F.H., K.F. and K.A.S. commented and edited the manuscript. All authors have read and approved the final version of the manuscript.

References

1. Bolay, P., Rozbeh, R., Muro-Pastor, M. I., Timm, S., Hagemann, M., Florencio, F. J., Forchhammer, K. and Klahn, S. (2021). The Novel PII-Interacting Protein PirA Controls Flux into the Cyanobacterial Ornithine-Ammonia Cycle. *mBio* 12(2): e00229-21.
2. Forchhammer, K. and Selim, K. A. (2020). Carbon/nitrogen homeostasis control in cyanobacteria. *FEMS Microbiol Rev* 44(1): 33-53.
3. FortéBio. (2005-2006). Octet System User's Guide.
4. FortéBio. (2019). Ni-NTA Biosensor Kinetic Assays.
5. Orthwein, T., Scholl, J., Spät, P., Lucius, S., Koch, M., Macek, B., Hagemann, M. and Forchhammer, K. (2021). The novel P_{II}-interactor PirC identifies phosphoglycerate mutase as key control point of carbon storage metabolism in cyanobacteria. *Proc Natl Acad Sci U S A* 118(6): e2019988118.
6. Pall FortéBio LLC. (2011). Octet® System Data Analysis User Guide. Release 7.1.
7. Santos, A. R. S., Gerhardt, E. C. M., Parize, E., Pedrosa, F. O., Steffens, M. B. R., Chubatsu, L. S., Souza, E. M., Passaglia, L. M. P., Sant'Anna, F. H., de Souza, G. A., Huergo, L. F. and Forchhammer, K. (2020). NAD+ biosynthesis in bacteria is controlled by global carbon/nitrogen levels via P_{II} signaling. *J Biol Chem* 295(18): 6165-6176.
8. Scholl, J., Dengler, L., Bader, L. and Forchhammer, K. (2020). Phosphoenolpyruvate carboxylase from the cyanobacterium *Synechocystis* sp. PCC 6803 is under global metabolic control by P_{II} signaling. *Mol Microbiol* 114(2): 292-307.
9. Selim, K. A., Ermilova, E. and Forchhammer, K. (2020). From cyanobacteria to Archaeplastida: new evolutionary insights into P_{II} signalling in the plant kingdom. *New Phytol* 227(3): 722-731.
10. Shah, N. B. and Duncan, T. M. (2014). Bio-layer interferometry for measuring kinetics of protein-protein interactions and allosteric ligand effects. *J Vis Exp*(84): e51383.

Please cite this article as: Orthwein, T. *et al.* (2021). Kinetic Analysis of a Protein-protein Complex to Determine its Dissociation Constant (K_D) and the Effective Concentration (EC_{50}) of an Interplaying Effector Molecule Using Bio-layer Interferometry. *Bio-protocol* 11(17): e4152. DOI: 10.21769/BioProtoc.4152.

11. Shang, J., Wan, Y., Luo, C., Ye, G., Geng, Q., Auerbach, A. and Li, F. (2020). Cell entry mechanisms of SARS-CoV-2. *Proc Natl Acad Sci U S A* 117(21): 11727-11734.

Publication 3

Structural elements of cyanobacterial co-factor-independent phosphoglycerate mutase that mediate regulation by PirC.

Tim Orthwein, Janette T. Alford, Nathalie Sofie Becker, Phillipp Fink and Karl Forchhammer

Available at: https://doi.org/10.1128/mbio.03378-24

AMERICAN SOCIETY FOR MICROBIOLOGY | mBio

Physiology and Metabolism | Research Article

Structural elements of cyanobacterial co-factor-independent phosphoglycerate mutase that mediate regulation by PirC

Tim Orthwein,[1] Janette T. Alford,[1] Nathalie Sofie Becker,[1] Phillipp Fink,[1] Karl Forchhammer[1]

AUTHOR AFFILIATION See affiliation list on p. 14.

ABSTRACT The 2,3-bisphosphoglycerate-independent phosphoglycerate mutase (iPGAM) has been identified as a regulating key point in the carbon storage metabolism of cyanobacteria. Upon nitrogen starvation, the iPGAM is inhibited by the P_{II}-interacting regulator PirC, which is released from its interaction partner P_{II} due to elevated 2-oxoglutarate levels. *In silico* analysis of 338 different iPGAMs revealed a deep-rooted distinctive evolution of iPGAMs in cyanobacteria. Remarkably, cyanobacterial iPGAMs possess a unique loop structure and an extended C-terminus. Our mass photometry analysis suggests that iPGAM forms a complex with three individual PirC monomers. Biolayer interferometry revealed that the PirC–iPGAM complex is affected by the unique loop and the C-terminal structural elements of iPGAM. A C-terminally truncated iPGAM enzyme showed loss of control by PirC and twofold increased enzymatic activity compared to the iPGAM-WT (wild type), as demonstrated by enzyme assays. By contrast, deleting the loop structure significantly reduced the activity of this variant. Physiological experiments were carried out with different iPGAM variant strains of *Synechocystis*, in which these structural elements were deleted. The strain expressing the C-terminally truncated iPGAM showed a similar overproduction of polyhydroxybutyrate as deletion of the iPGAM regulator PirC. However, in contrast to the latter, these strains showed higher overall biomass accumulation, making them a better chassis for the production of polyhydroxybutyrate or other valuable substances than the PirC-deficient mutant.

IMPORTANCE The primordial cyanobacteria were responsible for developing oxygenic photosynthesis early in evolution. In the pathways of fixed carbon allocation, the co-factor-independent phosphoglycerate mutase (iPGAM) plays a crucial role by directing the first CO_2 fixation product, 3-phosphoglycerate, toward central anabolic glycolytic-derived pathways. This work reveals a distinct evolution of iPGAM within oxygenic photosynthetic organisms. We have identified two specific segments in cyanobacterial iPGAMs that affect the control of iPGAM activity through its specific interactor protein PirC. This understanding of iPGAM has allowed us to engineer cyanobacterial strains with altered carbon fluxes. Since cyanobacteria can directly convert CO_2 into valuable products, our results demonstrate a novel approach for developing a chassis for biotechnical use.

KEYWORDS PirC, PII, iPGAM, enzyme regulation, phosphogylcerate mutase, *Cyanobacteria*, *Synechocystis*

Phosphoglycerate mutases (PGAMs) are enzymes present in almost every living organism. They connect the major sugar metabolic routes, the Embden–Meyerhof–Parnas pathway, the Entner–Doudoroff pathway, the oxidative pentose-phosphate pathway and its reductive pendant, the Calvin–Benson–Bassham cycle, with the reactions of lower glycolysis. At this metabolic linchpin, PGAM converts 3-phosphoglycerate (3-PGA) into 2-phosphoglycerate (2-PGA), allowing carbon flux into lower

Editor Haike Antelmann, Freie Universitat Berlin, Berlin, Germany

Address correspondence to Karl Forchhammer, karl.forchhammer@uni-tuebingen.de.

The authors declare no conflict of interest.

See the funding table on p. 14.

Received 12 November 2024
Accepted 4 March 2025
Published 3 April 2025

glycolysis and thereby into many pathways of anabolic metabolism, such as synthesis of fatty acids or amino acids.

There are two types of PGAM enzymes, which are affiliated with the same superfamily of alkaline phosphates (1): first, the 2,3-bisphosphoglycerate (2,3-BPG)-dependent PGAM (dPGAM) and, second, the 2,3-BPG-independent PGAM (iPGAM) (2–4). Other than dPGAM, iPGAM does not need activation by 2,3-BPG. iPGAMs exist in all plants, algae, some invertebrates, and fungi and are widespread in bacteria (2). In these enzymes, the reversible transfer of the phosphate of the glycerate core from the C3 to the C2 position is achieved in a two-step reaction induced by substrate binding. When no substrate is bound, the cleft between the phosphatase and transferase domains of iPGAMs is open, allowing the entrance of 3-PGA into the binding pocket. Substrate binding induces the closing of the open cleft by phosphatase and transferase domain movement, which enables the reaction to occur (3). 3-PGA first phosphorylates the active-site seryl residue through phosphatase sub-domain activity, followed by reorientation of the substrate and re-phosphorylation of the C2 oxygen by phosphotransferase activity (2). Two manganese ions coordinate the reaction, which makes this reaction highly pH-dependent (4). Species of the *Bacillota* (*Firmicutes*) phylum use this effect to regulate iPGAMs, which play a crucial role in endospore formation (5).

In analogy to the *Firmicutes*, iPGAMs possess a unique regulatory role in cyanobacteria, particularly in response to nitrogen starvation. In *Synechocystis* sp. PCC 6803 (now termed *Synechocystis*), two genes are annotated as iPGAMs, *slr1124* and *slr1945*. The product of *slr1124* was previously identified as a phosphoserine phosphatase and has an essential role in serine biosynthesis in cyanobacteria (6). Notably, we could demonstrate that the product of *slr1945* indeed is an iPGAM, and its regulation is crucial in the biosynthesis of carbon storage polymers during the adaptation to nitrogen-limiting periods (7). The acclimation response of non-diazotrophic cyanobacteria to nitrogen limitation occurs in a process termed chlorosis, which has been thoroughly studied in the strains *Synechococcus* PCC 7942 and *Synechocystis* PCC 6803 (8–10). In the early phase of chlorosis, cells undergo a final doubling before cell cycle arrest, and they immediately start degrading their pigments and forming glycogen as carbon storage (11, 12). Some species, including *Synechocystis* PCC 6803, also accumulate polyhydroxybutyrate (PHB) during the chlorosis process from glycogen turnover (9).

The P_{II} signal transduction protein is a critical factor in the adaptation to nitrogen limitation. It acts as a sensor of the intracellular energy via the binding of ADP and ATP and of carbon-nitrogen status via the binding of 2-oxoglutarate (2-OG). P_{II} directly or indirectly interacts with various enzymes and proteins, affecting a plethora of cellular mechanisms (13, 14). 2-OG binds to P_{II} in synergy with ATP and gives rise to a conformation of P_{II} that prevents interactions with many P_{II} target proteins (reviewed in reference 15). One example of direct interaction is N-acetyl-L-glutamate kinase (NAGK), serving as a model to study P_{II}–enzyme interactions (15, 16). More recently, a novel P_{II} interactor, PirA (P_{II}-interacting regulator of arginine synthesis), was discovered, whose interaction with P_{II} additionally regulates the NAGK indirectly (17). Activation of the global nitrogen control transcription factor NtcA is indirectly under P_{II} control via the NtcA co-activator PipX (P_{II}-interacting protein X). Under low energy or low 2-OG conditions, P_{II} binds and sequesters PipX, whereas this complex dissociates, releasing PipX when 2-OG levels increase due to low nitrogen conditions. Then, PipX co-activates NtcA to stimulate the expression of over 80 genes required for low nitrogen acclimation (18–20).

The newly discovered PirC (Sll0944, P_{II}-interacting regulator of carbon metabolism) is like PipX and PirA, a small protein with no enzymatic activity. Still, it modulates the activity of a particular interaction partner, in this case, iPGAM. During nitrogen-supplemented vegetative growth, when 2-OG levels are relatively low, P_{II} forms a complex with PirC, thereby preventing iPGAM inhibition. Upon nitrogen limitation, 2-OG levels increase, and PirC dissociates from the P_{II} complex, which can then inhibit iPGAM. This blocking of the iPGAM stimulates glycogen formation and reduces carbon flow

into lower glycolysis, from where many anabolic pathways, including the glutamine synthetase (GS) - glutamate synthase (GOGAT) cycle, are derived (7).

Unlike the regulation of iPGAM in *Bacillota*, the iPGAM in cyanobacteria is regulated via protein–protein interaction with PirC. This unique type of iPGAM regulation in cyanobacteria implies specific structural features of cyanobacterial iPGAMs. Within the iPGAM of cyanobacteria, we identified an internal loop structure and an extended C-terminus (CT). This study aimed to clarify the role of these sub-structures in cyanobacterial iPGAM and their involvement in the PirC interaction by using biochemical and physiological experiments.

RESULTS

In silico analysis reveals unique sub-domains in cyanobacterial iPGAM

To find out if cyanobacterial iPGAMs differ from other species, we performed a multiple sequence alignment with a simultaneous phylogenetic analysis of 338 different iPGAMs (reviewed according to https://www.uniprot.org) using Matlab and IQ-Tree (21). The tree illustrates the monophyletic evolution of cyanobacterial and red algae iPGAM, distinguishing them from all other tested iPGAMs of bacterial species, plants, and the rare metazoan iPGAMs (bootstrap 98). Furthermore, the tree shows a divergence of iPGAMs from α-cyanobacteria and β-cyanobacteria but with moderate confidence (bootstrap 50). Intriguingly, the chloroplastic iPGAMs of red algae share a common ancestry with the enzymes of cyanobacteria, indicating their origin from the cyanobacterial endosymbiont (bootstrap 91). In contrast, the iPGAM in green plants (kingdom Plantae) is distinct from the cyanobacterial and red algae iPGAMs, indicating that the iPGAM of the endosymbiont was replaced during green plant evolution (Fig. 1).

The multiple sequence alignment revealed two exclusive sequence segments in cyanobacterial iPGAMs: an inner segment of 17 amino acids near the end and an extended CT (Fig. S1). Accordingly, the sequence conservation of the two segments was tested based on multiple sequence alignment of 644 cyanobacterial iPGAMs (Fig. S1B and S1C). The inner segment comprises 17 highly conserved amino acids, which almost always start with a triplet of glutamate, glycine, and glutamate (EGE). The lysine residue at position 6 of the loop is also highly conserved, only replaced by arginine or glutamine and followed by hydrophobic amino acids at positions 14 and 16. There is a high probability of a hydrophobic amino acid, followed by arginine in most cases. By contrast, the CT segment, also unique to cyanobacteria, exhibits poor sequence conservation except for arginine and proline at this segment's seventh and ninth position, respectively.

For further analysis, the *Synechocystis* iPGAM (Slr1945) structure was predicted using the SWISS-MODEL and AlphaFold server (Google DeepMind) to get more information on Slr1945 and the segments (Fig. 2). The AlphaFold server uses the AlphaFold 3 algorithm. Due to the lack of structural prediction of substrate binding by AlphaFold, the SWISS-MODEL, which shows the bonded substrates, was also used.

The structure predictions of the iPGAM of *Synechocystis* showed the typical division in the phosphatase and transferase sub-domains of iPGAMs. Whereas the AlphaFold prediction shows the open structure without substrate (AlphaFold prediction, Fig. 2A), the SWISS-MODEL in the presence of substrate reveals the closed structure with the bonded substrate (SWISS-MODEL, Fig. 2C) in perfect agreement with the proposed reaction mechanisms. Both predictions revealed the cyanobacterial-specific loop structure of the inner segment. The extended CT was only revealed by Alphafold, predicting a random coil of the CT segment with local proximity to the loop (Fig. 2A and B). The Alphafold prediction was predicted with high accuracy. Most areas have a predicted local distance difference test (pLDDT, a measure for the local confidence of the prediction) value above 70 and close to 90. Additionally, the predicted template modeling (pTM) score of 0.81 and the interface pTM (ipTM) of 0.83 and the predicted aligned error (PAE) graph (Fig. 2B) indicate high confidence in the Alphafold prediction (pTM = measure of the confidence of the whole prediction; ipTM = measure of the confidence of the individual structures within the structure, PAE = graphical presentation

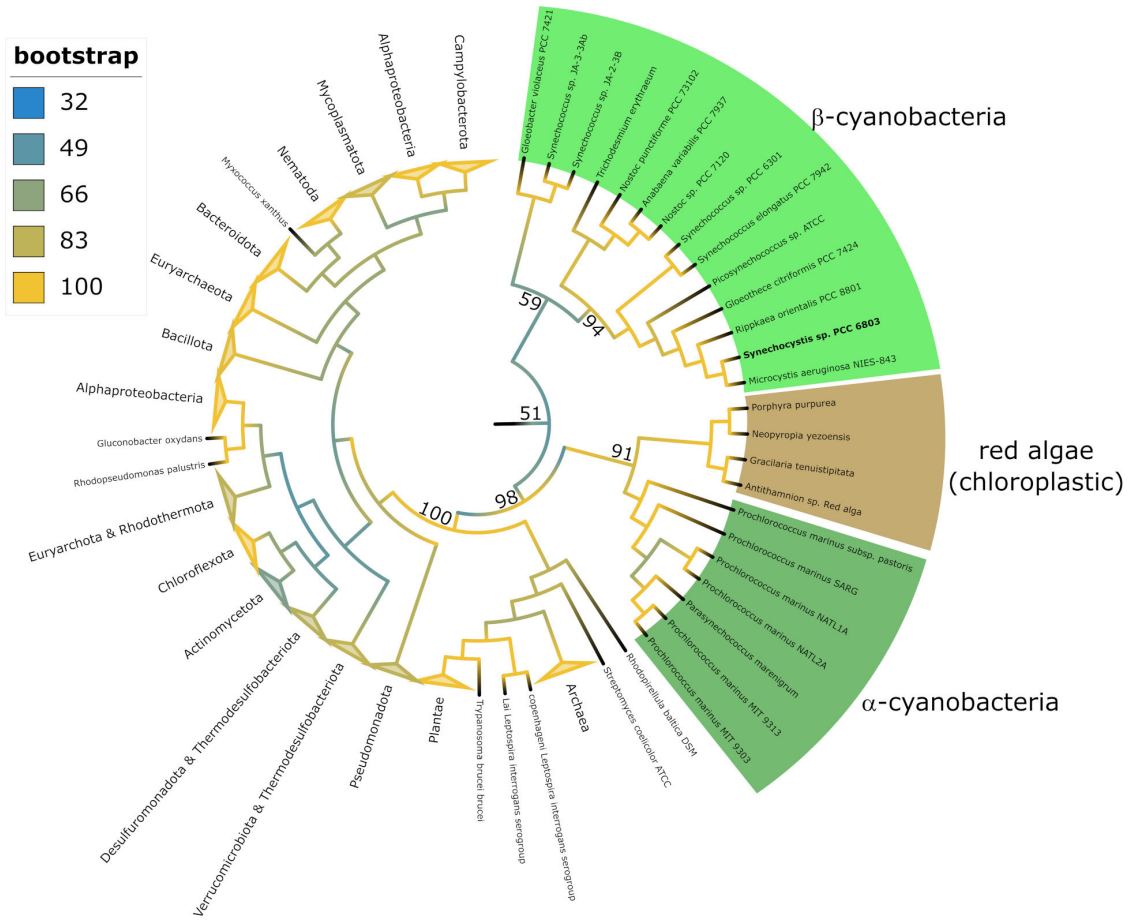

FIG 1 Phylogenetic tree computed with a multiple sequence alignment (MSA) of 338 different iPGAMS (reviewed, according to UniProt). MSA—progressive pairwise alignment using Blosum64 scoring matrix. Tree analysis—maximum likelihood with ultrafast bootstrap analysis (1,000 alignments) computed with IQ-Tree using a general matrix for proteins with a FreeRate heterogeneity +9 (21).

of estimated errors between two predicted residues). Only the areas of the exclusive cyanobacterial sub-structures show lower confidence (light areas). Based on SWISS-MODEL prediction, the amino acid residues contributing to the active site of the *Synechocystis* iPGAM could be elucidated (Fig. 2C). It appears that the loop segment is directly connected to the catalytic center, especially to histidine 457 (H457), by 10-amino-acid-long β-strand (Fig. 2D). A closer view into the loop structure revealed direct interaction between the two highly conserved amino acids E468 (glutamine at position 1 according to the segment position) and K473 (lysine at position 6) (Fig. S2).

Mass photometry indicates the involvement of three PirC monomers in the iPGAM interaction

Recombinant strep-tagged iPGAM and PirC proteins were produced in *Escherichia coli* and purified by Strep-Tactin Superflow affinity chromatography. The purified proteins were analyzed via mass photometry to assess the oligomeric structure of iPGAM, PirC, and the iPGAM–PirC complex. The individual protein measurements used iPGAM concentrations of 10 nM. In preliminary experiments, we tested the optimal ratios for the complex measurement. The iPGAM–PirC ratio of 1:3 showed the most accurate results according to the low appearance of additional peaks (monomers of iPGAM and higher oligomers of PirC) and significant protein counts.

Mass photometry determined monomeric iPGAM particles with masses between 73 and 88 kDa compared to a calculated size of iPGAM of 60 kDa. For purified recombinant

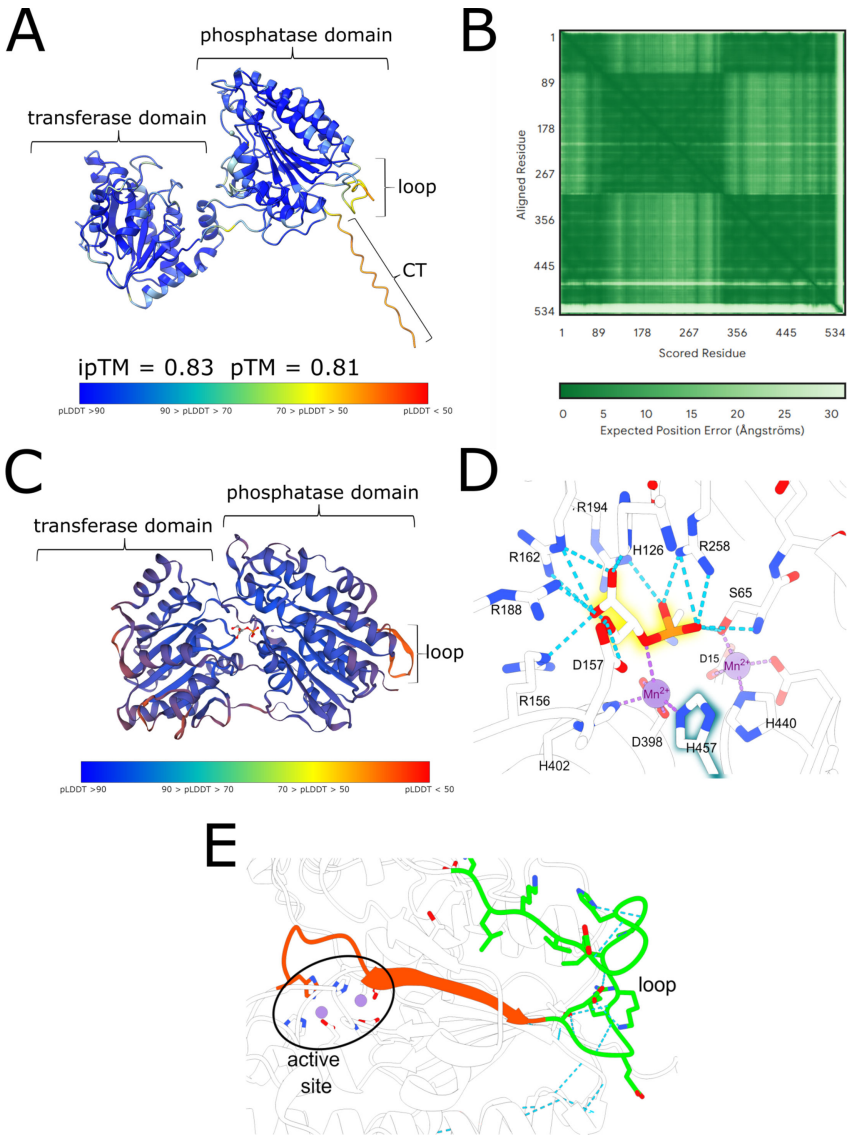

FIG 2 Structure of iPGAM of *Synechocystis* (Slr1945). (A) AlphaFold prediction of the Slr1945. Prediction confidence is shown by the interface predicted template modeling (ipTM) and pTM values and by colorization by the calculated predicted local distance difference test (pLDDT) with the color key below. The AlphaFold server provided by Google DeepMind, which uses the AlphaFold 3 algorithm, was used. (B) Predicted aligned error diagram according to the AlphaFold prediction. (C) SWISS-MODEL prediction of the Slr1945 (PDB template: 1o98, iPGAM of *Geobacillus stearothermophilus*). Prediction confidence is shown by the ipTM and pTM values and by colorization by the calculated pLDDT with the color key below. Exclusive domains and sub-domains are labeled with a bracket. (D) Contributing residues in the catalytic center of Slr1945 according to the SWISS-MODEL prediction. The numbers are based on the position in the *Synechocystis* sequence, shown in Fig. S1D. (E) Connection of the loop to the catalytic center over the β-strand.

PirC, mass photometry determined a maximum of particles between 100 and 114 kDa, fitting to a hexameric structure of the PirC protein (strep-PirC = 14,723.35 Da). Furthermore, a shoulder of around 180 to 210 kDa indicates a higher oligomerized species of PirC. Analyzing the PirC–iPGAM complex resulted in a maximum peak of 125 kDa (replicate 2 = 134 kDa, replicate 3 = 137 kDa). Again, a shoulder appeared at the same position as in the PirC graph. With a size of 125 kDa, the peak is about 55 kDa–65 kDa larger than that of iPGAM alone, which fits the size of three PirC monomers. This suggests

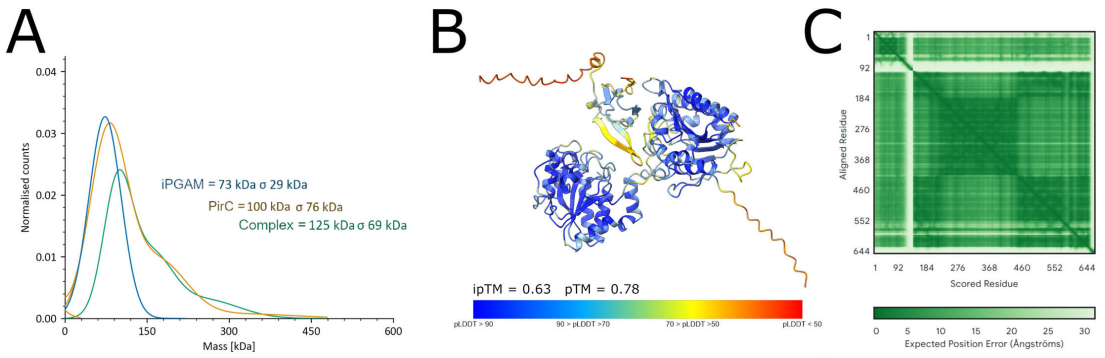

FIG 3 Mass photometry of strep-iPGAM, strep-PirC, and their complex (A), and structure of the iPGAM–PirC complex (B) and the corresponding PAE graph (C). (A) Representative graph of one individual measurement. Triplicates are shown in Fig. S2. (B) Complex of iPGAM and PirC in a ratio of 1:1. Colorized in pLDDT and depicted prediction confidence scores ipTM and pTM. (C) PAE graph based on the complex prediction.

the complex could consist of a monomeric iPGAM to which three PirC subunits are bound. According to the results, the structure of the complex was predicted using AlphaFold. However, AlphaFold could not predict such a complex with acceptable confidence (Fig. S4). By contrast, the prediction of a complex only with one PirC bound gave trustable confidence (ipTM of 0.63 and pTM of 0.78) (Fig. 3).

The Alphafold prediction revealed a PirC protomer located in the binding cleft of the substrate between the phosphatase and transferase domains of iPGAM. There, the PirC protomer covers the catalytic center of the phosphatase domain. The confidence of the predicted C-terminus of PirC is low, as indicated by a low pLDDT (Fig. 3A, orange coloring) and a high PAE (Fig. 3B, light areas in the graph)

Sub-structure-free variants alter the binding of PirC and inhibitory characteristics

The exclusive co-occurrence of PirC with the loop and CT segments in cyanobacterial iPGAM implied functional relations. To further investigate the functional significance of these structures, three variants of the *Synechocystis* iPGAM, each with an N-terminal strep-tag, were constructed. First was variant iPGAM-Δloop, where the entire loop was replaced by a five amino acid sequence (TKKGI) present at homologous localization in *Geobacillus stearothermophilus* iPGAM. Second, the CT segment was deleted, creating variant iPGAM-ΔCT, and third, a combination of both alterations, was iPGAM-ΔloopΔCT. In a preliminary experiment, we analyzed the interaction of the various iPGAM variants with PirC by pull-down analysis of Strep-Tactin with immobilized strep-iPGAMs as bait

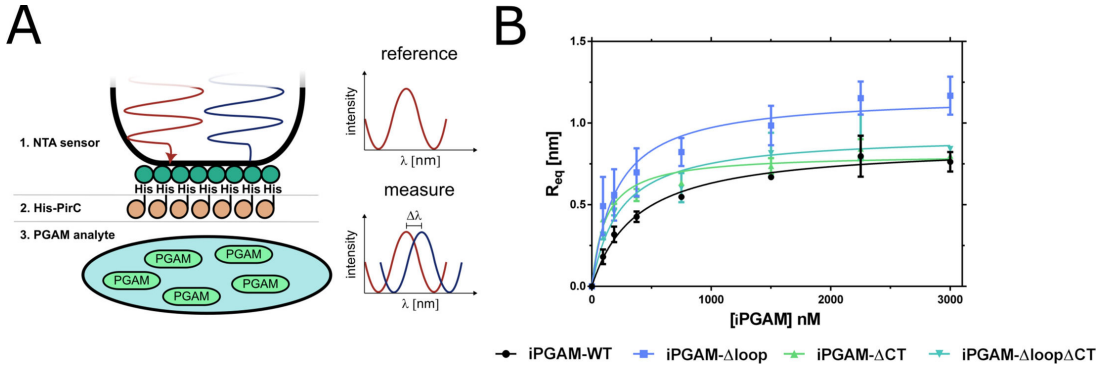

FIG 4 Binding of PirC and iPGAM variants. (A) Principle of BLI measurement with His-PirC and iPGAM variants. In BLI, binding ligands (His-PirC) and analytes (strep-PGAM) at the sensor tips alter the surface's reflection properties, resulting in a wavelength phase shift. This shift is proportional to the bound molecule. It allows real-time detection of binding, from which the kinetic constants can be calculated. (B) Binding kinetics of iPGAM-WT (wild type), iPGAM-Δloop, iPGAM-ΔCT, and iPGAM-ΔloopΔCT. Each point represents a mean of technical triplicates. The error bars represent the standard deviation.

TABLE 1 Binding kinetic parameters of the different iPGAM variants

Parameter	iPGAM-WT	iPGAM-Δloop	iPGAM-ΔCT	iPGAM-ΔloopΔCT
R_{max} [nm]	0.872 ± 0.033	1.170 ± 0.063	0.810 ± 0.025	0.9291 ± 0.047
K_D [nM]	378.4 ± 50.3	203.2 ± 45.0	113.6 ± 18.3	233.4 ± 45.3

and His-tagged PirC as analyte. Surprisingly, all three variants retained their interaction capacity with iPGAM (Fig. S5). To gain more insight into PirC binding, we performed biolayer interferometry (BLI) measurements using an Octet K2 system. The His-tagged version of PirC was immobilized on the surface of a Ni^{2+}-NTA sensor. The different strep-iPGAM variants were then used as analytes in various concentrations for binding kinetics (Fig. 4, Table 1).

The BLI experiments revealed significant differences between the variants. Deleting the loop, CT segment, or both caused an increased affinity for PirC. The K_D was reduced by half in the iPGAM-Δloop and iPGAM-ΔloopΔCT compared to the wild-type (WT). The

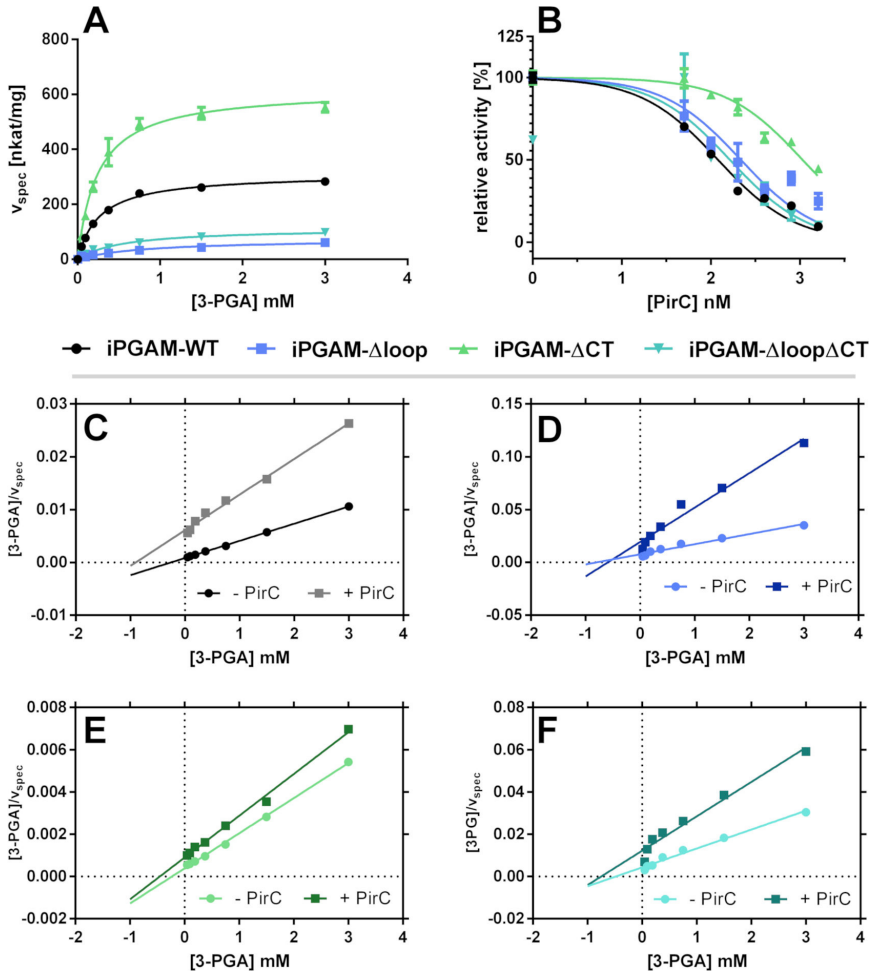

FIG 5 Activity of iPGAM variants of *Synechocystis* sp. PCC 6803 and the effect of PirC on activity. (A) Michaelis-Menten kinetics of iPGAM variants without PirC. (B) Dose-response curve of PirC on the iPGAM variants at 0.75 mM 3-PGA. Each point represents the mean of three independent measured triplicates. The error bar depicts the standard deviation of the triplicate. (C) HW kinetic transformation of WT with and without PirC (400 nM). (D) HW kinetic transformation of Δloop with and without PirC (400 nM). (E) HW kinetic transformation of ΔCT with and without PirC (400 nM). (F) HW kinetic transformation of ΔloopΔCT with and without PirC (400 nM). Each point represents the transformed HW value of the mean of the triplicates. HW transformation → *x*-axis = [substrate concentration], *y*-axis = [substrate]/v.

TABLE 2 Kinetic parameters of iPGAM-WT, -Δloop, -ΔCT, and -ΔloopΔCT[a]

Sample iPGAM	PirC	K_m (mM)	v_{max} (nkat · mg^{-1})	k_{cat} (s^{-1})	$k_{cat} \cdot K_m^{-1}$ ($s^{-1} \cdot M^{-1}$)
WT	–	0.265 ± 0.013	310.6 ± 4.5	18.6 ± 0.3	70,241.7 ± 3,588.3
	+	1.018 ± 0.070	154.4 ± 4.5	9.3 ± 0.3	9,096.3 ± 681.0
Δloop	–	1.087 ± 0.141	114.3 ± 6.4	6.7 ± 0.4	6,189.5 ± 873.9
	+	0.750 ± 0.132	32.1 ± 2.2	1.9 ± 0.1	2,522.3 ± 475.9
ΔCT	–	0.242 ± 0.019	617.9 ± 13.7	35.9 ± 0.8	148,468.5 ± 11,979.3
	+	0.482 ± 0.056	521.4 ± 20.7	30.3 ± 1.2	62,813.9 ± 7,711.8
ΔloopΔCT	–	0.547 ± 0.059	112.8 ± 4.3	6.4 ± 0.2	11,760.0 ± 1,355.4
	+	0.961 ± 0.182	65.7 ± 5.2	3.7 ± 0.3	3,900.7 ± 802.5

[a]Values represent the mean of triplicates with (+) and without (–) the addition of 400 nM PirC . The error range of K_m, v_{max}, and k_{cat} represents the standard error calculated by GraphPad Prism. The error of $k_{cat} \cdot K_m^{-1}$ was calculated using error propagation.

iPGAM-ΔCT had an even four-times lower K_D. The iPGAM-Δloop also had a 35% higher binding maximum than the WT.

The BLI experiment proved that the deletion of the loop and CT structures positively affected the binding of PirC. To reveal any effects of these modifications on enzyme activity, coupled enzymatic assays were carried out to determine the catalytic properties of the iPGAM variants and the inhibitory effects exerted by PirC. First, the effect of the co-factor Mn^{2+} was tested to find the optimal manganese concentrations for each iPGAM variant (Fig. S6). The iPGAM-Δloop and the iPGAM-ΔloopΔCT required 20 times more manganese to achieve maximum activity. Therefore, a concentration of 50 µM $MnCl_2$ was used in further experiments to achieve the maximum activity with all variants. First, the variants were tested in the absence of PirC (Fig. 5A). Next, the experiments were repeated in the presence of 50 nM, 100 nM, 200 nM, 400 nM, 800 nM, or 1,600 nM PirC to gain information on the inhibition mechanism (Fig. 5 and Table 2). In Fig. 5C through F and Table 2, only the results in the presence or absence of 400 nM PirC are shown for clarity (the full data set is shown in Fig. S7 and S8; kinetic parameters of all concentrations are shown in Table S1). In addition, a dose-response curve of the inhibitory effect of PirC on each iPGAM variant was plotted to calculate the half maximal inhibitory concentration (IC_{50}) of PirC, by taking the value at 0.75 mM 3-PGA for each iPGAM assay at the various PirC concentrations (Fig. 5B; Table 3). Moreover, the coupling enzymes were tested with 2-PGA as a substrate to ensure that PirC does not affect the coupling reactions (Fig. S7E). To analyze the inhibition of PirC on the different variants, the Michaelis-Menten (MM) kinetics were transformed to Hanes-Woolf kinetics (HW). The HW transformation of MM kinetics can show the strength and type of inhibition. The steeper the inhibition lines compared to the non-inhibited line, the more potent the inhibition. The convergence of the two lines without crossing before the *y*-axis indicates a non-competitive mode of inhibition (Fig. 5). We observed this for iPGAM-WT (Fig. 5C). Additionally, the increased K_m of the iPGAM-WT–PirC complex indicates competitive inhibiting properties, whereas the decreased v_{max} again showed non-competitive inhibition. This implies a type of mixed inhibition by PirC (Table 2).

Compared to iPGAM-WT, the iPGAM-Δloop variant had three times lower activity but was still inhibited by PirC. Interestingly, inhibition was less efficient, with a twofold increase in IC_{50} for PirC compared to inhibiting the iPGAM-WT ($IC_{50,\ iPGAM\text{-}WT}$ = ~120 nM,

TABLE 3 IC_{50} of PirC with the different iPGAM variants[a]

Sample	IC_{50} (nM)
iPGAM-WT	120.1 ± 1.06
iPGAM-Δloop	217.0 ± 1.14
iPGAM-ΔCT	1,069 ± 1.07
iPGAM-ΔloopΔCT	163.5 ± 1.25

[a]The IC_{50} was detected at 0.75 mM 3-PGA. Values represent the mean of triplicate. The error range represents the standard error calculated by GraphPad Prism.

$IC_{50,\ iPGAM\text{-}\Delta loop}$ = ~220 nM). More striking differences were observed for the iPGAM-ΔCT variant. First, the catalytic efficiency (CE) of iPGAM-ΔCT was severely enhanced with a CE value of 150,000 $s^{-1} \cdot M^{-1}$ compared to ~70,000 $s^{-1} \cdot M^{-1}$ for WT. Furthermore, the inhibitory effect of PirC on iPGAM-ΔCT was almost completely lost, as shown by the small difference in slope between the non-inhibited and inhibited states (Fig. 5E). The inhibited iPGAM-ΔCT still had a CE of 63,000 $s^{-1} \cdot M^{-1}$, which is close to the activity of non-inhibited iPGAM-WT (Table 2). The dose-response curves of PirC and the calculated IC_{50} demonstrated a 10-fold decreased efficiency of PirC to inhibit iPGAM-ΔCT compared to iPGAM-WT ($IC_{50,\ iPGAM\text{-}WT}$ = ~120 nM, $IC_{50,\ iPGAM\text{-}\Delta CT}$ = ~1070 nM, see Table 3). The iPGAM-ΔloopΔCT variant combined properties of the two single mutations: deleting the C-terminus in the iPGAM-Δloop variant increased its catalytic efficiency and partially decreased the inhibitory effect of PirC compared to the Δloop variant (Table 2).

Sub-domain-free variants influence the physiology during chlorosis

To investigate the effect of the above-described alterations of the iPGAM variants on the physiology of *Synechocystis*, mutant strains were generated by homologous recombination of native iPGAM with the iPGAM variants followed by spectinomycin (Δloop) or chloramphenicol (ΔCT and ΔloopΔCT) as selection markers. As controls, the WT was used as a reference for the standard interaction between iPGAM and PirC and a PirC deletion mutant (ΔPirC) for native iPGAM without PirC regulation.

Since the PirC–iPGAM interaction affects physiology during nitrogen limitation, we tested the effect in nitrogen deprivation experiments, in which we analyzed the OD_{750}, the glycogen amount, and the PHB levels after 14 days. As control experiments, we also tested the effect of nitrogen-rich conditions with nitrate or ammonia (Fig. 6).

All *Synechocystis* variants showed similar growth in the standard BG_{11} medium and reached a comparable maximal optical density (OD_{750}) after 7 days of cultivation. Also, when ammonium was used as a nitrogen source, no differences between the strains

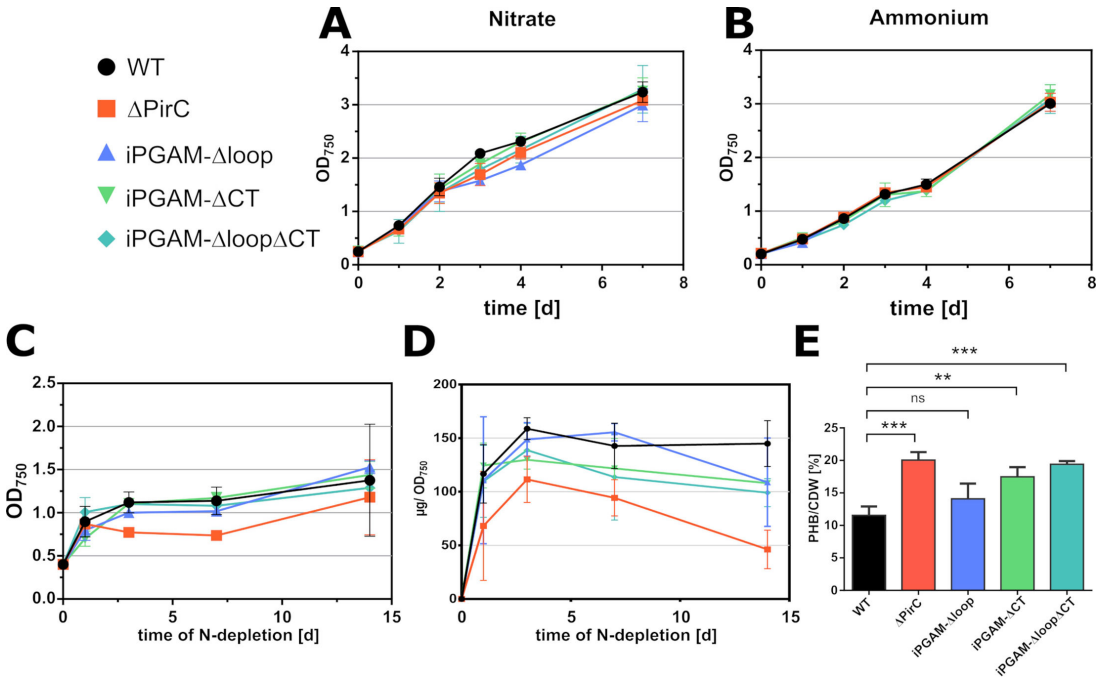

FIG 6 Effect of iPGAM-Δloop, -ΔCT, and -ΔloopΔCT on the physiology of *Synechocystis* sp. PCC 6803. (A) Growth curves of iPGAM variants with 17 mM $NaNO_3$. (B) Growth curves of iPGAM variants with 5 mM NH_4Cl. (C) OD_{750} of iPGAM variants during nitrogen depletion. (D) Glycogen content in iPGAM variant strains during nitrogen depletion. Each point represents the mean, and the error bars represent the standard deviation of independent triplicates. (E) PHB content after 14 days of nitrogen depletion in the iPGAM variants. Each bar and error bar represent the mean of biological triplicates. Statistical analysis was performed using a one-way analysis of variance. Each column was compared to the WT control. Dunnett's multiple comparisons test was used ($P < 0.05$).

showed up. However, upon nitrogen step-down, phenotypic differences to the wild-type became apparent. Upon nitrogen depletion, the wild-type carries out a final cell division before arresting the cell cycle, which is evidenced by an increase in OD_{750} until reaching a stationary value, which is double the initial OD_{750} (8, 10, 22). The ΔPirC strain, by contrast, was unable to carry out the doubling of OD_{750}. In contrast to the ΔPirC strain, the iPGAM variants exhibited the final increase in OD_{750} like the wild-type. The ΔPirC accumulated less glycogen and had twice as high levels of PHB compared to the WT. The iPGAM-Δloop mutant accumulated glycogen at similar levels as the WT but required more time to reach its maximum level. The iPGAM-ΔCT and -ΔloopΔCT strains showed intermediary phenotypes between ΔPirC and WT for glycogen accumulation. A hallmark of the *pirC* mutation was the strongly increased accumulation of PHB. In this respect, the iPGAM-ΔCT and -ΔloopΔCT strains resembled the ΔPirC strain. After 14 days of chlorosis, the PHB level per cell dry weight (CDW) of iPGAM-ΔCT (18.2 ± 0.4 mg · CDW^{-1}) and ΔloopΔCT (19.4 ± 0.3 mg · CDW^{-1}) strains reached PHB levels similar to the high PHB-producer ΔPirC (20.1 ± 1.0 mg · CDW^{-1}), whereas those of the iPGAM-Δloop strain were similar to the WT (12.9 ± 0.5 mg · CDW^{-1} compared to 1.5 ± 1.5 mg · CDW^{-1}).

DISCUSSION

This research unveils a unique insight into the pivotal role of the iPGAM in regulating carbon flux in cyanobacteria. Our bioinformatics analysis revealed two structural elements exclusively in cyanobacterial iPGAM, indicating a unique functional connection with PirC. The phylogenetic analysis showed that cyanobacterial iPGAMs diverged early from iPGAMs of other species. Notably, the iPGAMs of red algae show a phylogenetic relation to cyanobacterial iPGAM despite lacking the two characteristic segments. The chloroplasts of red algae have retained several features from the early endosymbiont, which were later lost in the evolution of green plants, such as components of the light-harvesting system. Furthermore, red algae exhibit P_{II} signaling features that resemble cyanobacteria, such as N-acetyl-L-glutamate kinase regulation by P_{II} (23). The phylogenetic tree of cyanobacterial iPGAM corresponds strikingly well with a recent whole-genome phylogeny of cyanobacteria (24), which considers many more genes than the usually used 120 housekeeping genes (25). If this refined phylogenetic tree accurately reflects the evolution of cyanobacteria, it suggests that the characteristic features of iPGAM and their regulation by PirC emerged early in cyanobacterial evolution. Alternatively, the prominent divergence of iPGAM homology between α- and β-cyanobacteria would indicate a different trend in protein evolution in these cyanobacterial groups. In red algae, the evolutionary loss of PirC led to the disappearance of the CT and loop segments, but other features of iPGAM were conserved, maintaining the phylogenetic clustering. In contrast, the evolution toward green plants involved significantly streamlining the P_{II} signaling system along with metabolic rearrangements. The endosymbiont's iPGAM was replaced by an unrelated enzyme, not associated with P_{II} signaling, along with the translocation of the *glnB* gene to the nucleus and the reorganization of the P_{II} signaling system (such as the acquisition of the glutamine-sensing C-terminal domain).

Detailed kinetic analysis of iPGAM now shows characteristics of both competitive and non-competitive inhibition by PirC. The enzyme has a lowered affinity to the substrate in the presence of PirC, as demonstrated by a lowered K_m. Furthermore, the iPGAM also has a reduced maximal activity in the presence of PirC (shown by v_{max} and k_{cat}). The PirC peptide, which AlphaFold predicted to be localized in the phosphatase-transferase interdomain cleft, possibly hinders the cleft closure, which is required to perform the reaction. Thereby, the catalytic reaction is inhibited.

The replacement of the loop reduced the activity of the iPGAM, reaching only one-third of the maximal activity as the iPGAM-WT, and the increased K_m evidence four times decreased substrate affinity. Residue H457 in the catalytic center in *Synechocystis* iPGAM, equivalent to H462 from the *G. stearothermophilus* iPGAM, is connected via a β-strand to the loop. This histidine residue contributes to the binding of manganese (Fig.

2D) (26). In agreement, the iPGAM-Δloop variant has a reduced affinity to Mn^{2+} ($K_{half, WT}(Mn^{2+})$ = ~1.3 µM; $K_{half, \Delta loop}(Mn^{2+})$ = ~10.5 µM), and the enzyme requires much higher Mn^{2+} concentrations to reach its maximal activity. The AlphaFold prediction of the iPGAM structure revealed an H-bond between K473 and E468 within the loop. This interaction possibly stabilizes the β-strand connection to the catalytic center, favoring the manganese binding. The iPGAM of *G. stearothermophilus,* which does not possess this loop, requires manganese concentrations that are 1,000-fold higher than the $K_{half}(Mn^{2+})$ of *Synechocystis* iPGAM for maximal activity (27). The low activity of the iPGAM-Δloop indicates that the lowered manganese affinity consequently affects the whole reaction. Hence, the H457 residue contributes to the coordination of the bond Mn^{2+}, which is essential in the phosphatase reaction of the enzyme. The H-bond K473-E468 within the loop structure keeps the H457 in an optimal position, and Mn^{2+} binds with higher affinity. Furthermore, the Mn^{2+} coordinates the phosphoester bond of 2- or 3-PGA and thus enables the hydrolyzation of the phosphate. In the iPGAM-Δloop variant, the K473-E468 interaction does not exist, and H457 could be in another orientation within the catalytic center, resulting in a lowered K_m. Intriguingly, the iPGAM-Δloop variant has a higher affinity for PirC, indicating a conformational change imposed by the loop deletion that facilitates PirC interaction.

In contrast to the iPGAM-Δloop, the iPGAM-ΔCT has a twofold increased v_{max} compared to iPGAM-WT, whereas the K_m is not altered. At the same time, the affinity toward PirC is strongly enhanced, but PirC only weakly inhibits the iPGAM reaction: the inhibitory effect of PirC on iPGAM-ΔCT activity is 10-fold lower than on iPGAM-WT ($IC_{50, PirC}$(iPGAM-WT) = ~120 nM, $IC_{50, PirC}$(iPGAM-ΔCT) = ~1,070 nM). This directly implies that the C-terminal flexible extension plays a crucial role in modulating the activity of iPGAM and transmits the inhibitory effect of PirC binding to the catalytic center. Possibly, this C-terminal extension lowers the v_{max} of the reaction by interfering with the domain closure. By removing this tail, the enzyme can work at its maximum pace. In agreement, the binding of PirC would place the C-terminal tail in a position where the inhibitory effect is augmented. Without the C-terminal extension, the binding of PirC cannot exert this inhibitory function but facilitates its binding to the iPGAM body. This can be explained by the assumption that the binding of the CT extension by PirC is thermodynamically unfavorable. Residual inhibition of the iPGAM-ΔCT variant requires 10-fold higher concentrations of PirC, although the affinity of these partners has increased, which appears counterintuitive. It suggests that additional binding of PirC protomers to low-affinity binding sites of iPGAM-ΔCT is required to achieve inhibition. These additional binding events may impair the catalytically driven domain closure of iPGAM. Additional binding sites also agree with the experimentally observed size of the iPGAM–PirC complex, suggesting that more than one protomer of PirC can bind to iPGAM.

Concerning the iPGAM-Δloop-ΔCT variant, it shows a similar increased K_m for Mn^{2+} as the single iPGAM-Δloop, which agrees with the obvious role of the loop segment in high Mn^{2+} affinity. Surprisingly, however, the combined removal of both the loop and the CT segments gave rise to compensatory effects concerning its catalytic properties, as the catalytic efficiency is in between that of iPGAM-Δloop and iPGAM-WT variants. The inhibition of iPGAM-Δloop-ΔCT variant activity by PirC affects the K_m in a similar way as iPGAM-ΔCT. Overall, the binding of PirC to different sites of iPGAM, sites near the unique loop structure, and the CT segment is likely the structural basis of the observed mixed-type inhibition. Although we showed that the substructures play an important role in iPGAM inhibition, PirC still inhibits all enzyme variants to some extent. This fits with the prediction of the PirC protomer within the binding cleft of iPGAM, which is independent of the sub-structures. To elucidate the details of the mechanism and how the loop and the C-terminus influence the inhibitory effect of PirC on iPGAM activity, it is necessary to solve the actual structure of the PirC–iPGAM complex.

Under nitrogen-replete conditions, all the iPGAM variant strains grow similarly to the WT. This shows that during nutrient-replete vegetative growth, the low activities

of the iPGAM-Δloop and iPGAM-ΔloopΔCT variants are sufficient to maintain metabolic homeostasis. Conversely, the excessive activity of the iPGAM-ΔCT variant during vegetative growth has neither a positive nor a negative effect on *Synechocystis* growth. However, a distinct phenotype of iPGAM variant strains appeared during nitrogen starvation. Unlike the ΔPirC strain, the iPGAM-Δloop, -ΔCT, and -ΔloopΔCT strains could carry out the final doubling of OD_{750} upon shifting to a nitrogen-depleted medium. Furthermore, all iPGAM strains formed similar amounts of glycogen, whereas the ΔPirC strain is strongly affected by glycogen accumulation, in agreement with earlier observations (7). During prolonged chlorosis, the iPGAM-Δloop, -ΔCT, and -ΔloopΔCT strains showed slightly increased glycogen degradation compared to the WT. Previously, we showed (7) that the levels of 3-PGA, a key activator of glycogen formation, in both the WT and the ΔPirC mutant doubled within the first 6 hours after N depletion, indicating that this initial 3-PGA accumulation does not require iPGAM inhibition by PirC. This also explains the initial glycogen increase in ΔPirC. During further nitrogen starvation, expression of PirC is strongly induced (28). This leads to a pronounced inhibition of iPGAM and, consequently, a further increase of 3-PGA levels in the wild-type, which is no longer observed in the ΔPirC. Consequently, glycogen synthesis continues in the WT to reach its maximal levels after approximately 2 days, whereas glycogen synthesis prematurely slows down in ΔPirC.

During prolonged nitrogen starvation, glycogen is slowly converted into PHB (9). In the ΔPirC strain, lack of iPGAM inhibition during chlorosis leads to accelerated carbon flow into lower glycolysis, finally resulting in PHB formation. Both strains expressing the CT-truncated iPGAM (iPGAM-ΔCT and iPGAM-ΔloopΔCT) show almost the same amount of PHB accumulation after 14 days of nitrogen starvation as the ΔPirC. This can very likely be attributed to the reduced inhibition of these variants by PirC, whereas the iPGAM-Δloop strain shows similar levels to the WT, in agreement with the low activity of the iPGAM-Δloop–PirC complex.

Although the iPGAM-ΔCT-expressing strains produce similar amounts of PHB during prolonged chlorosis as the PirC-deficient strain, they still are able to respond to nitrogen starvation in a similar way to the WT by accumulating glycogen and performing a final cell division, whereas, in the absence of PirC, the cells go immediately into growth arrest. This could indicate additional roles of PirC beyond iPGAM inhibition for the acclimation toward nitrogen starvation. However, concerning the effect on PHB accumulation, inhibition of iPGAM seems to be the most important function. Previously, Koch et al. (29) achieved higher PHB levels with the ΔPirC strain by introducing additional *phaA* (acetyl-CoA acetyltransferase) and *phaB* (acetoacetyl-CoA reductase) genes, whose products catalyze the initial steps of PHB synthesis. A similar approach should also increase the PHB amounts in iPGAM-ΔCT or the iPGAM-ΔloopΔCT. In contrast to ΔPirC, these strains do not have the disadvantage of biomass loss during nitrogen starvation, which seems beneficial for biotechnological applications.

MATERIALS AND METHODS

Detailed descriptions of the methods are shown in the supplemental methods.

Multiple alignments and phylogenetic tree calculation of phosphoglycerate mutases

The alignments were done with Matlab and the tree was computed with IQ-Tree (21). The resulting tree was visualized with iTol (30).

Structure predictions

The structure of the iPGAM was predicted using the SWISS-MODEL workspace and AlphaFold server (31–33). AlphaFold was also used to predict the structure of the complex.

Molecular cloning and mutagenesis

Gibson assembly (GA) and mutagenesis PCR were used to create the plasmids. The GA was done according to the manufacturer protocol (NEB E2611S/L, E5510S).

According to the manufacturer protocol, iPGAM was mutated with the Q5 Site-Directed Mutagenesis Kit (NEB, E0554).

Plasmid and strains

The physiological experiments on cyanobacteria were carried out with the unicellular non-diazotrophic *Synechocystis* sp. PCC 6803 wild-type glucose sensitive strain, which is based on the Kazusa strain. All created mutants are also based on the above-described background strain.

Plasmids and all other strains created and used in this study are listed in Table S1 and Table S2.

Cultivation of cyanobacteria

Growth experiments and precultures of *Synechocystis* were cultivated in BG_{11}, and the composition was explained by Mager et al. (34). Standard cultivation was performed at 28°C with continuous shaking at 125 rpm at constant illumination (24 $h \cdot d^{-1}$, ~50 $\mu E\ m^{-2} \cdot s^{-1}$). The BG_{11} was adjusted for different experiments, as explained in the supplemental material.

For nitrogen deficiency experiments, precultures of *Synechocystis* at an OD_{750} of 0.6–1 were washed with and resuspended in BG_{11},0 medium, and the nitrogen-free culture was inoculated to an OD_{750} of 0.4.

Escherichia coli cultures were grown on lysogenic broth (LB) medium and agar.

Expression and purification of proteins

E. coli Lemo21(DE3) was used to overexpress proteins induced depending on the vector either by 400 mM isopropyl-β-D-thiogalactopyranoside (IPTG) or 200 µg anhydrotetracycline. The His-tagged proteins were purified using HisTrap HP columns (Cytiva, Marlborough, USA) and strep-tagged protein using the Strep-Tactin Superflow columns (IBA Lifescience, Göttingen, Germany) by affinity chromatography.

Mass photometry using the Refeyn OneMP

A mass photometry experiment was used to study the variants' oligomerization and the stoichiometry of the iPGAM–PirC complex. For this purpose, the Refeyn OneMP was used. The data were analyzed using the DiscoverMP software.

BLI using the Octet K2 system

In vitro binding studies were done using BLI using the Octet K2 system (Sartorius, Göttingen, Germany) according to the Bio-Protocol (35).

Phosphoglycerate mutase assay

The iPGAM activity was determined by a coupled enzyme assay as adapted as described previously (7). The release of the product 2-PGA, by iPGAM, is coupled to enolase, pyruvate kinase, and lactate dehydrogenase (LDH). LDH transforms NADH to NAD^+ by its reaction, and the NADH decrease was measured spectrophotometrically at 340 nm.

Glycogen measurement

The glycogen content was quantified according to previous studies from 2 mL *Synechocystis* culture samples (36). Samples of 2 mL cell culture were lysed by boiling at 95°C in 30% (wt/wt) KOH. The released glycogen was washed, accumulated, and enzymatically cleaved to glucose and detected via reaction with o-toluidine and measurement of the resulting compound spectrophotometrically at 635 nm.

PHB quantification

PHB was detected using high-performance liquid chromatography as described previously (7, 29, 37).

ACKNOWLEDGMENTS

We thank the Weir Lab at Friedrich-Miescher Laboratory at the Max-Planck Institute in Tübingen for allowing us to use their ReFeyn OneMP mass photometer. We thank Sofía Doello for the introduction to the instrument.

The work was supported by a grant from the Deutsche Forschungsgemeinschaft (DFG) Fo195/21-1 and infrastructural support through the Cluster of Excellence EXC 2124 (Controlling Microbes to Fight Infections, CMFI, grant 390838134) at the Eberhard Karls Universität Tübingen.

T.O.: Conceptualization, methodology, overall Investigations, BLI measurements, writing—original draft preparation, writing—review and editing; K.F.: Conceptualization, methodology and interpretation of results, writing—review and editing, supervision; N.B.: BLI measurements, writing—review and editing; J.T.A.: Construction of pJA01 and construction of ΔPirC strain, writing—review and editing; P.F.: PHB analysis, writing—review and editing. All authors read and approved the final manuscript.

AUTHOR AFFILIATION

[1]Interfaculty Institute of Microbiology and Infection Medicine Tübingen, University of Tübingen, Tübingen, Germany

AUTHOR ORCIDs

Tim Orthwein http://orcid.org/0000-0002-4650-2554
Janette T. Alford http://orcid.org/0009-0009-1115-5175
Nathalie Sofie Becker http://orcid.org/0000-0002-6893-1181
Karl Forchhammer http://orcid.org/0000-0003-3199-8101

FUNDING

Funder	Grant(s)	Author(s)
Deutsche Forschungsgemeinschaft	DFG Fo 195/21-1	Tim Orthwein
Deutsche Forschungsgemeinschaft	DFG Fo 195 /23-1	Nathalie Sofie Becker
Deutsche Forschungsgemeinschaft	EXC 2124	Karl Forchhammer

AUTHOR CONTRIBUTIONS

Tim Orthwein, Conceptualization, Data curation, Investigation, Methodology, Validation, Visualization, Writing – original draft, Writing – review and editing | Janette T. Alford, Investigation, Writing – review and editing | Nathalie Sofie Becker, Investigation, Writing – review and editing | Phillipp Fink, Investigation, Methodology, Writing – review and editing | Karl Forchhammer, Conceptualization, Data curation, Funding acquisition, Methodology, Project administration, Resources, Supervision, Validation, Writing – original draft, Writing – review and editing

ADDITIONAL FILES

The following material is available online.

Supplemental Material

Supplemental material (mBio03378-24-S0001.docx). Figures S1 to S8, Tables S1 to S4, and supplemental methods.

REFERENCES

1. Galperin MY, Bairoch A, Koonin EV. 1998. A superfamily of metalloenzymes unifies phosphopentomutase and cofactor-independent phosphoglycerate mutase with alkaline phosphatases and sulfatases. Protein Sci 7:1829–1835. https://doi.org/10.1002/pro.5560070819
2. Jedrzejas MJ. 2000. Structure, function, and evolution of phosphoglycerate mutases: comparison with fructose-2,6-bisphosphatase, acid phosphatase, and alkaline phosphatase. Prog Biophys Mol Biol 73:263–287. https://doi.org/10.1016/s0079-6107(00)00007-9
3. Roychowdhury A, Kundu A, Bose M, Gujar A, Mukherjee S, Das AK. 2015. Complete catalytic cycle of cofactor-independent phosphoglycerate mutase involves a spring-loaded mechanism. FEBS J 282:1097–1110. https://doi.org/10.1111/febs.13205
4. Kuhn NJ, Setlow B, Setlow P. 1993. Manganese(II) activation of 3-phosphoglycerate mutase of *Bacillus megaterium*: pH-sensitive interconversion of active and inactive forms. Arch Biochem Biophys 306:342–349. https://doi.org/10.1006/abbi.1993.1521
5. Loshon CA, Setlow P. 1993. Levels of small molecules in dormant spores of *Sporosarcina* species and comparison with levels in spores of *Bacillus* and *Clostridium* species. Can J Microbiol 39:259–262. https://doi.org/10.1139/m93-036
6. Klemke F, Baier A, Knoop H, Kern R, Jablonsky J, Beyer G, Volkmer T, Steuer R, Lockau W, Hagemann M. 2015. Identification of the light-independent phosphoserine pathway as an additional source of serine in the cyanobacterium *Synechocystis* sp. PCC 6803. Microbiology (Reading) 161:1050–1060. https://doi.org/10.1099/mic.0.000055
7. Orthwein T, Scholl J, Spät P, Lucius S, Koch M, Macek B, Hagemann M, Forchhammer K. 2021. The novel P_{II}-interactor PirC identifies phosphoglycerate mutase as key control point of carbon storage metabolism in *Cyanobacteria*. Proc Natl Acad Sci USA 118:e2019988118. https://doi.org/10.1073/pnas.2019988118
8. Klotz A, Georg J, Bučinská L, Watanabe S, Reimann V, Januszewski W, Sobotka R, Jendrossek D, Hess WR, Forchhammer K. 2016. Awakening of a dormant cyanobacterium from nitrogen chlorosis reveals a genetically determined program. Curr Biol 26:2862–2872. https://doi.org/10.1016/j.cub.2016.08.054
9. Koch M, Doello S, Gutekunst K, Forchhammer K. 2019. PHB is produced from glycogen turn-over during nitrogen starvation in *Synechocystis* sp. PCC 6803. Int J Mol Sci 20:1942. https://doi.org/10.3390/ijms20081942
10. Görl M, Sauer J, Baier T, Forchhammer K. 1998. Nitrogen-starvation-induced chlorosis in *Synechococcus* PCC 7942: adaptation to long-term survival. Microbiology (Reading) 144 (Pt 9):2449–2458. https://doi.org/10.1099/00221287-144-9-2449
11. Sauer J, Schreiber U, Schmid R, Völker U, Forchhammer K. 2001. Nitrogen starvation-induced chlorosis in *Synechococcus* PCC 7942. Low-level photosynthesis as a mechanism of long-term survival. Plant Physiol 126:233–243. https://doi.org/10.1104/pp.126.1.233
12. Schlebusch M, Forchhammer K. 2010. Requirement of the nitrogen starvation-induced protein Sll0783 for polyhydroxybutyrate accumulation in *Synechocystis* sp. strain PCC 6803. Appl Environ Microbiol 76:6101–6107. https://doi.org/10.1128/AEM.00484-10
13. Forchhammer K, Schwarz R. 2019. Nitrogen chlorosis in unicellular *Cyanobacteria* - a developmental program for surviving nitrogen deprivation. Environ Microbiol 21:1173–1184. https://doi.org/10.1111/1462-2920.14447
14. Forchhammer K, Selim KA. 2020. Carbon/nitrogen homeostasis control in *Cyanobacteria*. FEMS Microbiol Rev 44:33–53. https://doi.org/10.1093/femsre/fuz025
15. Forchhammer K, Lüddecke J. 2016. Sensory properties of the PII signalling protein family. FEBS J 283:425–437. https://doi.org/10.1111/febs.13584
16. Rozbeh R, Forchhammer K. 2021. Split NanoLuc technology allows quantitation of interactions between PII protein and its receptors with unprecedented sensitivity and reveals transient interactions. Sci Rep 11:12535. https://doi.org/10.1038/s41598-021-91856-2
17. Bolay P, Rozbeh R, Muro-Pastor MI, Timm S, Hagemann M, Florencio FJ, Forchhammer K, Klähn S. 2021. The novel P_{II}-interacting protein PirA controls flux into the cyanobacterial ornithine-ammonia cycle. MBio 12:e00229-21. https://doi.org/10.1128/mBio.00229-21
18. Giner-Lamia J, Robles-Rengel R, Hernández-Prieto MA, Muro-Pastor MI, Florencio FJ, Futschik ME. 2017. Identification of the direct regulon of NtcA during early acclimation to nitrogen starvation in the cyanobacterium *Synechocystis* sp. PCC 6803. Nucleic Acids Res 45:11800–11820. https://doi.org/10.1093/nar/gkx860
19. Forcada-Nadal A, Bibak S, Salinas P, Contreras A, Rubio V, Llácer JL. 2024. Structural understanding of NtcA regulation and of its coactivation by the adaptor PII/NtcA shuttling protein PipX, which connects PII regulation with gene expression regulation. bioRxiv
20. Forcada-Nadal A, Llácer JL, Contreras A, Marco-Marín C, Rubio V. 2018. The P_{II}-NAGK-PipX-NtcA regulatory axis of *Cyanobacteria*: a tale of changing partners, allosteric effectors and non-covalent interactions. Front Mol Biosci 5:91. https://doi.org/10.3389/fmolb.2018.00091
21. Trifinopoulos J, Nguyen LT, von Haeseler A, Minh BQ. 2016. W-IQ-TREE: a fast online phylogenetic tool for maximum likelihood analysis. Nucleic Acids Res 44:W232–W235. https://doi.org/10.1093/nar/gkw256
22. Collier JL, Grossman AR. 1992. Chlorosis induced by nutrient deprivation in *Synechococcus* sp. strain PCC 7942: not all bleaching is the same. J Bacteriol 174:4718–4726. https://doi.org/10.1128/jb.174.14.4718-4726.1992
23. Selim KA, Ermilova E, Forchhammer K. 2020. From *Cyanobacteria* to *Archaeplastida*: new evolutionary insights into PII signalling in the plant kingdom. New Phytol 227:722–731. https://doi.org/10.1111/nph.16492
24. Strunecký O, Wachtlová M, Koblížek M. 2021. Whole genome phylogeny of *Cyanobacteria* documents a distinct evolutionary trajectory of marine picocyanobacteria. bioRxiv. https://doi.org/10.1101/2021.05.26.445609
25. Strunecký O, Ivanova AP, Mareš J. 2023. An updated classification of cyanobacterial orders and families based on phylogenomic and polyphasic analysis. J Phycol 59:12–51. https://doi.org/10.1111/jpy.13304
26. Jedrzejas MJ, Chander M, Setlow P, Krishnasamy G. 2000. Structure and mechanism of action of a novel phosphoglycerate mutase from *Bacillus stearothermophilus*. EMBO J 19:1419–1431. https://doi.org/10.1093/emboj/19.7.1419
27. Chander M, Setlow P, Lamani E, Jedrzejas MJ. 1999. Structural studies on a 2,3-diphosphoglycerate independent phosphoglycerate mutase from *Bacillus stearothermophilus*. J Struct Biol 126:156–165. https://doi.org/10.1006/jsbi.1999.4112
28. Muro-Pastor MI, Cutillas-Farray Á, Pérez-Rodríguez L, Pérez-Saavedra J, Vega-de Armas A, Paredes A, Robles-Rengel R, Florencio FJ. 2020. CfrA, a novel carbon flow regulator, adapts carbon metabolism to nitrogen deficiency in *Cyanobacteria*. Plant Physiol 184:1792–1810. https://doi.org/10.1104/pp.20.00802
29. Koch M, Bruckmoser J, Scholl J, Hauf W, Rieger B, Forchhammer K. 2020. Maximizing PHB content in *Synechocystis* sp. PCC 6803: a new metabolic engineering strategy based on the regulator PirC. Microb Cell Fact 19:231. https://doi.org/10.1186/s12934-020-01491-1
30. Letunic I, Bork P. 2024. Interactive Tree of Life (iTOL) v6: recent updates to the phylogenetic tree display and annotation tool. Nucleic Acids Res 52:W78–W82. https://doi.org/10.1093/nar/gkae268
31. Guex N, Peitsch MC, Schwede T. 2009. Automated comparative protein structure modeling with SWISS-MODEL and SWISS-PdbViewer: a historical perspective. Electrophoresis 30 Suppl 1:S162–S173. https://doi.org/10.1002/elps.200900140
32. Waterhouse A, Bertoni M, Bienert S, Studer G, Tauriello G, Gumienny R, Heer FT, de Beer TAP, Rempfer C, Bordoli L, Lepore R, Schwede T. 2018.

SWISS-MODEL: homology modelling of protein structures and complexes. Nucleic Acids Res 46:W296–W303. https://doi.org/10.1093/nar/gky427
33. Abramson J, Adler J, Dunger J, Evans R, Green T, Pritzel A, Ronneberger O, Willmore L, Ballard AJ, Bambrick J. 2024. Accurate structure prediction of biomolecular interactions with AlphaFold 3. Nature New Biol 630:493–500. https://doi.org/10.1038/s41586-024-07487-w
34. Mager M, Pineda Hernandez H, Brandenburg F, López-Maury L, McCormick AJ, Nürnberg DJ, Orthwein T, Russo DA, Victoria AJ, Wang X, Zedler JAZ, Dos Santos FB, Schmelling NM. 2023. Interlaboratory reproducibility in growth and reporter expression in the cyanobacterium *Synechocystis* sp. PCC 6803. 12:1823–1835. ACS Synth Biol 12:1823–1835. https://doi.org/10.1021/acssynbio.3c00150
35. Orthwein T, Huergo LF, Forchhammer K, Selim KA. 2021. Kinetic analysis of a protein-protein complex to determine its dissociation constant (K_D) and the effective concentration (EC_{50}) of an interplaying effector molecule using bio-layer interferometry. Bio Protoc 11:e4152. https://doi.org/10.21769/BioProtoc.4152
36. Doello S, Klotz A, Makowka A, Gutekunst K, Forchhammer K. 2018. A specific glycogen mobilization strategy enables rapid awakening of dormant *Cyanobacteria* from chlorosis. Plant Physiol 177:594–603. https://doi.org/10.1104/pp.18.00297
37. Koch M, Berendzen KW, Forchhammer AK. 2020. On the role and production of polyhydroxybutyrate (PHB) in the cyanobacterium *Synechocystis* sp. PCC 6803. Life (Basel) 10:47. https://doi.org/10.3390/life10040047